Smoothing Silver Nanowires for Optoelectronic Applications

by

Richard Michael Steuben Swartwout

B.S. Rensselaer Polytechnic Institute (2015)

Submitted to the Department of Electrical Engineering and Computer Science
in partial fulfillment of the requirements for the degree of

Master of Science

at the

MASSACHUSETTS INSTITUTE OF TECHNOLOGY

June 2018

Author . . . .
Department of Electrical Engineering and Computer Science
May 21, 2018

Certified by. . . . .
Vladimir Bulović
Professor of Electrical Engineering
Thesis Supervisor

Accepted by . . . .
Leslie A. Kolodziejski
Professor of Electrical Engineering and Computer Science Chair,
Department Committee on Graduate Students

Smoothing Silver Nanowires for Optoelectronic Applications

by

Richard Michael Steuben Swartwout

Submitted to the Department of Electrical Engineering and Computer Science
on May 21, 2018, in partial fulfillment of the
requirements for the degree of
Master of Science

Abstract

Silver nanowire meshes have shown potential for becoming a more robust, flexible alternative to traditional ceramic and brittle metal oxides. However, the current methods employed at making these films are not scalable and the high aspect ratios limit their final use. Spray coating is a technique that is widely used in many industries and has proven effective in many coating applications but continues to be limited by drying defects when used traditionally. A simple modification; pulsed spraying can decouple rheology and chemistry and allow for deposition of more uniform silver nanowire mesh films. Additional processing methods, such as metal mesh compression and matrix infilling with a CVD deposited plastic, Parylene-C, can yield a composite that solves roughness issues present with bare films. By combining all of these methods, a silver nanowire-parylene composite can be fabricated using fully scalable techniques ready for sheet-to-sheet or roll-to-roll processing. The composite is flexible, optically transparent, surface smooth, atmospherically stable and conductive, proving itself as a potential replacement for traditional transparent electrodes.

Thesis Supervisor: Vladimir Bulović
Title: Professor of Electrical Engineering

Acknowledgments

Thank you to my parents for conceiving me

Thank you to Marty for believing in me

Thank you to Vladimir and ONELab for working with me

Thank you to the Tata Center for funding me

Thank you to beer for all the fun times and getting me through

Thank you to Lisa for making me finish what I started, I love you

Shout out to CMSE for reminding me over the summer of 2017 that its important for students and their equipment to shower every now and again

Contents

List of Figures

10

11

List of Tables

Chapter 1

Introduction

Since the development of the first semiconductor single heterostructure and double heterostructure based devices based on silicon and germanium compounds in the middle of the 20th century, technology, chemistry and materials science has progressed to the point where heterostructures devices are the most important device architecture of our age. Today, heterostructure based optoelectronic devices are becoming a mainstay in our everyday lives. Organic light emitting diode (OLED) displays are the main technology used in the smartphone screens used by companies like Apple, Samsung and Google. OLED displays are also beginning their entrance in the television market with companies like LG, Sony and Samsung selling OLED screen TVs as their flagship models. In fact, heterojunction based optoelectronic devises are responsible for the most efficient and color accurate light emitting diodes currently used in research and on the market today [4] [8] [48].

In addition, but to a lesser extent, the solar cell industry (a sister technology to LEDs) has also taken up and commercialized heterstructured devices. Miasole has successfully commercialized flexible copper gallium indium selenide (CIGS) technology and First Solar has successfully commercialized Cadmium Telluride (CdTe) on glass. In academic research, the highest absorbing, efficient, cost effective and scalable solar cells are also heterstructure-based devices [55] [39] [58]. Nevertheless, for every success story there are many failed companies. Konarka a company that raised $170 million in investor funding, promising to produce cheap and flexible polymer and

17

organic based heterostructure solar cells, but still ended up going bankrupt in 2012. This is just the most notable example from many failed organic solar cell companies that went bankrupt in the early to mid 2000s. There are currently no notable organic solar cell products on the market despite their prevalence and growth in the display industry.

The difficulty seems to be in the heterostructure device itself; by allowing greater degrees of freedom for material selection, electronic structuring and application specific tunability, heterostructures bring further challenges in materials processing, material compatibility and multi-material property control during fabrication that is difficult to control on a manufacturing scale [44] [6]. Although heterostructured optoelectronic devices have the ability to be highly engineered and tailored to specific applications, the difficulty in bringing them to market, and having a market willing to pay for that development, limits their scope and use in industry despite the many thousands of published structures at a research level.

Additional difficulties and engineering challenges present themselves when trying to fabricate a flexible electronic heterostructued device. Not only is materials processing still a significant issue, but also the available materials that are possible to be incorporated in the device is severely limited. In addition, material mechanical properties can be just as significant to material electrical properties in terms of device performance and decide longevity. Finding an intersection of adequate and cost effective material processing, electronic structuring and mechanical flexibility is therefore a daunting problem. Despite the flexible display market being valued over a billion dollars, the display industry has failed to release any significant mass produced product in this space leaving this market largely uncaptured [37].

1.1 Review of Device Architecture

Most modern double heterostructured devices have at least six thin film material layers as seen in Figure 1-1. In terms of overall manufacturing of this structure, there are no physical limits as to which layer needs to be processed first. Generally, due

to ease and simplicity of material handling the device is constructed in order from one electrode to the other on top of a support material. In solar cell literature, if the device is manufactured from the opaque *back* electrode toward the transparent *front* electrode, the support material is referred to as a *substrate* and the entire stack of materials is referred to as having a *substrate configuration*. Since most devices are usually encapsulated by sandwiching between two materials, there tends to be a second sheet of material in-between the transparent electrode and the environment. This transparent material is referred to as the *superstrate* as it sits above the device and does not need to mechanically support the device, just allow light to enter and exit the device.

It is possible, to build a device from the transparent electrode toward the back opaque electrode. The supporting material in this case (again only in solar cell literature) would be called the *superstrate* to distinguish itself from the previous example and said to be built in a *superstrate configuration*. This configuration, although basing its nomenclature on the substrate configuration is the most common configuration for heterojunction based devices to be built. This is due to multiple factors. First, superstrates tend to be chemically resistant, if not more chemically resistant than substrates. Second, superstrates tend to be cheap to produce. Third, it is common for manufacturers to manufacture transparent conducting electrodes on top of superstrates, which can then be purchased by the one making the optoelectronic device, reducing time of manufacturing. Lastly, transparent oxides, which are the most common transparent oxide can be processed relatively smooth, and usually require the highest temperature annealing of any layer. Therefore, almost all modern day heterostructure based devices used in research and academia, both solar cells and light emitting diode architectures are manufactured in the superstrate configuration. There are notable exceptions to this rule in industry however, like the CIGS devices from Miasole, which processed in the substrate configuration on metal foil and silicon solar cells, which can also be grown in a substrate configuration.

Due to its commonality to build a device from transparent electrode to opaque back metal electrode, the LED literature has referred to the supporting transparent

material as the substrate. Due to all solar devices being referred to in this thesis being of the superstrate configuration, I will be referring to the transparent supporting material as the substrate in all cases to avoid confusion.

1.2   Review of Flexible Heterostructured Devices

As stated in the last section, a modern day heterostrucutred device is composed of at least six material layers, with one layer being the bulk substrate. In general, the device is manufactured from a transparent electrode to an opaque metal electrode with transport layers and active layers in between. A flexible device is therefore a device that is manufactured upon a flexible substrate and takes advantage of ductility, flexibility and thin film characteristics in the electrodes, charge transport and active layers.

In recent years, there has been a push in literature to move toward flexible, planar heterojunction electronics and there are many demonstrations showing applications of flexible architectures [10-14]. Joel Jean et al [21] published a report, which integrates a flexible substrate fabrication in situ with additional thin film layers to create a fully flexible and lightweight organic solar cell. The flexible substrate, in this case Parylene-C, was deposited on a ridged carrier substrate before additional thin film processing and additional back encapsulation. The entire flexible organic device was then be peeled off the carrier substrate, which could be reused, isolating a free standing, flexible and ultra-thin substrate. This demonstration, despite having low overall efficiency and mechanical stability, shows the novelty of using traditional material handling techniques to fabricate a flexible device. Overall device dimensions was 2.3 micrometers.

Moon Kee Choi et al. [7] produced a flexible quantum dot display using a novel printing technique. Their device is also based around in situ growth of parylene, and additional growth of other layers, but this time included a solution processed quantum dot layer in an LED structure. To demonstrate flexibility and the biocompatibility of parylene, this device was then laid on human skin to create an electrically and

optically functional tattoo. Although not studied, this device was also mechanically instable as the device is non-uniform and shorting in sections as seen in a supplementary reported video about the device.

Martin Kaltenbrunner et al. [25] reported an ultra-flexible organic solar cell using only ductile materials. Due to the ultra-flexibility of the device, the sample could be compressed and stretched, using wrinkles to increase optical path length despite being a planar device. Four years later Martin repeated the device with organometallic perovskite as the absorber layer, seeing a large increase in power conversion efficiency, which allowed the manufacture of a solar powered plane using perovskite solar cells [24].

Lastly, Juho Kin et al. [26] fabricated an ultra-thin and flexible GaAs solar cell in the substrate configuration. Not only does this show that flexible architectures are not limited to novel material systems, but also do not require transparent substrates in order to achieve a high efficiency and flexible product.

1.3   Review of Transparent Electrodes

Transparent electrodes are a class of electrode that is transparent to the visible spectrum but remains electronically favorable for device making and has high conductivity for long-range current extraction out of a device or current injection into a device. For crystalline materials, this is usually a material that has a bandgap in the ultraviolet spectrum and is n+ doped to be highly conducting due to longer electron mobility and lifetime [36] [17] [42] [12] [38] [42]. Poylmeric and organic materials are usually long chains of delocalized pi bonds which provide conduction, but have a HOMO/ LUMO energetic gap outside the visible spectrum. Organic materials may also be doped to increase free charge concentration and therefore conductivity [47] [27] [22] [52]. Lastly, metal or conducting carbon grids can also be used as transparent conductors, but are not a periodic or homogeneous material film on their own. A summary of common transparent electrodes reported in literature and their properties can be seen in Table 1.1.

Table 1.1: Common transparent electrodes and basic properties

Material	$R_{sheet}(\Omega/\square)$	$\%T_{550}$	Reference
Sputtered ITO	15-50	>90%	[36] [17] [42] [12]
Sputtered FTO	7-100	>80%	[38] [42] [17] [12]
PEDOTT:PSS	100-1000	>90%	[47] [29] [27] [22] [12]
CVD Graphene	100-1000	>70%	[52] [51] [53]
Graphene Oxide	100-1000	>60%	[52]
Silver Nanowires	15	85%	*This Work*
Metal Grids	1-10	>80%	[30] [12] [57] [15]

Many of these technologies however are not commercialized. Most commercial products fall in the category of being transparent metal oxides, mostly tin compounds doped to have higher conductivity than normal tin oxide. Common ridged products in this space include indium doped tin oxide (ITO) deposited on glass and fluorine doped tin oxide (FTO) on glass. When moving to a flexible architecture, materials selection becomes limited and commercial products are almost exclusively indium doped tin oxide deposited on PET or PEN. There is however, one commercialized flexible silver grid electrode: *Flextrode* produced by infinityPV.

The limited commercialization shows that for a flexible transparent conducting electrode to be successful, it must adhere to some very strict requirements. It must be smooth to have good electrical contact for layers deposited upon it [13] [17] [12]. In addition, under mechanical and thermal stress these traditionally brittle layers can delaminate and crack, creating a poor interface with the active layers, increase electrode resistivity, or cause shorting of the device altogether [2]. Reproduced sheet resistivity data over the course of cyclic bending cycles is reproduced in Figure 1-2. Lastly traditional TCEs are usually vacuum coated and annealed at high temperature, an energy intensive and slow manufacturing process that is difficult to accomplish on plastics such as PET on a large area for low cost, an issue for traditional ITO coated PET. Therefore, it is important to find a suitable replacement to vacuum coated TCEs that are mechanically ductile, smooth, deposited quickly at low temperature, cheap and stable [13].

There have been many reports of novel TCEs that attempt to meet these needs [9] [40] [49] [35] [41] [15] [1] [57] [51] [20] [33] [9] [29] [31] [11], however as the needs for
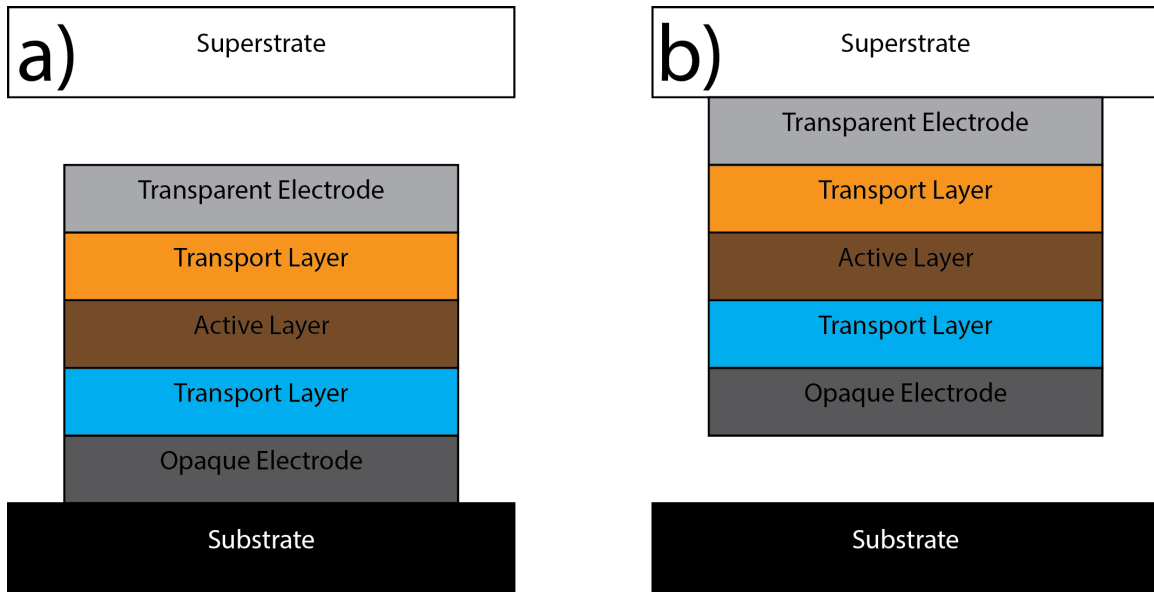
Figure 1-1: a)Substrate and b) Superstate device configurations

such a material are high, none are perfect replacements. Novel organic semiconductors are transparent, conductive, flexible, and cheap but suffer from poor environmental and chemical stability [27] [47] [29]. In addition, most require electrical compatibility and alignment with the target device. This can be beneficial in some circumstances, but in general limit the scope of possible architectures. Sol-Gel based metal oxides have been shown to have better mechanical stability than their vacuum deposited relatives at reasonable transparency and conductivity (90%T at 20 $\Omega/\square$) but suffer from higher material cost, long anneal times, and have yet to be proven on high efficiency flexible optoelectronic devices [49] [40]. Graphene is promising as it is highly flexible and environmentally stable, but is still difficult to produce in large areas, at reasonable cost, and at high transparency and conductivity (90%T at < 50 $\Omega/\square$) [51] [52] [53]. Nanowire meshes and grids have shown good mechanical stability as well as transparency and conductivity (90%T at 20 $\Omega/\square$) and can be manufactured quickly and cost effectively, but suffer from high surface roughness and low environmental lifetime (usually due to oxidation) [9] [31] [33] [20] [16]. They also have the challenge of being an inherently non-uniform layer, which may cause issues if injection or collection layers if not taken into account. Bare nanowire roughness data is seen in Chapter 3 and 4.
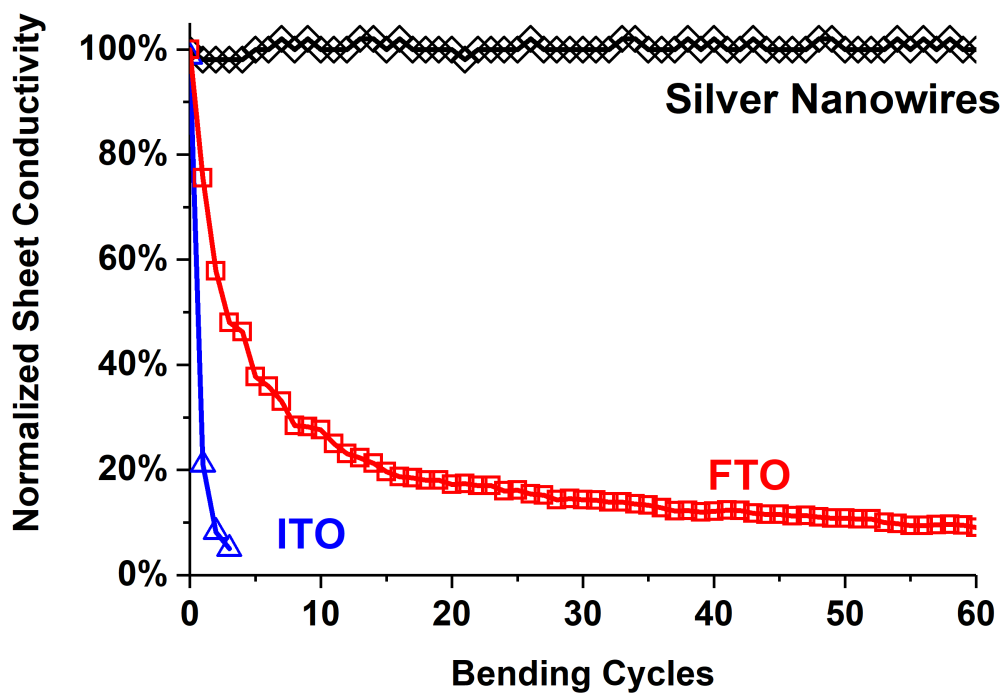
Figure 1-2: Degradation of transparent conducting metal oxides with cyclic bending radius of r=5mm [31]

Composites materials of nanowires and other materials show the greatest promise as they solve many of the issues present in a single component material [41] [11] [15] [35] [57] [45] [1]. The general tactic is to combine silver nanowires with other TCE materials to increase conductivity while also keeping surface roughness low. However, for this approach to be a true replacement, both materials must meet the needs that current transparent conducting oxides provide. Nanowire and organic composites increase conductivity but are still limited by poor stability. Nanowire and sol-gel composites are costly and still require long annealing times. Nanowire and graphene composites are highly flexible but still have high roughness and graphene is not proven at scale in large quantities.

1.4   Thesis Outline

This thesis will explore the use of a lab built solution processed spray coating technique, and traditional vacuum processing to deposit and surface smooth silver nanowire networks. I first introduce basic theory of spray coating and parylene CVD deposition. I then discuss surface modification and silver nanowire chemistry. Lastly, I discuss the fabrication of the smoothed metal nanowire mesh composites and report on its properties.

Chapter 2

Thin Film Deposition Theory and Techniques

Almost all thin film deposition techniques relay on a carrier (vacuum, gas or liquid) to transition and deposit a bulk material into a thin film of material on a surface. In practice, each technique is limited by the manufacturing restrictions of the carrier for obtaining a quality, uniform and homogeneous thin film. In traditional thermal evaporation, a physical vapor deposition process, the technique is limited by the mechanical constraints needed to maintain a high atmospheric vacuum and the power required to sublimate or evaporate the base material. Traditional solution processing, where a liquid solvent is a carrier for a given material is limited by solvent interactions and solvent-atmosphere drying effects. This section will discuss two thin film deposition techniques used later for fabrication of a composite nanowire substrate. This section will begin by discussing drop drying physics, its extension for traditional spray coating and the construction of a lab-built spray coater. Lastly, pyrolysis CVD and its application will be discussed, specifically for parylene materials.

2.1 Drop Drying

To understand solution processed thin film techniques it is important to understand one of the most basic systems, drop drying. Drop drying is where a solution loaded

with a solute or dispersed particles is placed on a surface and allowed to dry, leaving a solid behind. How a drop dries and the resulting film can give us a wealth of knowledge about the mechanisms behind solution based thin film deposition and allows us to engineer solutions and inks to meet device needs.

2.1.1   Contact Angle and Drop Shape

When a liquid is placed on a surface, it can either ball up or spread out. This phenomenon is characterized by the contact angle. Contact angle is the characteristic angle defined by a liquid-vapor-solid interface. Mathematically it can be defined by the Young equation and visually in Figure 2-1.

$$y_{S,G} - y_{S,L} - y_{L,G}cos(\theta) = 0$$
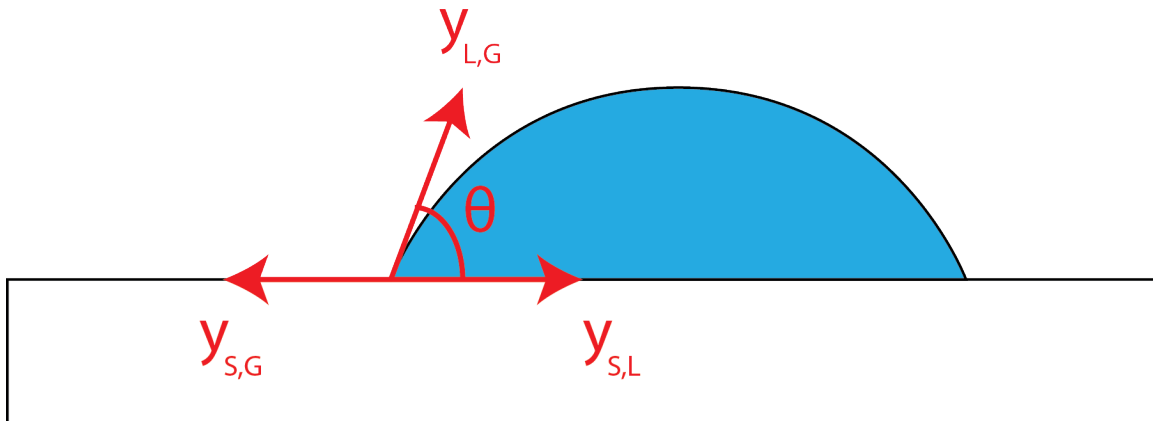
Figure 2-1: Visual description of the Young equation

For this analysis, contact angle is important for determining drop shape and therefore has an impact on microfluidic forces that are possible for drying.

2.1.2   Microfluidics and the Coffee Ring Effect

The liquid-vapor interactions during drying and the subsequent microfluidic phenomenon it induces has generally been studied in the form of the coffee ring effect. The coffee ring effect is when solute is forced to the edges of a drop during drying,

creating a ring around the drop. The effect was first given a capillary flow model by Robert D Deegan et al. in which fluid is forced to the edges of a drop while drying [10]. The model shows that to balance flow in the system, and due to higher evaporation at the edges of the drop rather than the middle, there must be a convection flow outwards while the drop is drying. Mainak Majumder et al. then reported that these forces can be overcome by controlling the capillary forces and inducing Marangoni flow, an internal convection, for more even particle distribution after drying [34]. Others have shown similar effects when manipulating internal capillary forces through solution chemistry engineering and temperature. Pictorial descriptions of this theory are shown in Figure 2-2 and 2-3 below.
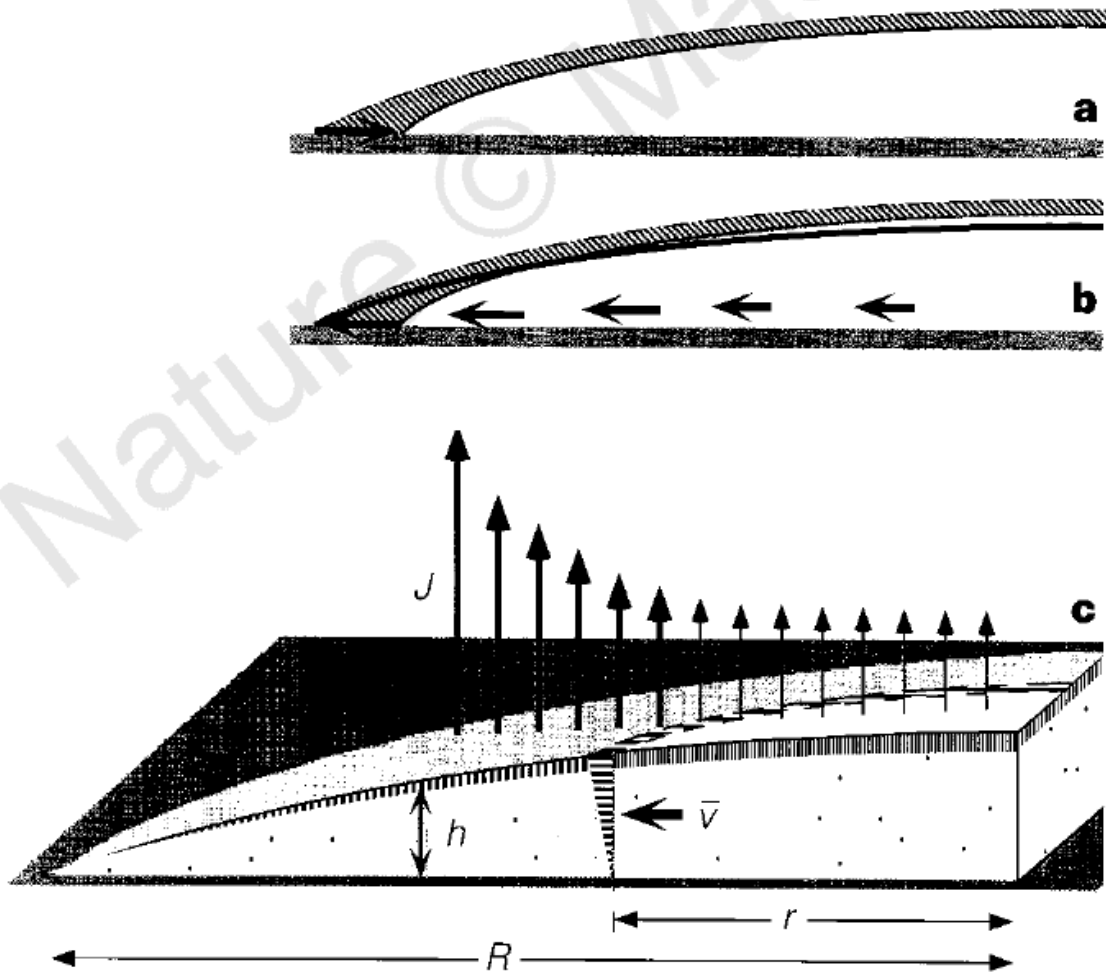
Figure 2-2: Representation of the coffee stain effect. Taken from [10]
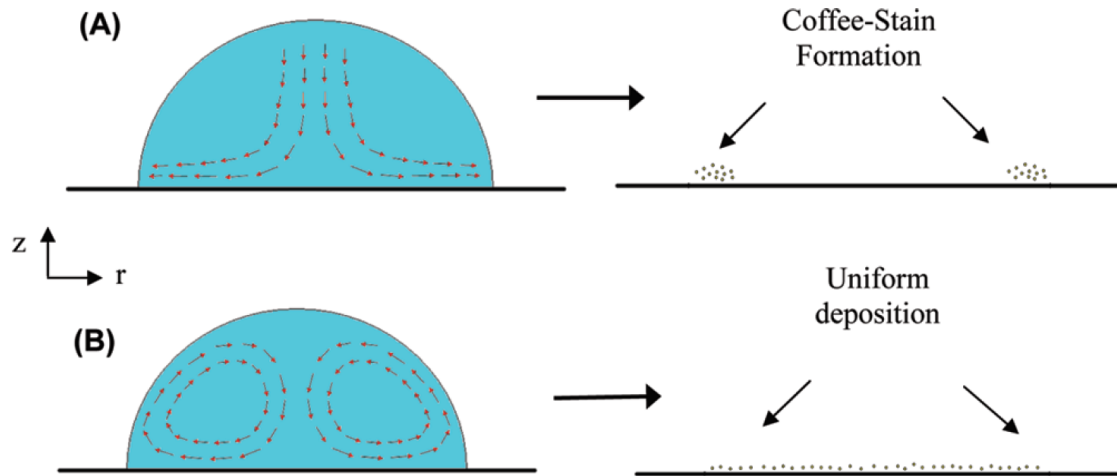
Figure 2-3: Representation of Marangoni flow to avoid the coffee stain effect. Taken from [34]. Traditional microfluidics that result in the coffee stain is shown in (A) Marangoni flow is shown in (B)

Understanding the capillary forces of drop drying shows that there is an inherent connection between the solute within a solution and its film formation within a given atmosphere. As contact angle, manufacturing and environment can all play a role in influencing microfluidic capillary forces, we can then postulate that engineering an ink system for a given application requires knowledge of the chemistry, but also the rheology of a given system and the interaction with the manufacturing process and global environment.

2.2   Spray Coating

An extension of drop drying is the technique known as spray coating. Unlike drop drying, spray coating is a two phase coating technique where a liquid is atomized by some means and then carried delivered to a surface by way of a carrier gas. There are many different methods and techniques for accomplishing this, from pressure induced to ultrasonically induced atomization. For this work we will be focusing on mostly venturi style self fed spray coating as this style is the main method used in paint airbrushes. This makes them cheap, simple to obtain and accurate enough with their

drop distribution to be useful for thin film purposes.

2.2.1 Traditional Spray Coating

The physics of creating a homogenous sized aerosol, the momentum and mass transport of the aerosol to the surface and the transient effects associated with spray coating can be complicated, and is not covered in comprehensive solution coating textbooks [46] [50]. For a more thorough coverage of the topic it, I direct the reader to reference Fluid Dynamics and Transport of Droplets and Sprays by William Sirignano [43].

For a venturi style airbrush a simple description is as follows: a medium pressure gas flows over a needle primed with an ink. That ink, which due to the venturi effect is pulled out of the needle, then interacts with the flowing gas. The gas, which has a high speed relative to the liquid ink then creates a high amount of sheer and liquid instability. The liquid then breaks into micron sized or multi-micron sized spheres and is aerosolized. Since the gas flow is directed at a surface, the aerosolized particles are then forced in the same direction by momentum transfer. At, or close to the surface, the carrier gas will begin to move around the surface where the solution will be deposited. The particles on the other hand do not change direction as quickly and instead they impact the surface. Surface energy and van der waals forces keep the liquid adhered to the surface. If enough particles attach to the surface at any given time, the particles will mesh into each other and create a thin film of liquid, on the order of microns thick. Fluid transfer and evaporation kinetics will then determine the rate of wet film growth, drying and dry film deposition rate. In an extreme case, fluid transfer will be high relative to drying and flood the surface. If drying is high and fluid transfer rate is low, a continuous wet film will never fully form. Therefore film growth is similar to drop drying. Pictorial descriptions of this can be seen in Figure 2-4.
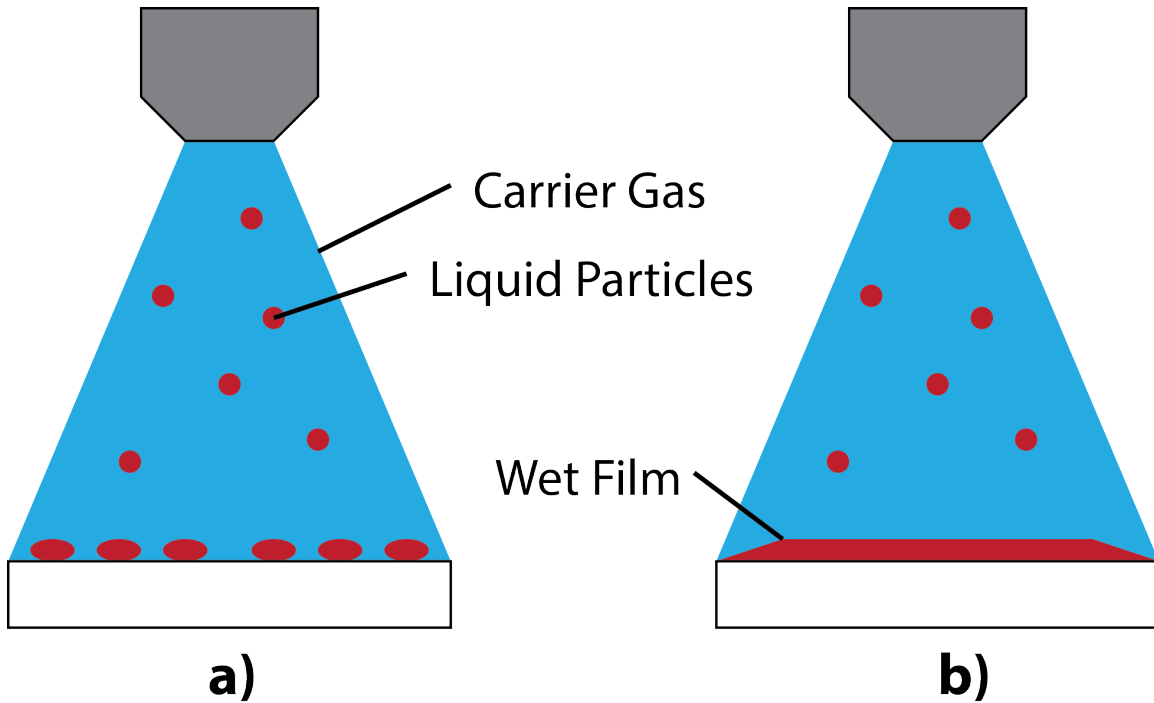
Figure 2-4: Representation of spray coating used in a traditional continuous flow

2.2.2 Pulsed Spray Coating

Both regimes of continuous spray coating can have significant impact on how the final film forms. Full wet film coverage and fast fluid transfer can allow for very fast manufacturing but slow fluid transfer can allow drops to pile on dry drops, increasing deposition control and uniformity if the chemistry allows for it. Despite this, there is still an inherent coupling of rheology and film formation. Things that dry slowly may build up too fast to be highly controllable and it may be hard to transition to solvents that are more volatile. In addition drying dynamics change between a continuous wet film and a discontinuous one. Therefore there is need to move toward decoupling solution rheology and final film formation.

One solution is to introduce carrier gas pulsing rather than a continuous jet like in traditional spray coating. The advantage of this is that rather than optimizing rheology and drying dynamics, pulsing can be used to deposit small liquid drops onto a surface and allowing them to completely dry before depositing another group of liquid drops. This prevents flooding of the surface with liquid and allows for less

rheological control, as the final film is built up little by little rather than all at once. This allows for a disconnection of solution rheology, negating the need for ink reformulation and rather optimization just requires tooling a mechanical system. A pictorial description can be seen in Figure 2-5
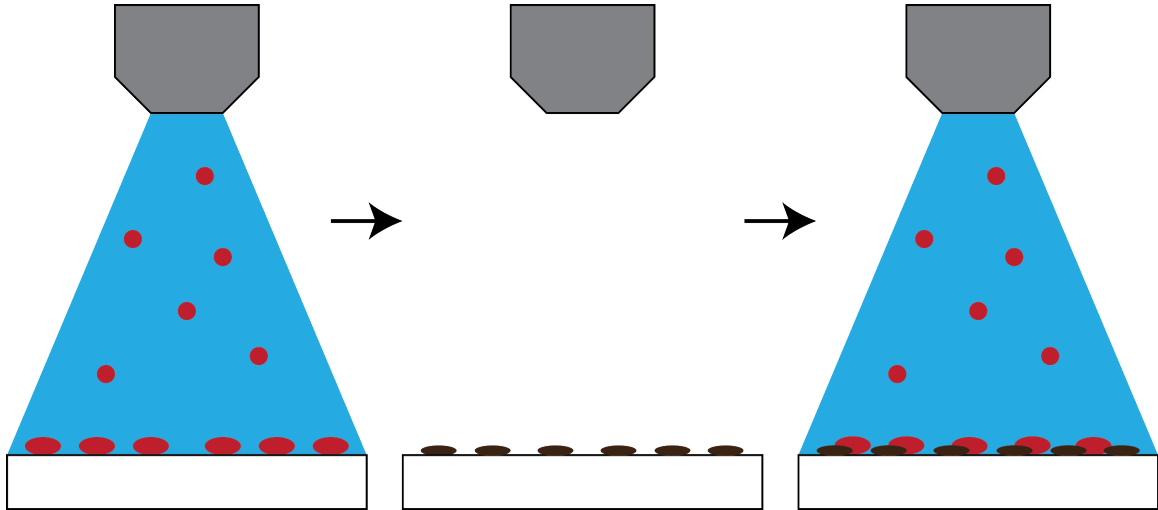
Figure 2-5: Representation of the pulsed spray coating method used in this work

For the nanowires solutions presented in this thesis, due to their high aspect length to diameter ratio (400:1), they also interact differently in each direction with the solution during dying. During full wet film drying, the wires tend to align to the drying direction and align in solution and aggregate. This creates a non-uniform film. Since the intent is to create a uniformly random nanowire film, this is considered a defect. With pulsed spraying, despite potential drying defects, the film fully dries between each pulse. With the introduction of new droplets, the wires are not dissolved readily. The result is that this creates a uniform film despite rheological limitations inherent in the wire ink dispersion. This difference can be seen in Figure 2-6 and Figure 2-7. This is shown further in Figure 2-8 where the left sample is pulse sprayed with a drying time of 10 seconds between each pulse and the right is a drying time of 0.5 seconds between each pulse. Each sample was sprayed with 30 pulses and rotated halfway though. The bed temperature was 100^oC and environmental conditions were 21^oC and 75% relative humidity. With the right sample, there are clearly large drying defects, where wires aggregated. The left sample is more uniform overall.

HV	mode	det	mag ⊞	WD	HFW	
5.00 kV	SE	ETD	350 x	4.3 mm	366 µm	100 µm
						Helios
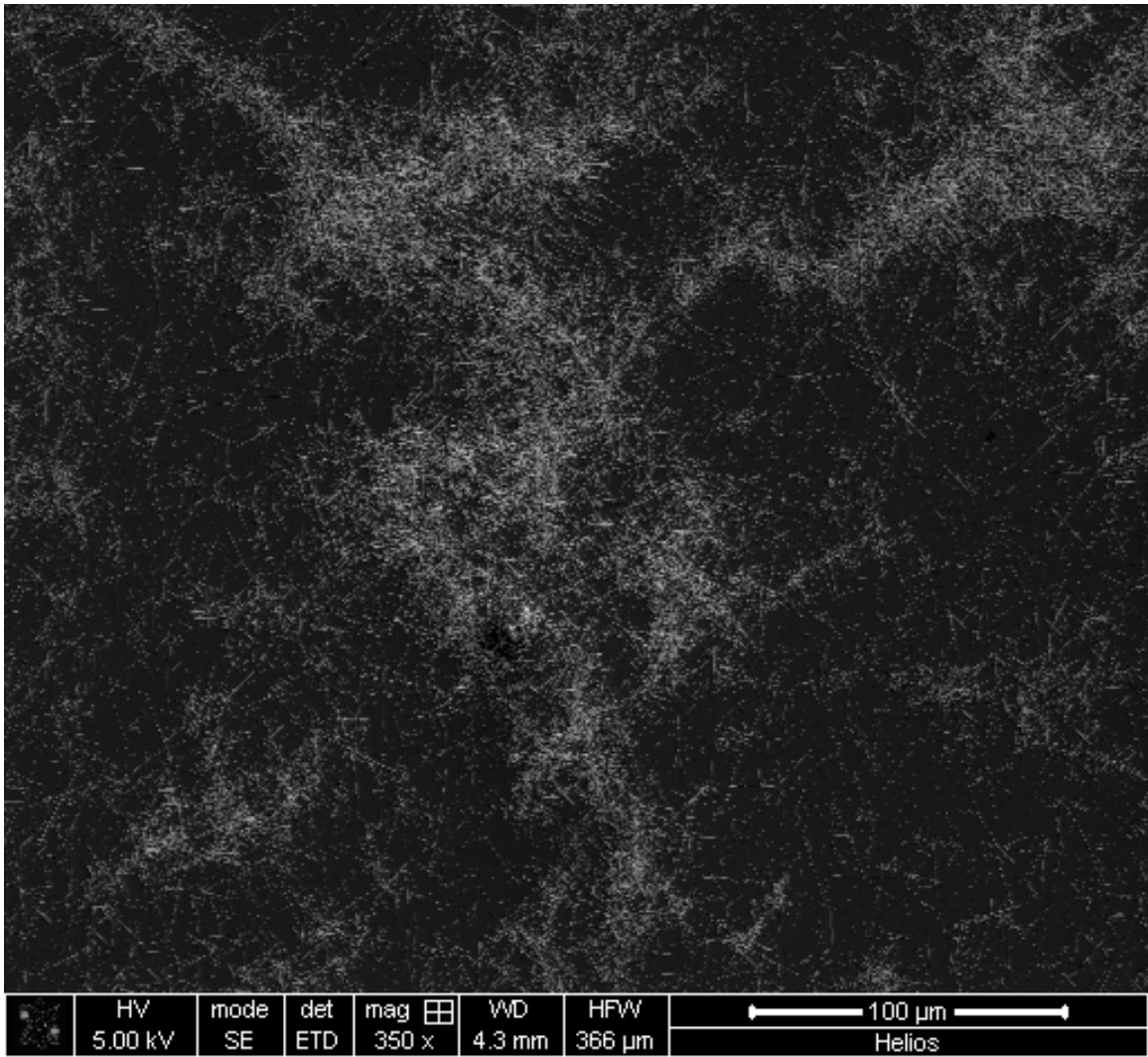
Figure 2-6: SEM image of nanowire film produced by continuous spray coating
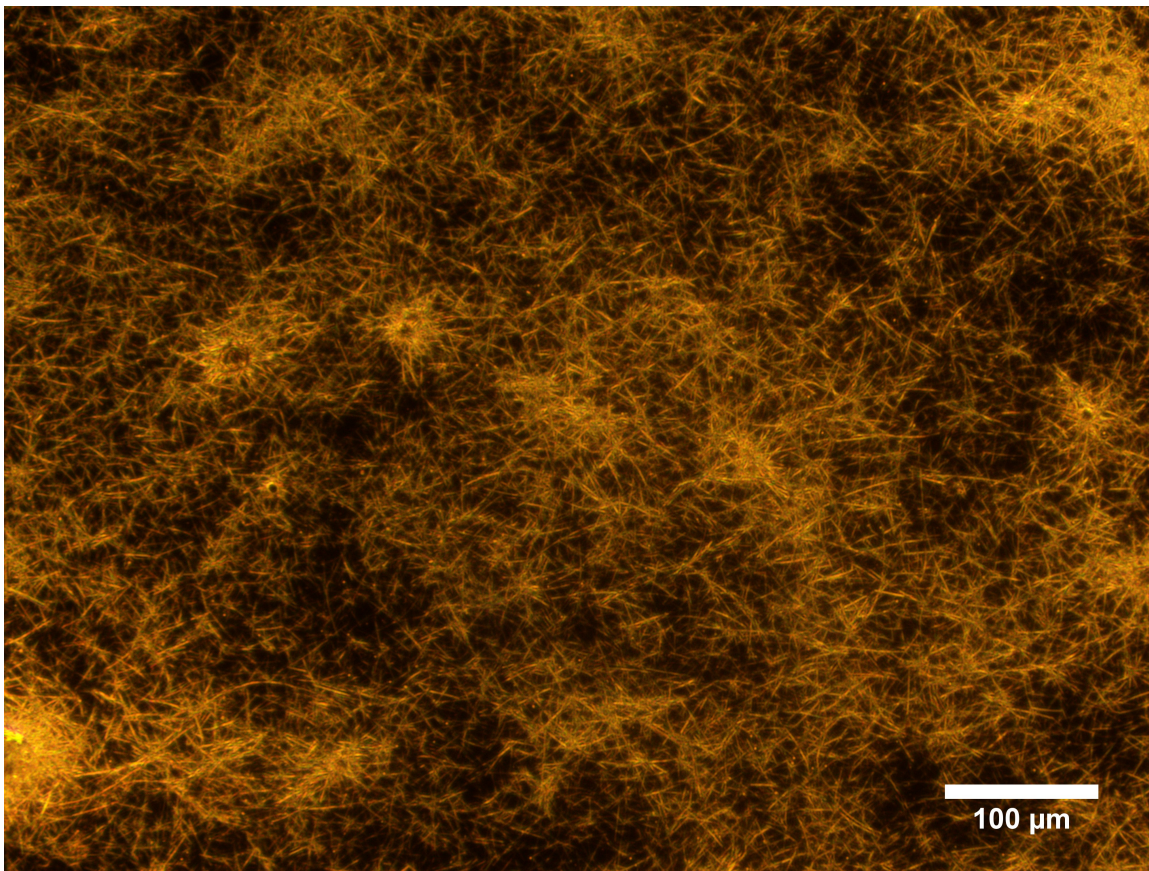
Figure 2-7: Dark Field optical image of nanowire film produced by pulsed spray coating

Figure 2-8: Visual uniformity of samples pulse sprayed at different times. Left: pulsed 30 times with 10s drying time. The solvent is fully removed between each pulse. Right: pulsed 30 times with 0.5s drying time. The solvent drops are therefore not dry before the next pulse.

2.3 Design and Usage of a Pulsed Spray Coating Tool

In order to decouple the drying dynamics with overall film quality for nanoparticle dispersion, a pulsed spray coater was designed and constructed. The overall design relies on simple materials and is made to be reproducible and low cost for developmental purposes.

2.3.1 Design Overview

To be as simple and reproducible as possible, the spray coater is kept as simple as possible and uses off-the-shelf components. The spray coater utilizes a simple single action airbrush for its main atomizing spray head. This allows for simplicity of replacement and cleaning while keeping atomization uniformity and quality relatively high. Since the system is fully stationary without any multi-axis control, the wet film uniformity and spray uniformity is assumed to be constant over the substrate so long as the spray cone is much larger than the substrate. In this case, the spray coater is designed to have a maximum substrate size of one inch, with a spray cone of 2 to 5 inches in diameter. The system has a heated bed in order to control drop drying characteristics and wet film drying. The system has minor isolation to prevent influence from external air currents (i.e. fume food) on the spray cone and to allow extraction of solvent vapors. Control is done through a microcontroller with a software frontend for machine programming, simple relays and pneumatic switches. The spray coater is designed to be compatible with five different spray heads at once and can therefore in theory spray coat 5 different materials in a single method. A pictorial description of the system can be seen in Figure 2-9

2.3.2 Mechanical System Design

The mechanical system can be broken down into two mains sections: the pneumatic section and the heating section. The pneumatic section comprises of the air control
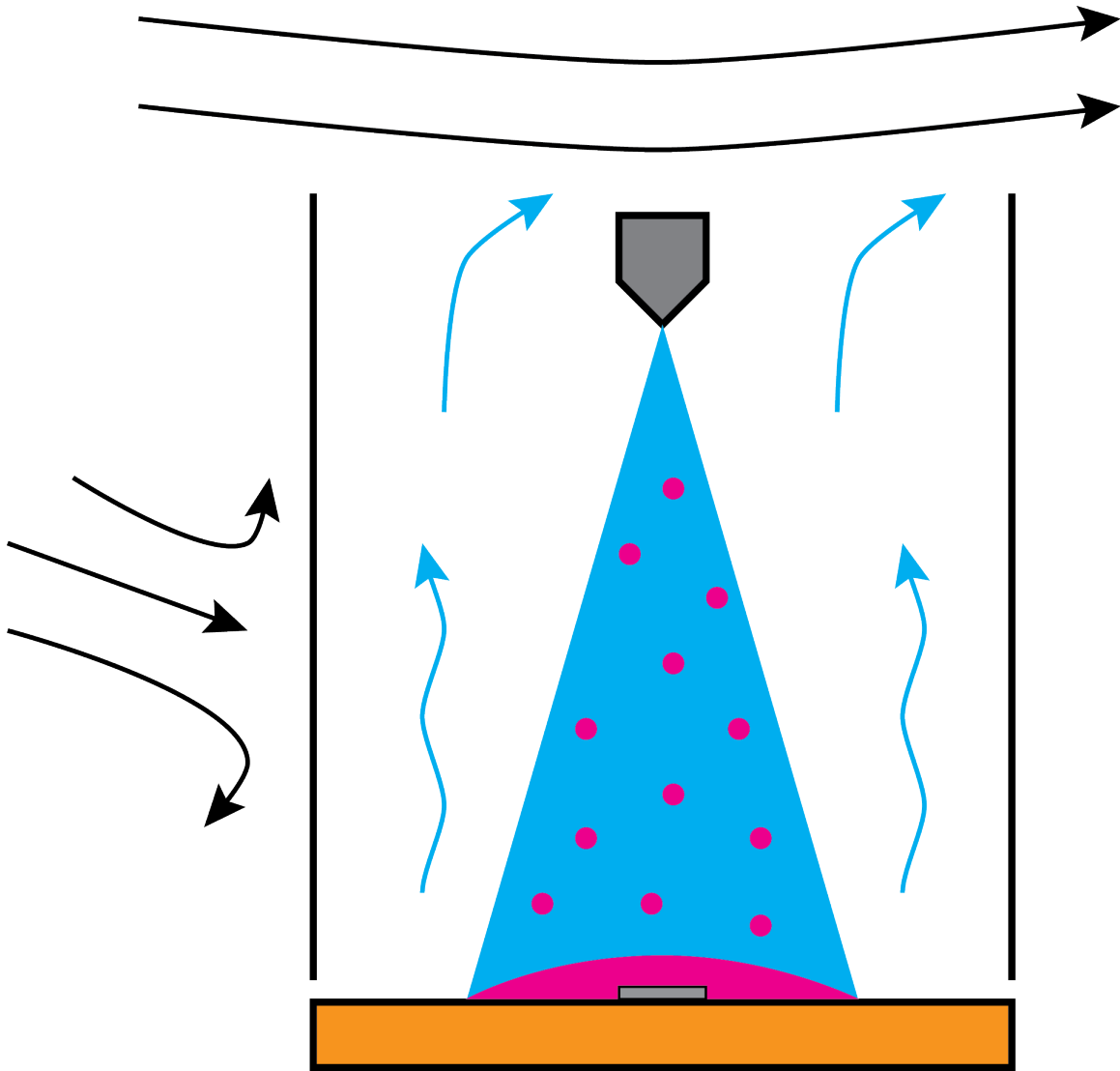
Figure 2-9: Pictoral description of the lab-built spray coater

systems and the atomizer and the heating section comprises of the substrate holder and temperature control.

The pneumatic section comprises of a Paasche Model H single action airbrush seen in Figure 2-10. It uses compressed air or nitrogen between 20 and 40 PSI which flows over a needle. The needle has a center pin, which can be adjusted in and out of the needle to adjust the size of needles orifice exposed to the gas flow. This in turn allows adjustment of the flow rate of the liquid ink in which you would like to spray. Since flow rate is coupled to droplet size and distribution in this configuration, lower flow equates to a finer mist and a faster flow rate equates to a slightly larger drop

size and larger size distribution. The needle can also be adjusted in and out of the air flow, thereby allowing control of how the air interacts with the tip of the needle and the fluid flow.

Figure 2-10: Paashe Model H used as the main atomizing head

The airbrush is made to be used by an artist by hand using a single action pneumatic plunger in a mostly horizontal position. For this application, the hand actuated plunger is bypassed with a custom 3D printed part and a screw, which allows the plunger to be constantly depressed. Control is then done by a 12V pneumatic solenoid to control airflow upstream. This has a drawback of not having a fast response time in terms of full pulse cutoff (about a tenth of a second delay for full cutoff in this design), but it is good enough for most applications. Better designs would move the valve upstream to achieve millisecond or even faster cutoff times. With the solenoid modification, the spray head can therefore be mounted vertically needing minimal mechanical attachments for stability. Since fluid feed in a horizontal position is done by the venturi effect *sucking* ink up from a container that is below the needle, this needed to be replicated the vertical positioning. Luckily the Paasche Model H uses a compression fitting to make a hermetic seal with the ink reservoir rather than a more custom fitting. The ink reservoir is remounted in a vertical position and an extension tube was made out of nylon tubing. Ink feeding is still done naturally by adjusting the pin and using the venturi effect. To account for pressure differences in height adjustment, the ink reservoir vial is held at constant height for every experiment.

To determine correct placement of the needle within the nozzle in order to least obstruct airflow while maintaining atomization, as well as determine proper geometry of the head in relation to the substrate, a CFD simulation was carried out in Solidworks 2016 Flow Simulation. For this a model geometry was made where the spray head was spraying into a square tube. The nozzle was pressurized at 35 PSI, and the feed line and the other end of the tube were kept at atmospheric pressure. Since Solidworks is incapable of doing two phase flow, and a two phase flow if this size would be unreasonable to simulate, the feed line did not contain any liquid but only air. Steady state results shown in Figure 2-11, 2-12 and 2-13 show that the airbrush requires a tilting of about 15 to 20 degrees for with constant needle position in order to have constant, strait flow down the tube. Flow perpendicular to the needle is unaffected since the airbrush is symmetric in that plane. Flow around the needle remains high, which is needed for proper shearing of the liquid for atomization. To account for differences in real life and the ability for adjustment the airbrush is mounted on a ball mount to allow for tilting and general spray cone adjustment. Dynamic results show that there is significant transient flow of for about 1 seconds before flow becomes uniform. In this time, a vortex travels down the length of the spray cone until steady state is achieved. Due to the needle this vortex is non uniform. Transient flow can be seen in Figures 2-14, 2-15 and 2-16.
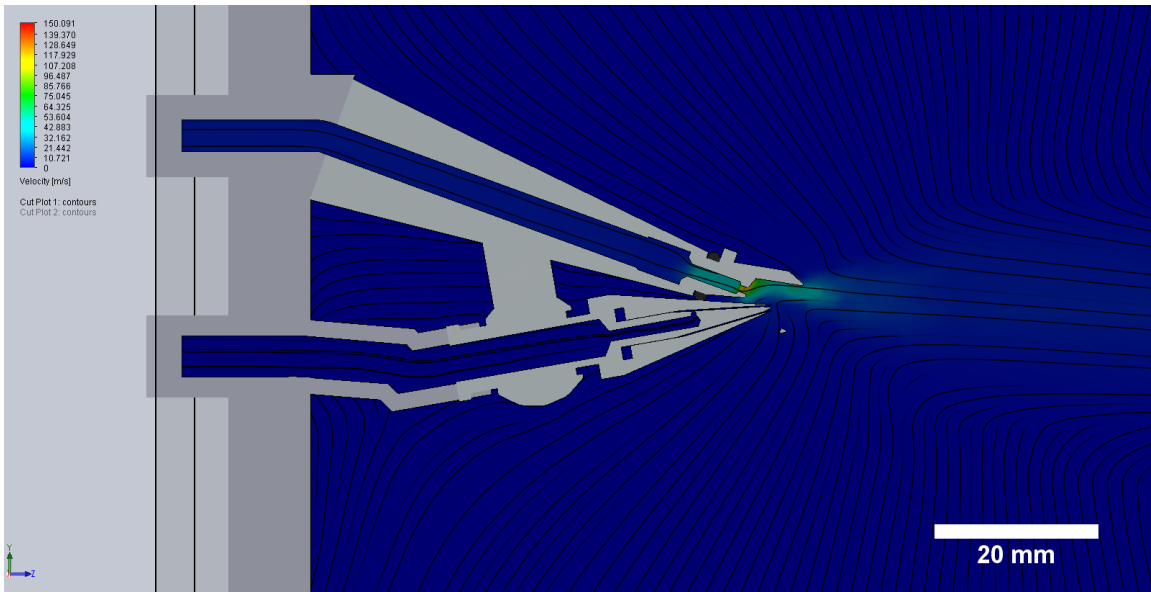
Figure 2-11: Flow dynamics within the Paasche Model H nozzle and needle
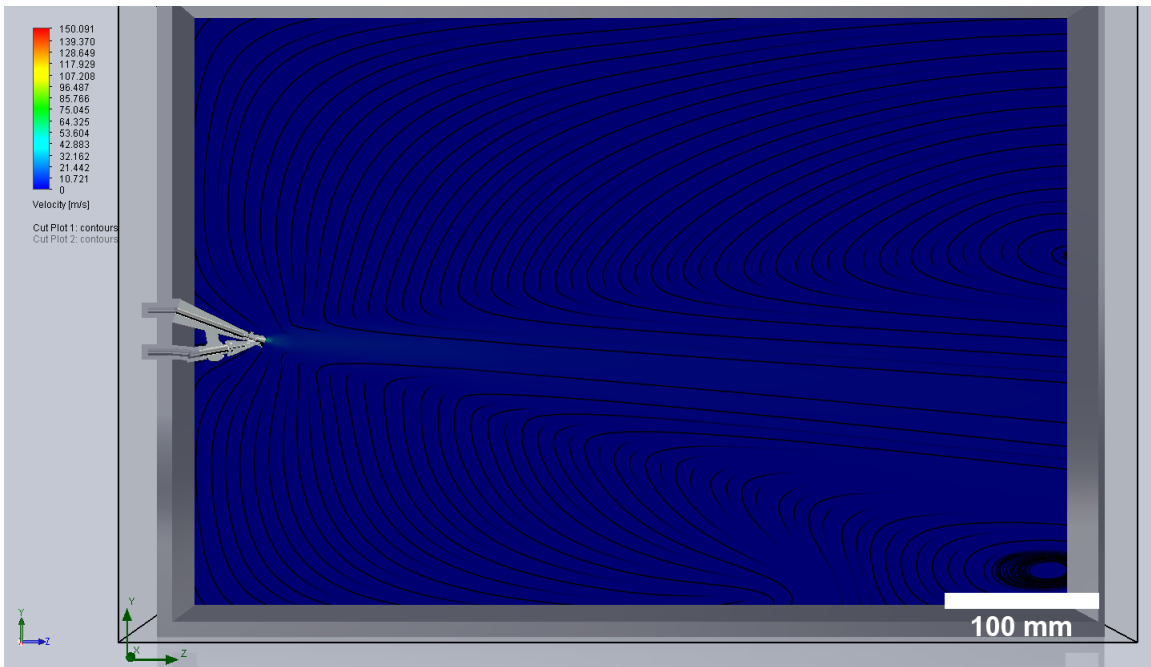
Figure 2-12: Flow dynamics of the Paasche Model H in steady state in the needle/nozzle plane
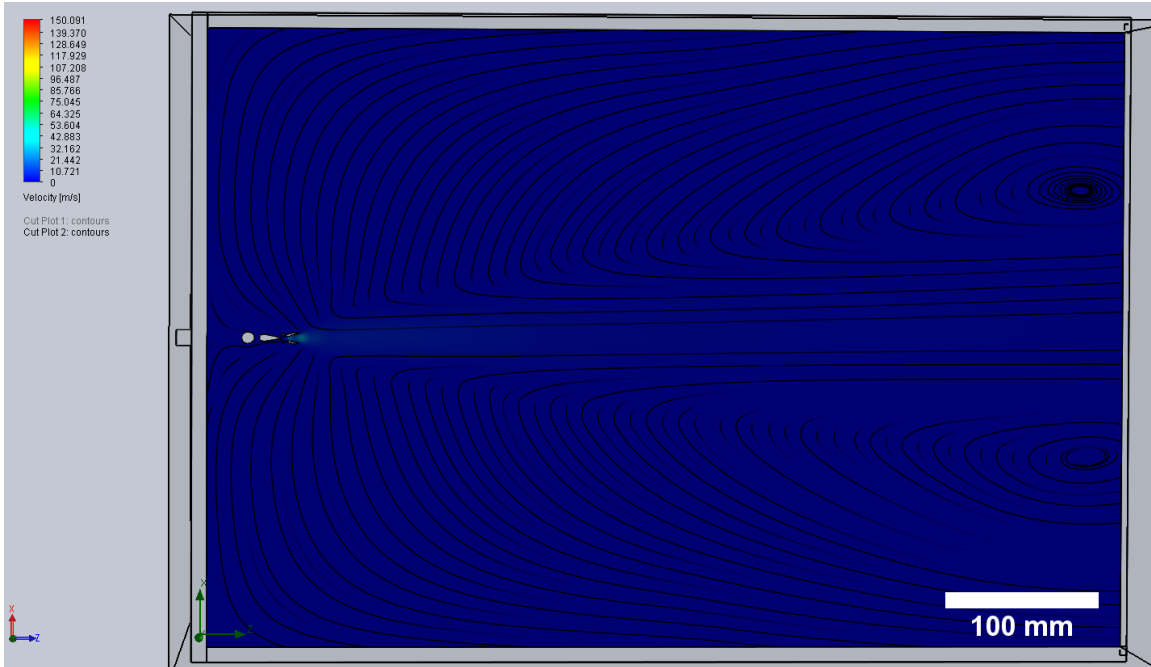
Figure 2-13: Flow dynamics of the Paasche Model H in steady state perpendicular to the needle/nozzle plane
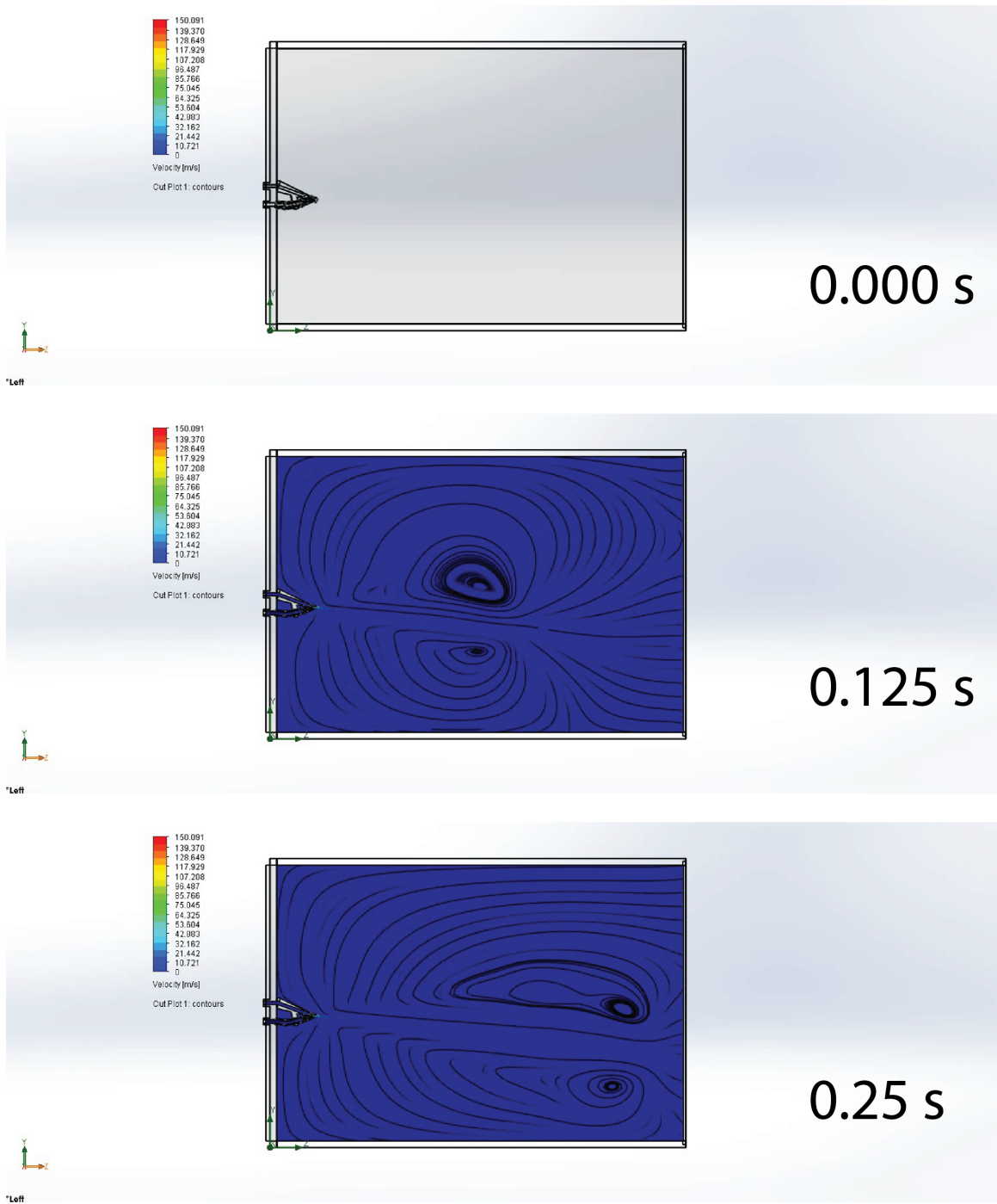
Figure 2-14: Transient flow 0.000s to 0.250s
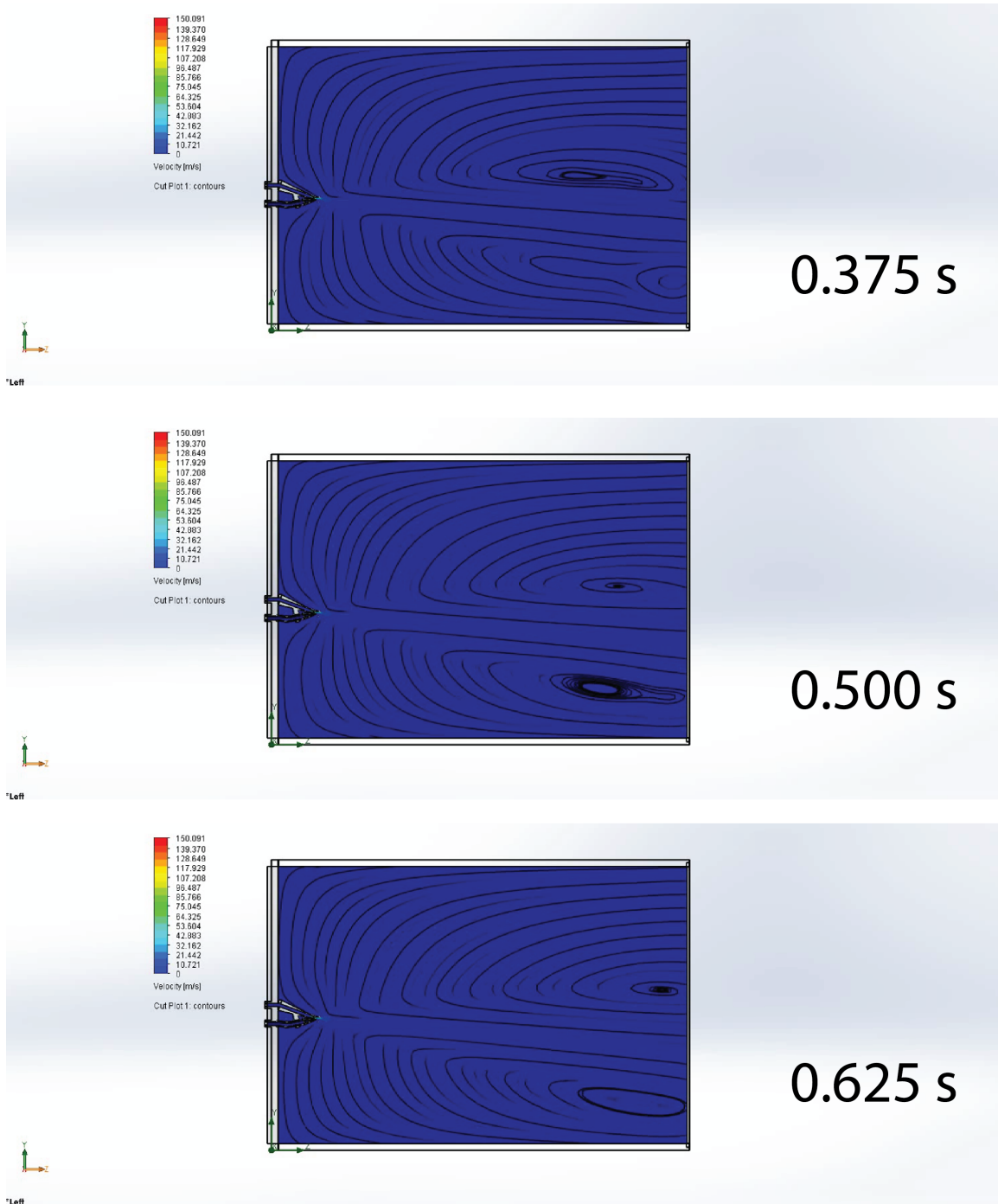
Figure 2-15: Transient flow 0.375s to 0.625s

0.750 s

0.875 s
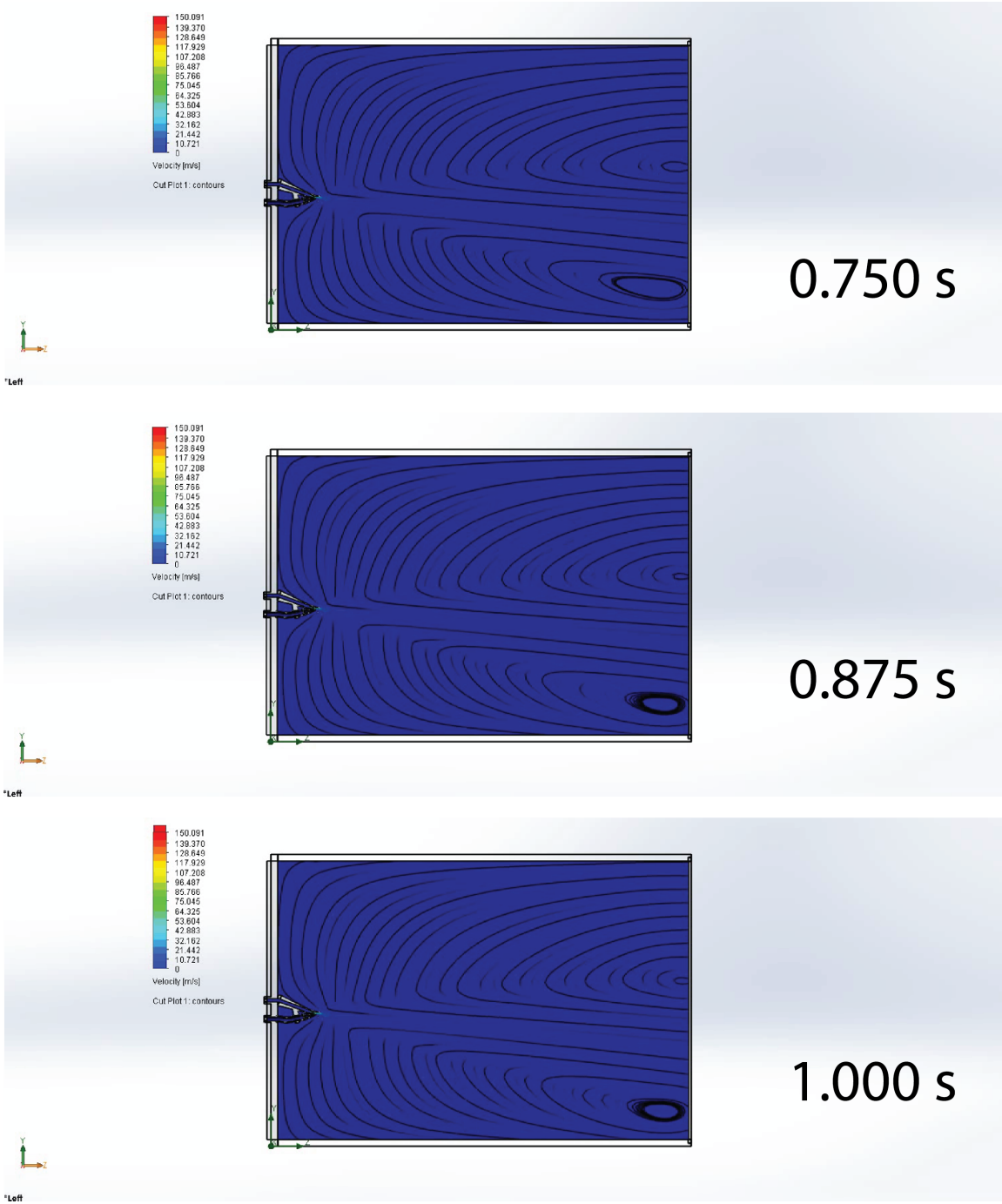
1.000 s

Figure 2-16: Transient flow 0.750 to 1.000s

The heating section consists of a custom built heated plate. The plate consists of a 120V silicone-heating mat glued to a 1/4 inch aluminum plate to act as a thermal bath. The aluminum plate is covered with a Teflon sheet, glued with RTV silicone adhesive. This allows for easy cleaning after spray coater use and to hide a thermocouple that runs to the center of the hotplate. Since sample location is important, but sample size may change, the heating plate is designed to have a 0.1 inch removable aluminum sample holder plate, which can be exchanged to allow for different sample holder sizes while maintaining spray cone alignment. The sample holder plate sits in a cutout in the Teflon sheet, and therefore can be aligned on the plate if removed. The sample holder is covered in a Teflon sheet for easy cleaning except the sample holder. The sample holder is nothing more than cutouts in the Teflon to allow samples to sit on the aluminum sample holder plate. In practice, this feature of having a removable sample plate is never used since spray cone alignment is difficult. Instead, since 1/2 inch samples and 1 inch samples are the most common used sizes, the sample holder plate is designed for holding four 1/2 inch samples and a separate external adapter allows to the use of a single 1 inch sample. For all normal uses, the sample holder plate is therefore permanent. The heating plate sits on four screws that allows pitch and yaw adjustment in relation to the spray head. A model of the heating plate can be seen in Figure 2-17.

The final mechanical construction is done out of aluminum extrusion. Simple air flow encasement is done with two steel sheets bent in a hexagonal shape. One sheet acts as the main encasement and the other acts as a door. All fittings are 3D printed in either PLA, ABS, or PETG. Final renderings of the design can be seen in Figure 2-18 and completed construction photos can be seen in Figures 2-19, 2-20, 2-21, 2-22 and 2-23.
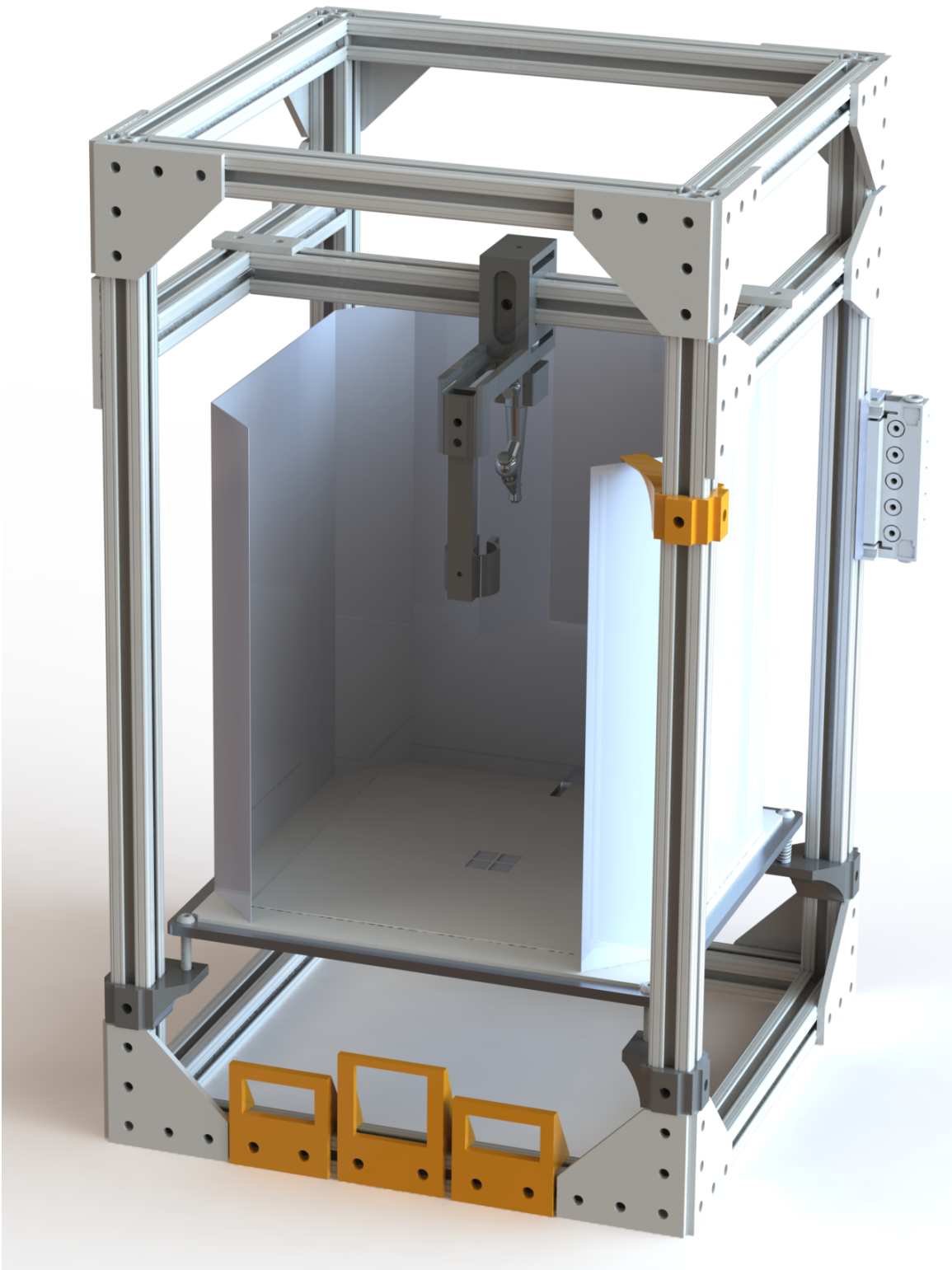
Figure 2-18: Rendering of the lab-built pulsed spray coater
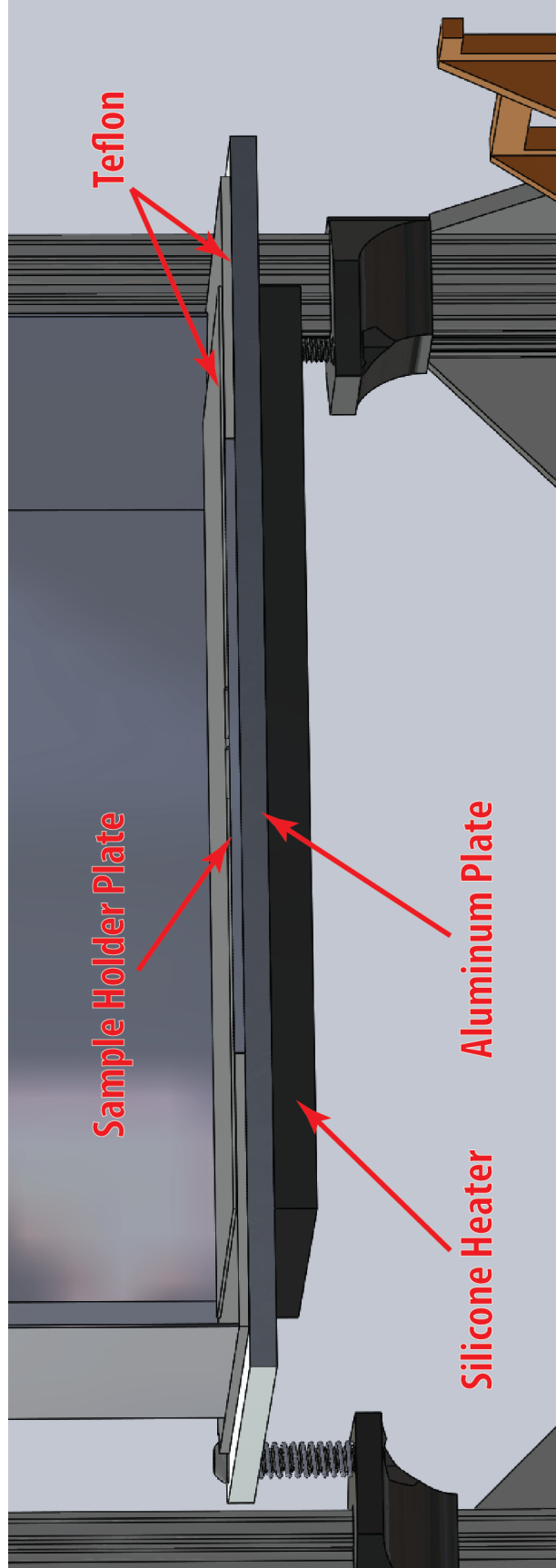
Figure 2-17: CAD of the heating plate
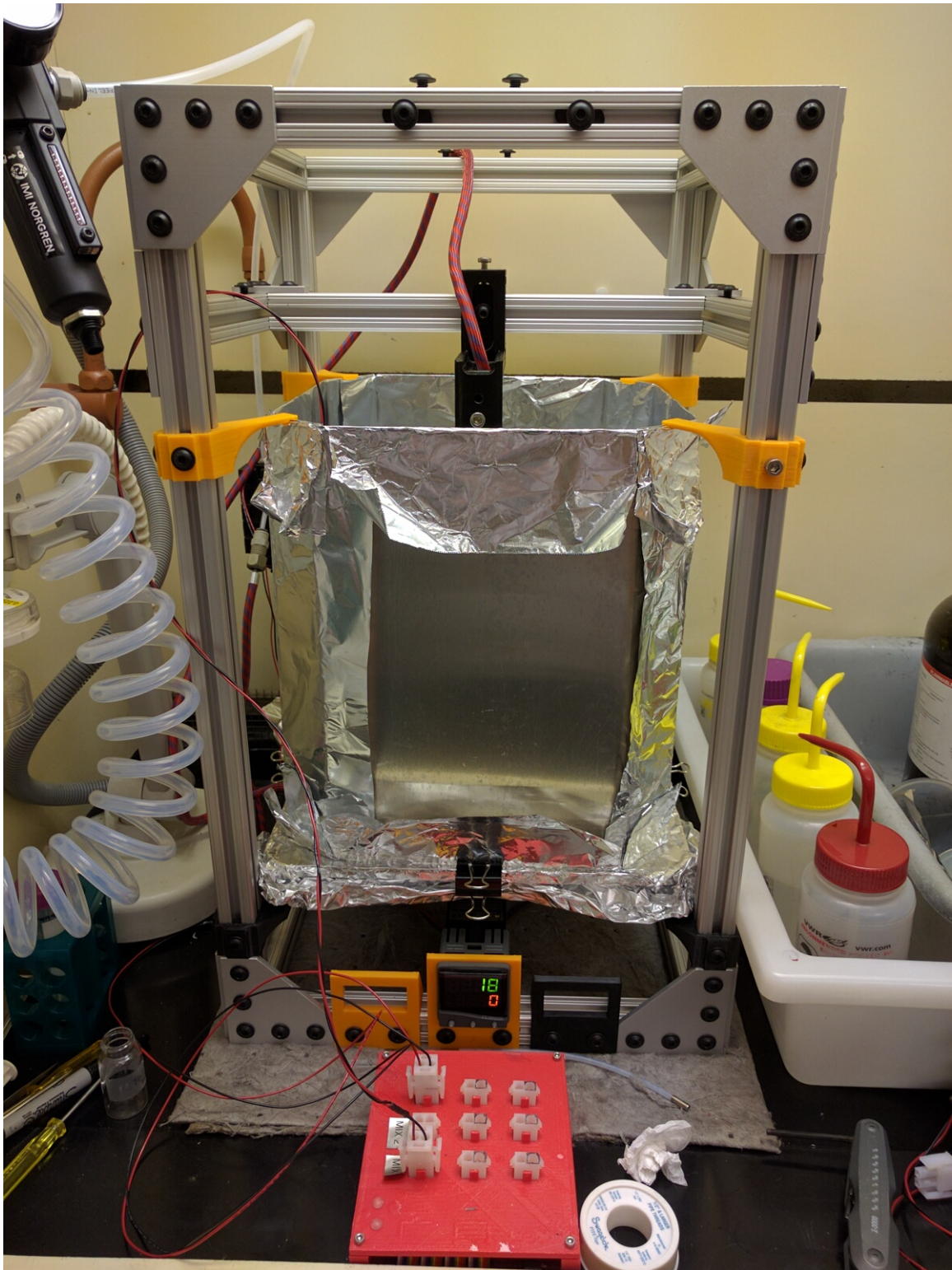
Figure 2-19: Lab-built pulsed spray coater - front
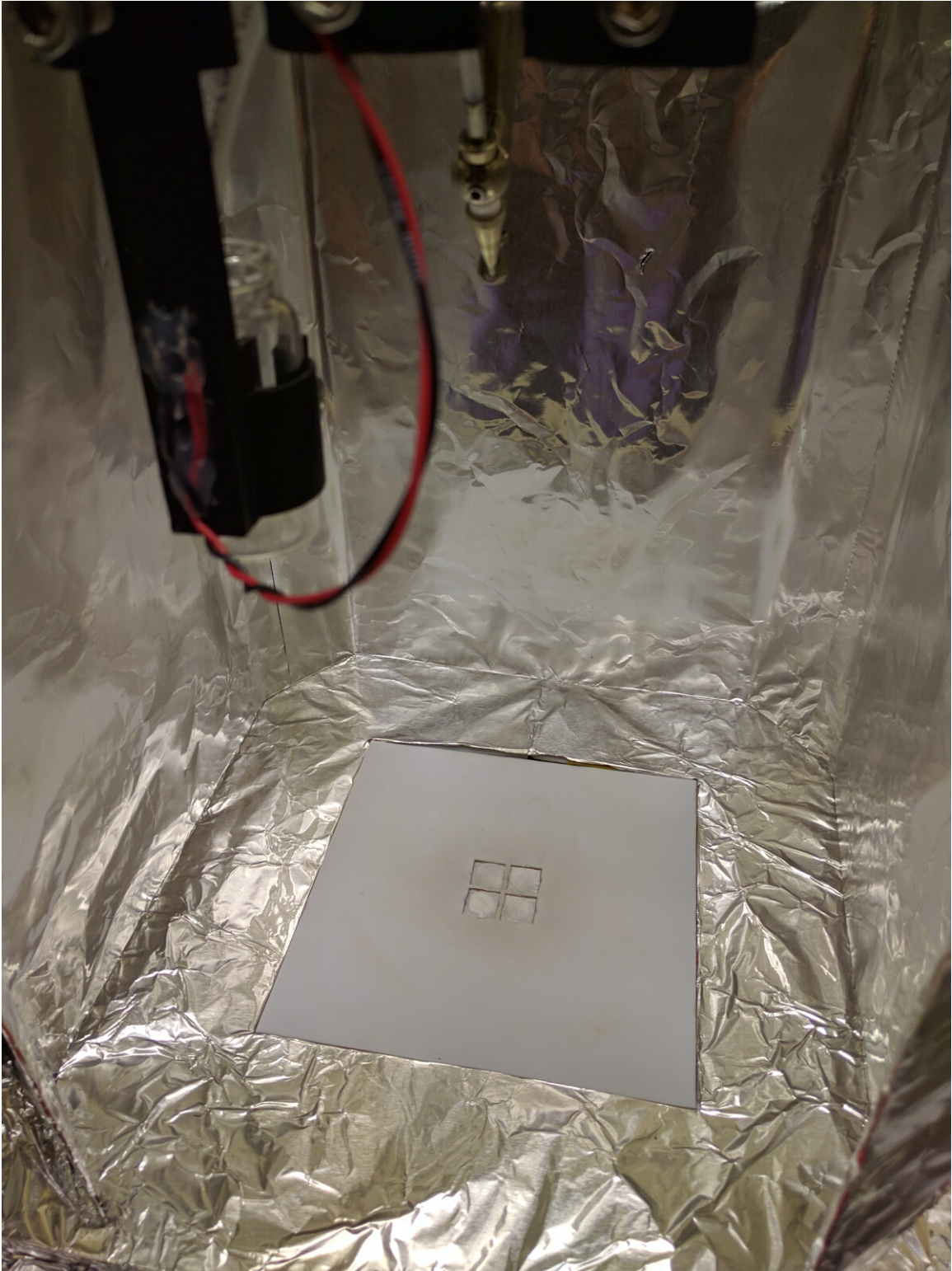
Figure 2-20: Lab-built pulsed spray coater - sample holder and heated bed
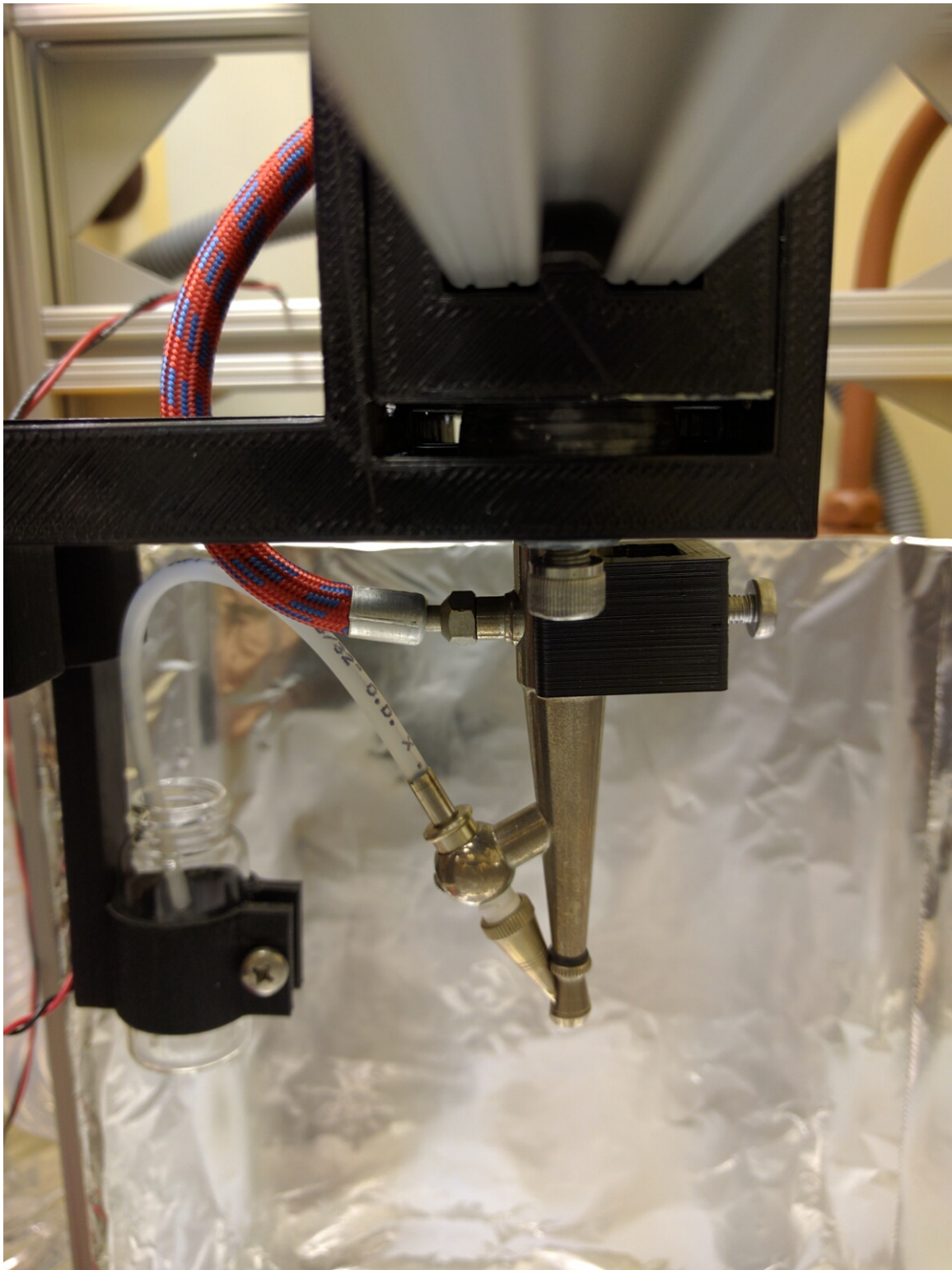
Figure 2-21: Lab-built pulsed spray coater - ink reservoir and spray head

Figure 2-22: Lab-built pulsed spray coater - pneumatic control
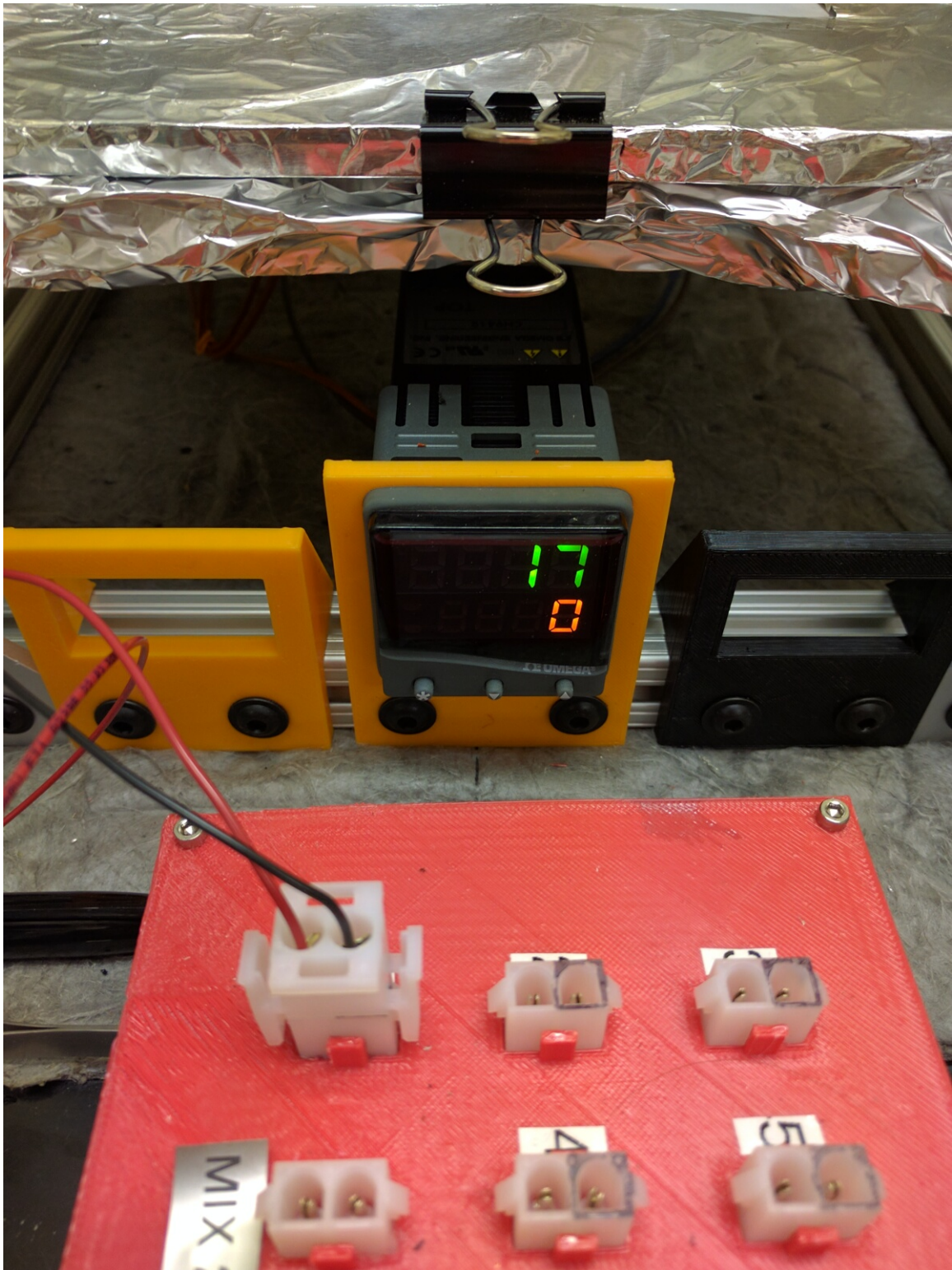
Figure 2-23: Lab-built pulsed spray coater - PID heating control and relay board
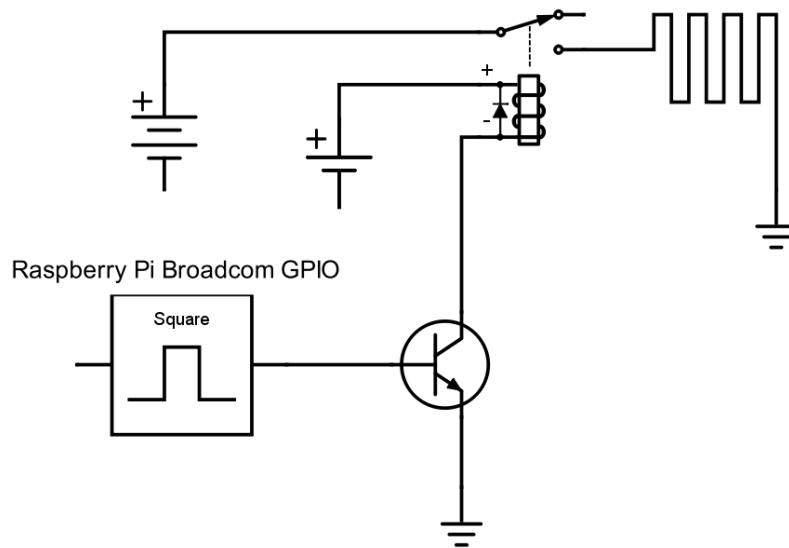
Figure 2-24: Diagram for the custom built relay system to control air supply

2.3.3 Control System Design

Similarly to the mechanical design, the control system can be split into the pneumatic control section and the heating control section. Pneumatic control is done with a binary on/off Bimba Isonic 12V 3-way compressed air control valve (McMaster part 62095K11) which is mounted to a DIN rail style connector. Control of the solenoid valve is done through a simple relay triggered by a Raspberry Pi. A PNP transistor acts as a logic level shifter to shift the 3.3V of the Raspberry Pi GPIO to 5V required to trigger the relay. The 5V is supplied by a 5V power supply but accessible through the Raspberry Pi on one of its pinouts. A 12V external power source is used to actuate the pneumatic solenoid and is isolated from the Raspberry Pi. The custom relay board includes seven 12V relays which allows control of up to seven solenoids or other 12V components. The board also includes two 5V sources, which simply do not include the relay, to control two 5V components. A circuit diagram can be seen in Figure 2-24 and a photo of the board can be seen in Figure 2-25.

A graphical user interface python program was created to allow the creation of manufacturing recipes using a pseudo machine code. A pictorial description of the algorithm can be seen in Figure 2-26, a description of the code can be seen in Equation
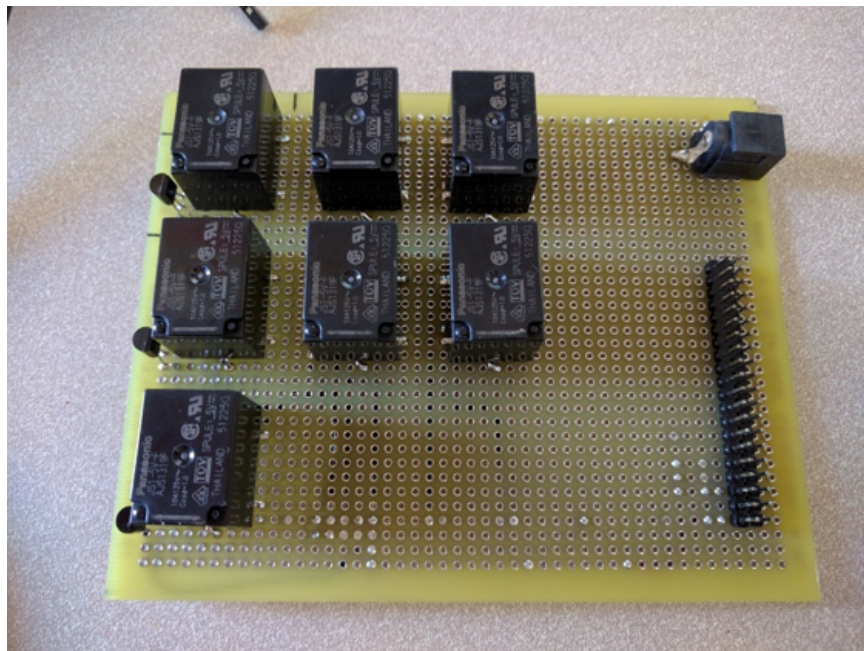
Figure 2-25: Photo of the 7 relay systems on the custom relay circuit board

2.1 and the graphical user interface used to program the coater can be seen in Figure 2-27. Red in Equation 2.1 indicates a numerical variable, black denotes the variable delimiter. The python code used to create the program can be seen in Appendix A. Additional features that were added to the GUI include a system purge, which can be used for priming and cleaning of the nozzle, and a mixing feature, which turns on one or both of the 5V sources designed to be used with a vibration or small stirring motor.

$$HeadNumber; StartDelay(s); Cycles; TimeOn(s); TimeOff(s); \qquad (2.1)$$

The control system for the heated bed is comparatively simple. It utilizes an Omega CN9600 PID controller to control a 12 inch silicone heating pad through a solid state 30A relay (see Figure 2-32. A K-Type thermocouple then probes the center of the bed next to the sample holder to provide the proper feedback loop. The bed is then autotuned to 100C to determine the correct Kp, Ki, and Kd settings. The max temperature possible for the bed is 200C due to limitations with the silicone heater.
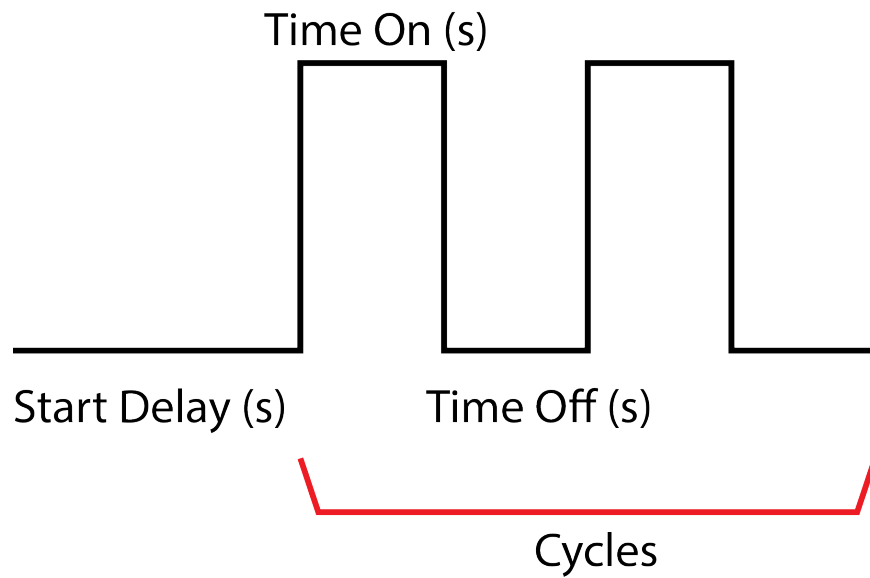
Figure 2-26: Control algorithm used by the python code to control the spray coater

Figure 2-27: GUI for the spray coater. Left panel (white) is pseudo-machine code programming and left (grey) is a log output

2.3.4 Alignment and Tooling of the Spray Coater

In order to use the spray coater, one must learn how to align the tool as well as tool the coater to make uniform layers across the sample holder. For basic operation, these two tasks are relatively decoupled, but can still be challenging depending on the level of uniformity required. A procedure for aligning the tool is as follows:

Setup the spray head

1. Adjust the spray head manually until it gives a consistent spray cone and drop formation, or adjust based on CFD calculations.

2. Mark measurements and positioning of the needle down for future use.

3. Any adjustments of the needle will result in the need for realignment.

Rough align the spray cone

1. Release the ball mount tensioning screw until the spray head moves freely but stays in position when not being actively held.

2. Position the spray nozzle so that it points in the direction of the sample holder.

3. Tighten the locking screw so that the spray nozzle is held in place.

4. Place a piece of aluminum foil over the sample holder to keep it clean and emboss the sample holder pattern by taking a wipe and smoothing out the foil on the sample holder. If necessary, hold down the aluminum foil in the corners so that it does not move during alignment.

5. Fill the ink reservoir with the main solvent of the ink that is expected to be sprayed.

6. Purge the head, filling the transfer tube and spray needle.

7. Wipe the aluminum foil dry with a lint free cloth.

8. Close the front door of the spray coater.

9. Using the purge setting, spray the head for between 1 and 5 seconds.

10. Remove the front door, and look to see if the spray pattern is centered on the samples.

11. Adjust the spray nozzle direction as necessary

12. Repeat this process until centered

Rough tool the spray parameters for alignment

1. Load a desired ink formulation into the ink reservoir or a solvent and a dye. Purge the head. Protect the sample holder with aluminum foil in order to prevent dirtying.

2. Heat the bed, 85-100$^o C$ is a good start for using alcohols. If heating is undesirable, leave the bed at room temperature.

3. Load half inch glass samples into the sample holder and allow them to heat.

4. Create pseudo code to pulse in order to pulse-spray the head. Ten cycles with half-second on, and five to ten seconds off is a good start. This allows minimal material to be deposited and long times for drop drying.

5. Check visually that the film is roughly uniform. High uniformity, or uniformity between samples is not needed at this stage.

6. The concentration of the ink/ or dye solution may need to be adjusted to get desirable results.

Fine align the spray cone

1. Fill the ink reservoir with the ink expected to be used, or with the solvent and a dye.

2. Pulse spray half of the ink onto glass samples until the samples have built up a noticeable film.

3. Rotate the samples 180 degrees and spray the rest of the ink onto the glass samples.

4. Measure the optical transparency with a spectrometer. Sample location and transparency will indicate the positioning of the cone relative to the samples.

5. Move the spray head accordingly.

6. Repeat this process as many times as needed until desired uniformity between samples is acquired. It is recommended the spray heads position be glued to prevent unwanted movement after positioning is finalized.

A visual description of the alignment process can be seen in Figures 2-28and 2-29.

2.3.5   Possible Improvements

While using this coater for the deposition of nanowires for use in the remainder of this thesis, there are a few improvements that may make using and operating the spray coater easier. First, the nozzle head needed to be modified and enlarged in order to prevent the nanowires from jamming in the head. It seems that at environmental conditions and with IPA as a solvent, the smallest orifice length to nanowire size of about four or five is needed to keep the wires from piling up in the spray head. This requires opening the needle orifice all the way and therefore shrinking the spray cone. Although uniformity is still possible, it is difficult. Therefore integrating spray heads that have a larger spray orifice is ideal for spraying large nanoparticles or microparticles. Secondly, although controlling ink-drying dynamics is possible, it does change seasonally with changes in environmental humidity. Therefore, having the entire coater in an environmentally controlled chamber is ideal.

Figure 2-28: Photo of the rough alignment process. The spray cone limits can be seen visually through the drops on the foil. Embossing the foil helps with rough positioning.
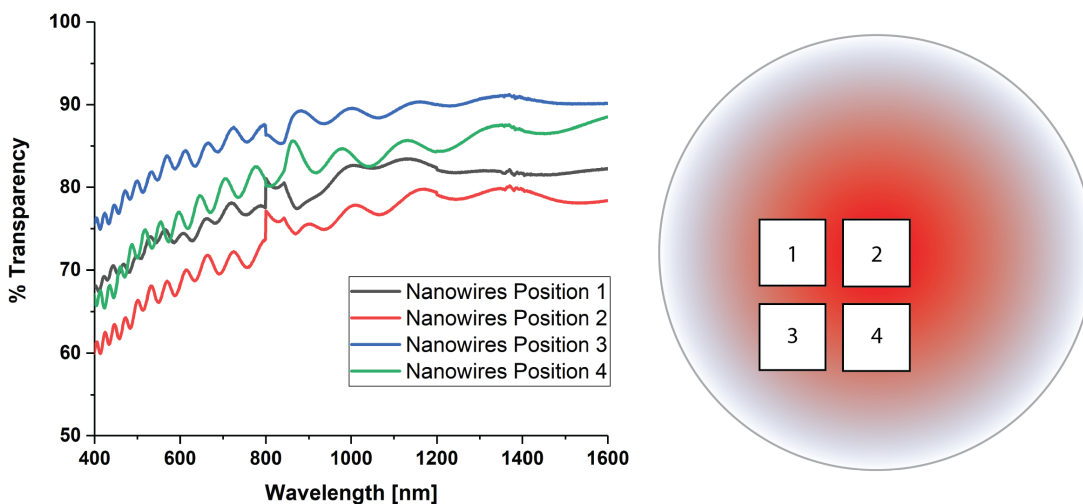
Figure 2-29: Representative transparency data in relation to the spray cone and wet film generation. As shown, Position 2 has the highest absorption. Samples 1 and 4 have similar transparency, and sample 3 is the least transparent. This is represented on the right with the red circle representing the spray cone. Since the amount of liquid particles diminishes away from center, this means the spray cone is more centered on sample 2

2.4   Parylene Deposition Theory and Practice

Parylene is a CV deposited single chain thermoplastic. It is a trade name for a variety poly-xylene polymers. In general, parylenes are a xylene base monomer with halogen or other modifications. The two most common variants of parylene are Parylene-N, a poly-xylene chain with no functional side group and Parylene-C, which is function-alized with chlorine. Parylene-C is more hydrophobic than Parylene-N allowing it to have better moisture barrier properties, making it a useful barrier for PCB en-capsulation and medical device encapsulation. Parylenes are vapor deposited by the Gorham CVD process, a pyrolysis CVD process, and are generally solvent insoluble and UV instable except for AF-4 (fluorine functionalized). For this work, we will only be using Parylene-C.

2.4.1 Theory of Deposition

Parylene is a vacuum deposited polymer and was first discovered and studied by William Gorham in 1966 [18]. Gorham discovered that a group of polymers could be formed on a surface through a sublimation and pyrolysis method under vacuum of a xylene dimer. In his original paper, he studied temperature ranges of the substrate, polymer conversion and mechanical, dielectric, and barrier properties on a variety of parylene polymers. Subsequent studies showed that parylenes can only be formed in certain vacuum pressure ranges [14]. In general the process is as follows: a xylene dimer is sublimated under vacuum. It passes through a high temperature pyrolysis tube. The high temperature furnace *cracks* the $CH_2 - CH_2$ bond keeping the xylene dimer together and forms a xylene free radical. This free radical then flows to the deposition surface where it is undergoes physical adsorption, a process that can be described by inverse Arrhenius kinetics. During adsorption, the radicalized monomer then undergoes polymeric growth as more radicalized monomers are adsorbed on the surface. Initiation is said to be stable and begin when three monomers meet at the surface [14]. Every parylene type has a condensation temperature, above which no polymerization will occur. Therefore, temperature and pressure control is important deposition. Pictorial description of the process can be seen in Figure 2-30 and relevant figures reproduced from Gorham's original paper can be seen in Figure 2-31 and 2-32.

Another important concept for parylene deposition is the mean free path distance before scattering. This can be calculated using Equation 2.2 where k is the boltzman constant, T is the temperature of the gas, d_m is the diameter of the gas molecule and P is the pressure.

$$l = \frac{k * T}{\sqrt{2} * \pi * d_m^2 * P} \tag{2.2}$$

For a medium vacuum (1-100 mTorr), which parylene deposits in, the mean free path is about 1 cm for a mostly nitrogen atmosphere. This, combined with the fact that parylene is a surface initiated polymer means that parylene growth is a highly conformal, and can even undercut shadow masks and mold to nanometer features.

$$T < T_c$$
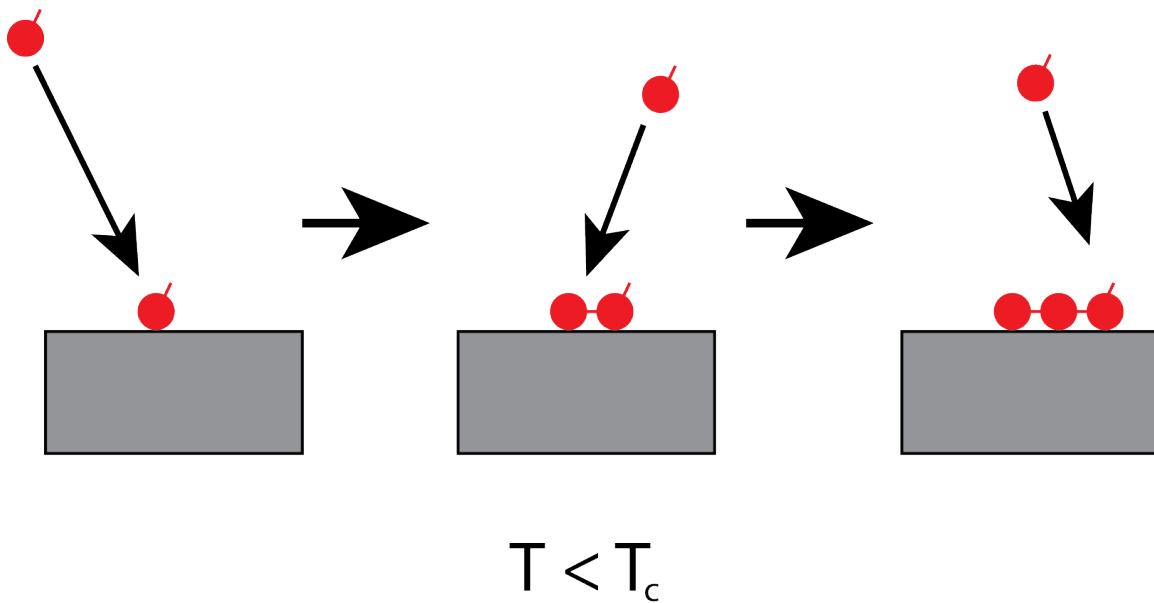
Figure 2-30: Pictorial description of the parylene deposition process
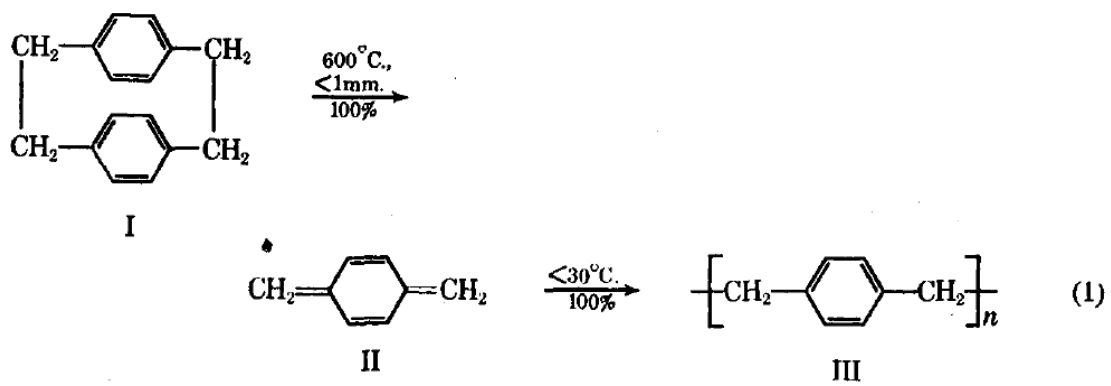
Figure 2-31: The Gorham process for Parylene-N as described by Gorham [18]

TABLE I

Monomer	Condensation temperature, °C.
p-Xylylene	30
2-Methyl-*p*-xylylene	60
2-Ethyl-*p*-xylylene	90
2-Chloro-*p*-xylylene	90
2-Cyano-*p*-xylylene	130
2-Bromo-*p*-xylylene	130
Dichloro-*p*-xylylene	130

Figure 2-32: A list of condensation temperatures measured by Gorham for different parylene derivatives [18]

2.4.2 Deposition Chamber

The deposition vacuum chamber to deposit Parylene-C in this thesis was custom built and designed to have feedback control using a quartz crystal monitor. This is unlike other parylene deposition systems where parylene thickness is controlled by loading more or less dimer into the system. The benefit of this is that thickness control is monitored during deposition, which is useful when depositing very thin films. An outline of the various components of the system can be seen in Figure 2-33. Components are labeled below:

1. **Z-axis adjustment and rotation stage:** powered by a MDC 665505-01 compact single axis stage and a MDC 670002-01 rotary motion actuator.

2. **Custom sample stage:** 4 inch square and coupled to MDC 670002-01

3. **Pyrolysis furnace:** powered by a Watlow 550W 120V band heater and insulation, controlled by a Watlow CLS204 controller on Channel 1.

4. **Evaporation furnace:** powered by standard cloth heat tape and controlled by a Watlow CLS204 controller on Channel 2.

5. **Genesis right angle poppet valve:** purchased from Nor-Cal Vacuum, used to control dimer evaporation into the pyrolysis heater. Heated to 120ÂřC during deposition.
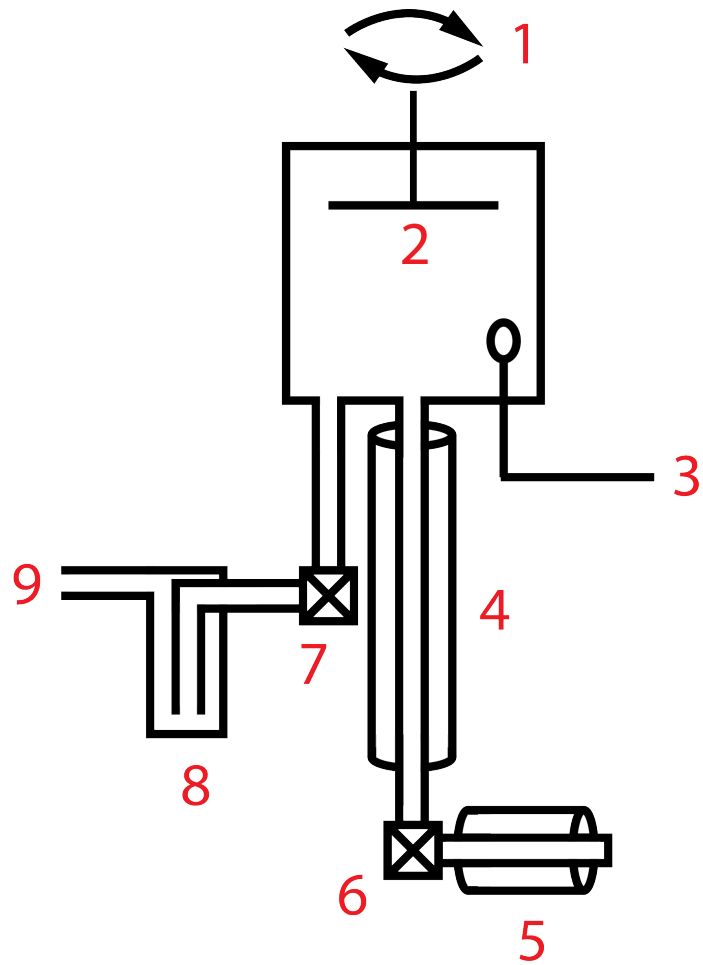
Figure 2-33: A description of the parylene system used in this thesis

6. **Genesis right angle poppet valve:** purchased from Nor-Cal Vacuum, used to control dimer evaporation into the pyrolysis heater. Heated to 120ÅřC during deposition.

7. **Cold Trap:** cooled by a Thermo Scientific NESLAB recirculating chiller

8. **Roughing Vacuum:** Edwards RV5 rotary vane oil vacuum pump.

Chapter 3

Surface Functionalization and Nanowire Growth

Surface chemistry is an important part of engineering, thin film development and the core of the novelty of this thesis. Controlling surfaces allows us to modify of interface interactions as well as modify growth kinetics for nanoparticles. Through careful engineering we can make two materials stick to each other that normally would not, we can make two materials repel each other that normally would not, we can make mono-disperse nanoparticles particles and high aspect ratio nanowires.

3.1 Silane Chemistry and Surface Treatment

One of the most important ways of surface treatment is by silane chemical treatment. The silane covalent bond is strong and therefore the coatings can be quite durable, and silane chemistry allows a wide range of chemical surface functional groups. Surface functionalization can range from making a surface act like a fluorinated polymer, thereby decreasing surface energy, or by treating with reactive and polar groups to increase adhesion and surface energy. In addition, since silane treatment takes advantage of oxygen bonds a wide variety of materials are possible to be surface treated with this method [3] [23] [32].

In theory, silane chemistry is fairly simple and entirely revolves around the idea
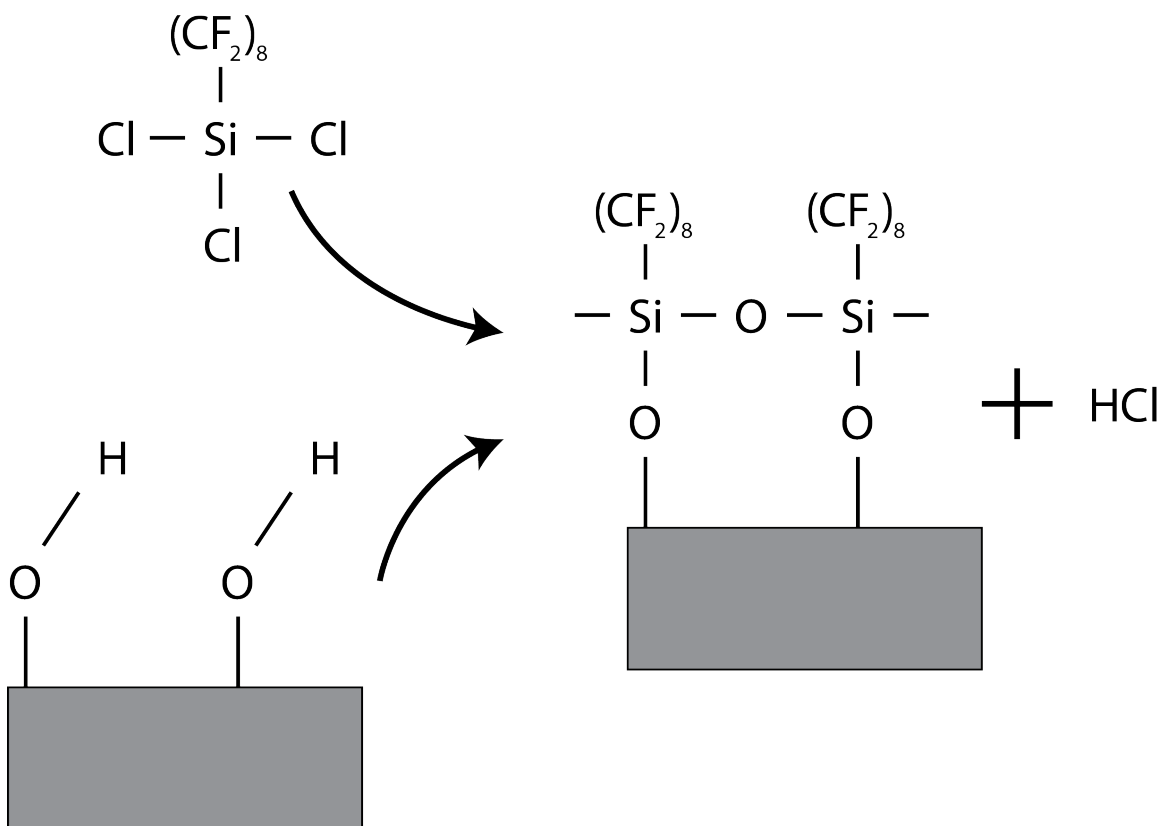
Figure 3-1: A description of the silane treatment process using a chlorosilane as an example

of surface oxidation and the oxygen bond. Most surface functioning silanes are based on a single silicon atom, usually with one sp orbital bonded to a carbon or functional group, and three sp bonded to a halogen like chlorine, or another leaving group. The carbon based functional group represents what surface properties you would like to obtain on the base substrate material. The leaving groups are to ensure that there is a strong silicon bond with the surface. Usually, the silane leaving groups interact with a hydrated surface, thereby creating a Si-O- bond to the surface [3]. For chlorosilane based surface treatments, a side product is hydrogen chloride. For oxysilane based surface treatments, the side product is water. All surface functionalizing silanes are considered self-assembling monolayers, however side reactions and van der waals forces can cause multilayer growth as well. A description of the surface functionalization process can be seen in Figure 3-1.

For the purposes of this work, we will mostly focus on fluorosilane treatments,

which include a single chain fluorinated carbon backbone and either chlorine or hydroxyl leaving groups. As a demonstration, Figure 3-1 includes the reaction for chlorine leaving groups.

3.1.1 Methods and Results

Although silane treatment of any surface oxidizing and surface hydrating substrate is possible, we will only focus on silicon/ silicon dioxide and glass substrates. There are three typical methods for silane surface treatment, vapor, liquid and boiling.

Vapor Method

Vapor treatment methods attempt to initial the self assembly of a silane molecule through the use of a gaseous delivery method. Since this method negates the use of liquid delivery, it either requires the use of a pre surface activation to break the O-H surface bond and allow the silane to bind to the surface, or post annealing to drive the reaction forward. A common procedure for the vapor based silane treatment method is as follows:

1. Clean the substrates as well as possible, with soap, solvent and with UV Ozone or O_2 Plasma

2. In a desiccator, place a drop of liquid silane on a watch glass, placing the watch glass on one end. Place the substrates face up on the other end.

3. Pull vacuum on the desiccator for 10 minutes

4. Turn off the vacuum to the desiccator and let sit for an hour

5. Vent the desiccator and remove the samples

6. Post anneal on a hotplate if necessary, usually at $80 - 100^o C$

The main benefit of using a vapor based treatment is that is fast, and generally inhibits the formation of multi-layer films. In that way it is usually a better technique
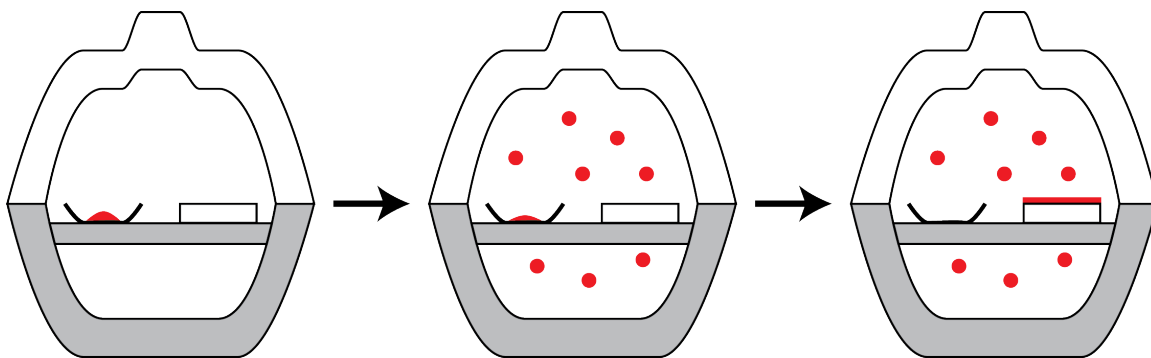
Figure 3-2: A description of the vapor silane treatment method

to functionalize patterned substrates as it prevents the loss of sharp features in the silane coating process. However, due to silane requiring a hydrated surface to properly bond, this method is the most uncontrolled and most prone to failure. A description of the process can be seen in Figure 3-2.

Liquid Method

Liquid treatment methods use a solvent as a transfer medium to allow for self-assembly of a silane molecule. The solvent is can be aqueous or non-aqueous depending on the type of silane. In general, liquid treatments are slower than vapor, but are also more compact as the silane has enough time to re-orient and create a dense layer. A common procedure for the liquid based treatment method is as follows:

1. Clean the substrates as well as possible, with soap, solvent and with UV Ozone or O_2 Plasma

2. Mix a solution of the silane in ethanol. Concentration depends on the amount of free surface. In general, 1-5 mMol is enough for eight half inch substrates using a flurosilane.

3. Place substrates in a glass petri dish face up

4. Pour the solution over the substrates, making sure to completely cover them

5. Cover the petri dish and let sit overnight
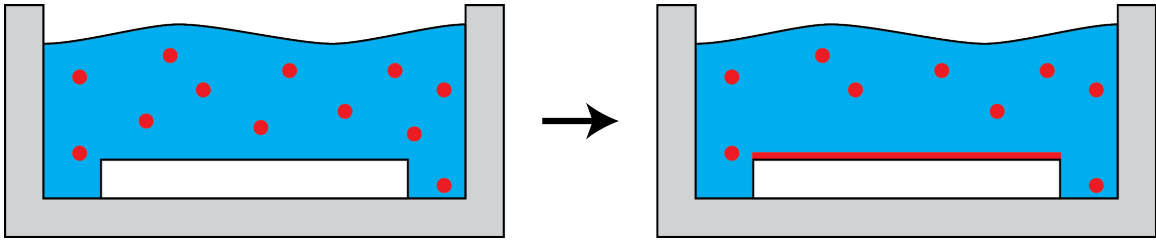
Figure 3-3: A description of the liquid silane treatment method

6. Pull the substrates out of the solution and rinse with isopropyl alcohol or ethanol

7. Post anneal or post treat if necessary

A description of the process can be seen in Figure 3-3. Surface data, taken by atomic force microscopy can be seen in Figure 3-4 using this method for surface treatment, silicon/silicon dioxide as the substrate and Trichloro(1H,1H,2H,2H-perfluorooctyl)silane as the functional silane. Statistical quantities can be seen in Table 4.1 The layer is dense relative to untreated silicon, which is assumed atomically smooth (about 1 ÅRMS Sq). The coated surface has a roughness of 0.22 nm RMS and thereby does not change the surface geometry to a significant degree.
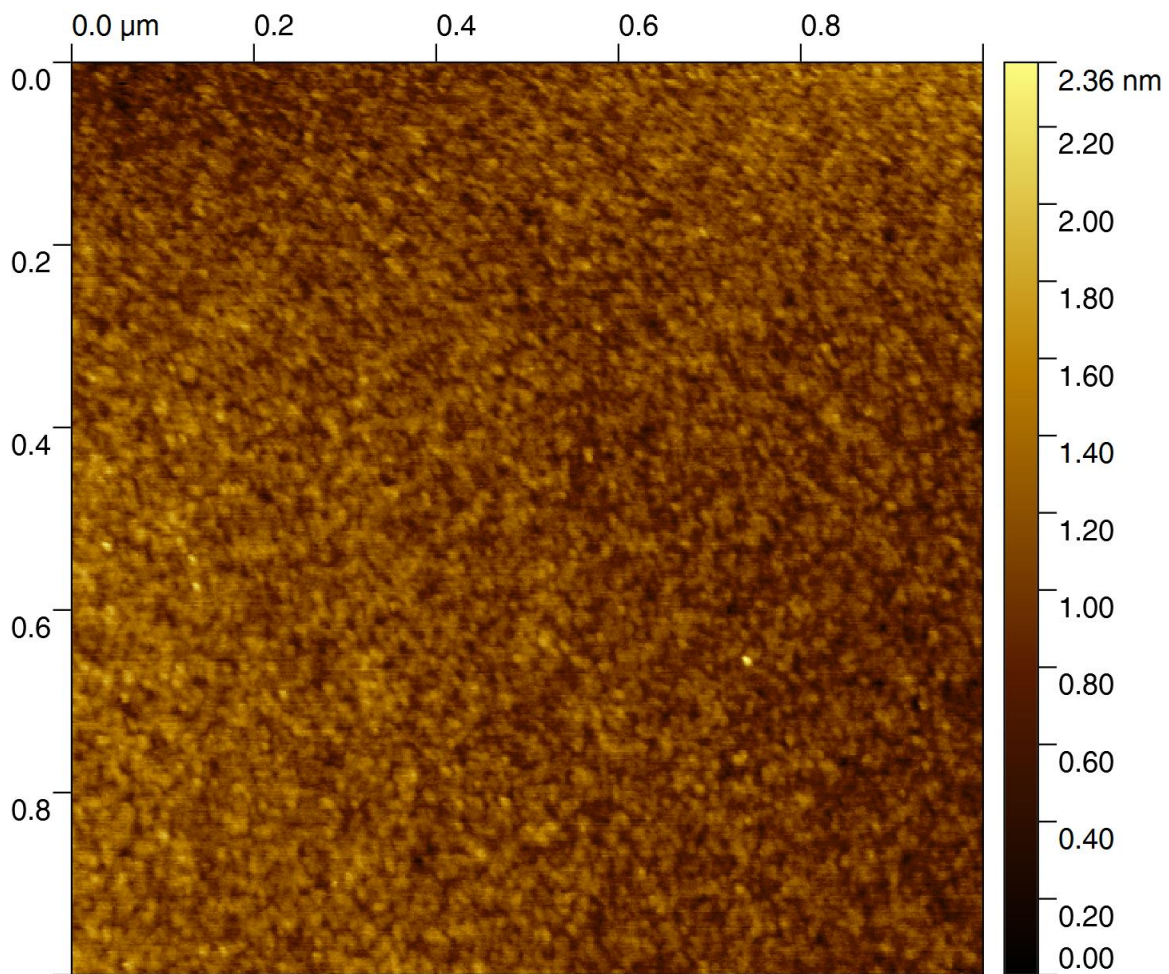
Figure 3-4: Atomic force microscopy image of a fluorosilane treated silicon surface. Statistical quantities are in 3.1

Table 3.1: Statistical quantities for Figure 3-4

Quantity	Value
Minimum	0.00 nm
Maximum	2.36 nm
Average Value	1.03 nm
Median	1.07 nm
Ra (Sa)	0.22 nm
Rms (Sq)	0.22
Skew	0.10
Kurtosis	0.09
Projected Area	1.00 μm

Boiling Method

The boiling method is a similar method to the liquid treatment but designed to create a more durable coating by hydrating the sample surface and pushing the silane reaction forward with heat all in one step. It is useful when dealing with large and uneven samples, but has the drawback of being uncontrolled, and therefore hard to obtain a single silane monolayer. A typical procedure for the boiling method is as follows:

1. Clean the substrates as well as possible, with soap, solvent and with UV Ozone or O_2 Plasma

2. Boil water and place the substrates in the boiling water

3. Add oxysilane into the boiling water. Usually a few drops is sufficient.

4. Boil the substrates in the water for 10 to 20 minutes

5. Remove the substrates and wash with isopropanol or ethanol

This method is very similar to the liquid method and is therefore similar to Figure 3-3. The main difference is that this method is faster and ensures that water and
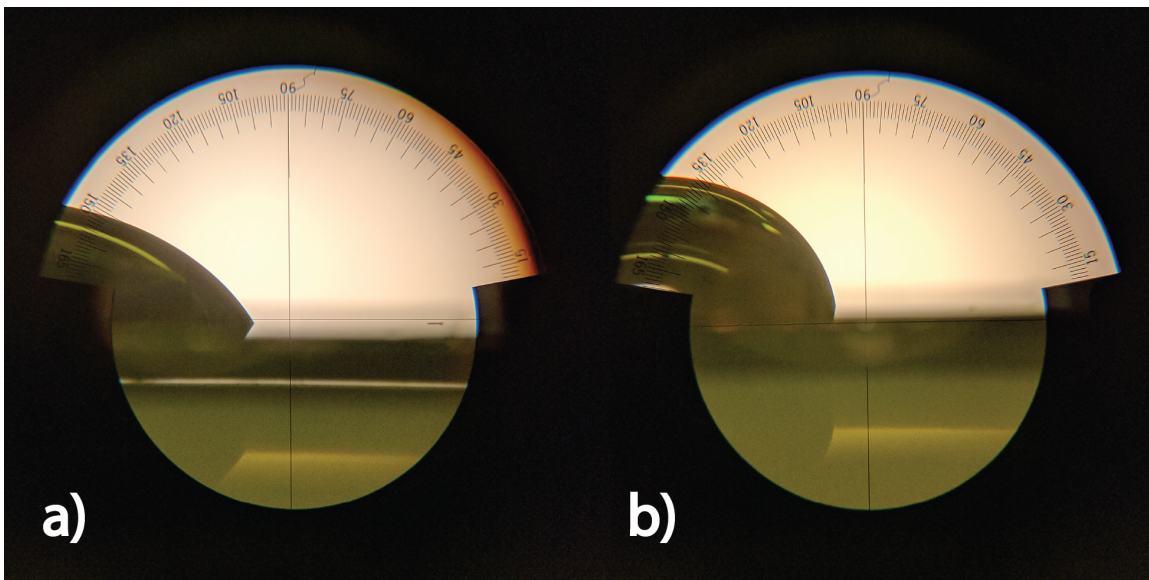
Figure 3-5: Contact angle for an a) untreated silicon sample and b) fluorosilane treated silicon sample

thermal energy are present for the reaction to move forward. Chlorosilanes cannot be used in this method due to their habit of polymerizing in aqueous environments.

All of these methods produce similar changes in surface energy due to the surface being similar with all methods. Photos of wetting angles of treated and untreated substrates are shown in Figure 3-5.

3.2   Silver Nanowire Growth

Silver nanowires are solution-grown nanoparticles that takes advantage of differences plane selective capping ligands, resulting in single dimensional growth. In silver and gold chemistry chemistry, adjusting the amount ligand or ligand ratios can result is a wide variety of interesting structures, from stars to cubes to hexagonal platelets, rods and wires [54]. For the purposes of transparent electrodes, silver nanowires have gained a lot of attention since they are highly conductive, easy to manufacture in a one-pot synthesis and have the potential to be cheaper than their metal oxide counterparts at scale [5] [56] [28] [19] [48].

3.2.1 Synthesis Procedure

Synthesis procedure for silver nanowires has been under development for many years. The simplest method is to reduce a silver salt in ethylene glycol with polyvinylpyrrolidone (PVP) acting as a coordinating ligand [28]. In this reaction, ethylene glycol acts as a solvent as well as a reducing agent at the high temperatures where this reaction takes place. Polyvinylpyrrolidone molarity, when controlled correctly allows for single dimensional growth. In this method, the wires can be self-seeding under the correct conditions, but often it is easier, more reproducible, and does not affect electrical properties if seeded with a copper or gold salt. A visual description of the chemistry can be seen in Figure 3-6. A procedure for synthesis can be seen below:

1. 5mL of anhydrous ethylene glycol is heated to 150^oC for one hour with stirring in an oil bath. Heating is done is a disposable, clean vial in order to reduce contamination.

2. 40 μL of 4mM Copper Chloride Dihydrate in ethylene glycol is added to the solution and allowed to heat for 15 minutes.

3. 1.5 mL of 114mM PVP in ethylene glycol is added to the vial

4. 1.5mL of 94mM Silver Nitrate in ethylene glycol is added to the solution

5. The solution is allowed to stir for one to 1.5 hours until the solution becomes silver and whispery, indicating the formation of long micron length nanowires.

6. The resulting product is washed with acetone and water three times before re-dispersing in IPA

The progressing reaction can be seen in Figure 3-7, and the resulting synthesized wires can be seen in Figure 3-8 right. An orange color indicates the correct faceted seed formation.
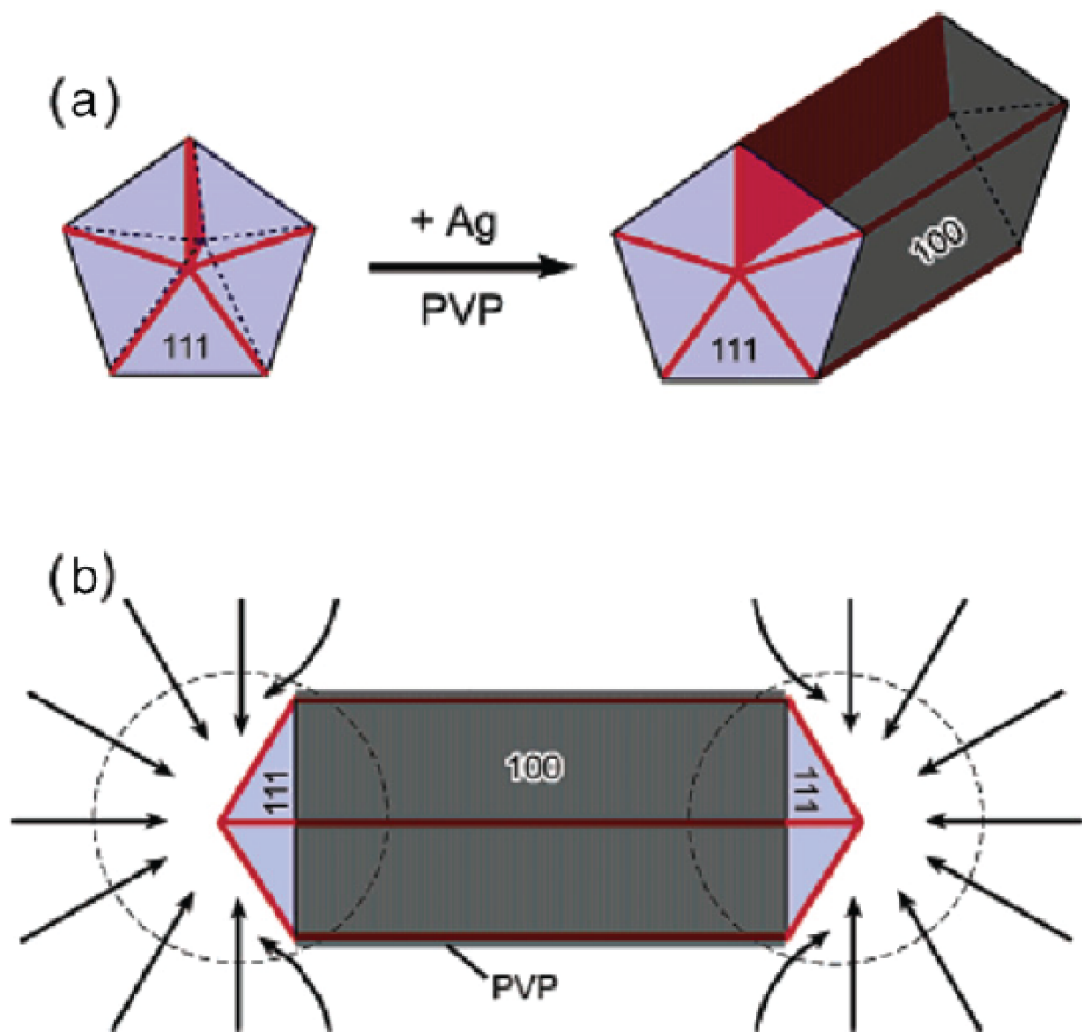
Figure 3-6: Growth Mechanism of silver nanowires. Starting from a twin-faceted nanoparticle (in this case copper) (a) PVP selectively caps the 100 plane and allows for growth along the 111 plane (b) reproduced from [31]
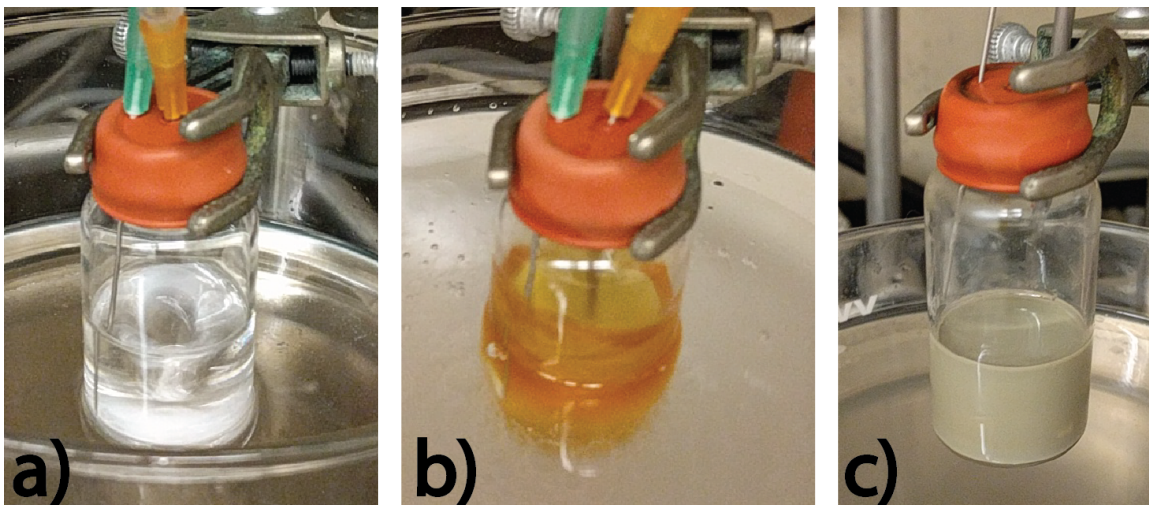
Figure 3-7: Nanowire reaction progressing a) right before copper chloride addition b) after 15 minutes c) right after stopping the reaction and before washing

3.2.2 Results

Growth of long silver nanowires needed for transparent conductors is highly dependent on compositional purity, and even small amounts of impurities can impinge on nanowire growth. This can be seen in Figures 3-8 and 3-9 in which the same silver solution is used two weeks later to synthesize nanowires. During that time, slight degradation of the solution causes a decrease in the number of nanowires formed, particle impurities and an overall decrease in length. This same degradation happens over time as silver nitrate naturally degrades from oxygen and light. Silver nitrate is also sensitive to chemical contamination, and therefore it is possible prevent wire formation due to slight amounts of organic contamination (i.e. from a glovebox for example). If all goes smoothly, typical wire formation can be seen in Figure 3-8 (right) and a length distribution, as measured from electron microscope images in ImageJ can be seen in Figure 3-8 (left).

Films generated by these wires can be rough and have high aspect ratios. An AFM image of two wires crossing can be shown in Figure 3-10.

Due to the increased presence and lower cost of silver nanowires by chemical suppliers, silver nanowires are purchased from various suppliers for simplicity and reproducibility for the majority of this work.
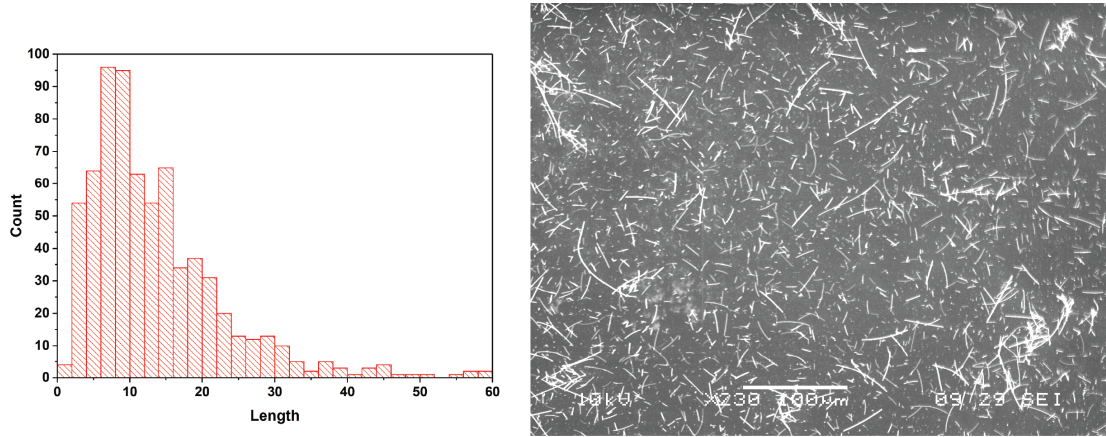
Figure 3-8: Nanowire length distribution as prepared (left) and SEM image of prepared nanowires (right) using fresh materials
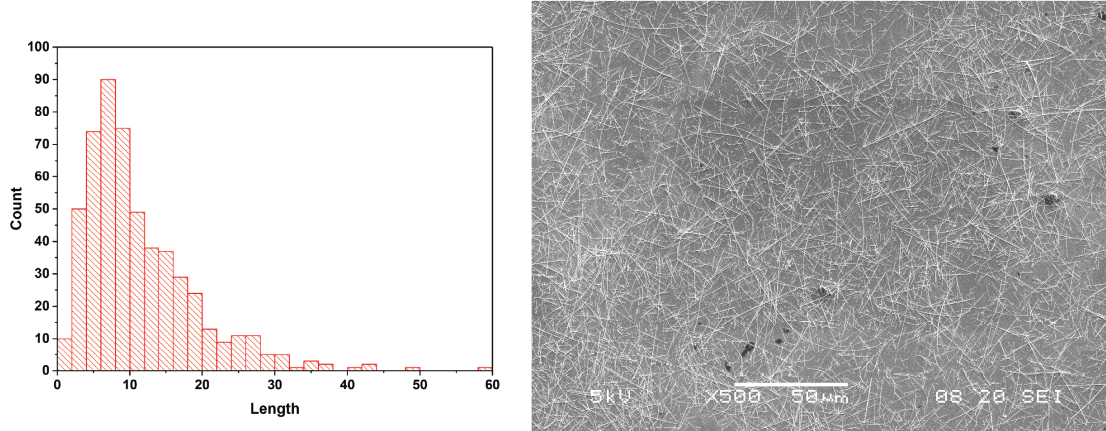
Figure 3-9: Nanowire length distribution as prepared (left) and SEM image of prepared nanowires (right) using two week old material
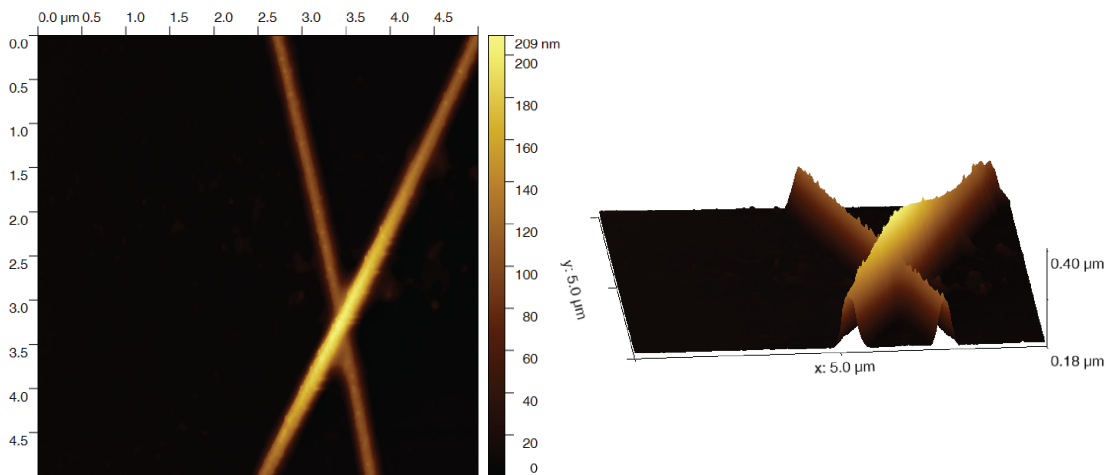
Figure 3-10: AFM image of two nanowires crossing

Chapter 4

Fabrication of Low Roughness Metal Nanowire Meshes

4.1 Fabrication Overview

Silicon and glass, processed for electronics through chemical mechanical polishing and cleaning are considered one of the smoothest engineered and widely available surfaces. When vacuum depositing ITO onto glass, roughness in increased, but still remains low (about 5 nm RMS) and also doesn't have any high aspect ratios. This smoothness is critical for creating heterojunction devices, as layer can be less than 10 nm in thickness. If a roughness approaches the thickness of your film, pinholes, or shorts can occur where the underlying layer is exposed to the next layer. This can be detrimental for device performance or even short the device all together. When transitioning flexible structures and silver nanowires, aspect ratios can be orders of magnitude larger than the actual device size. This can be seen in Figure 4-1. This makes it impossible to fabricate small structures utilizing flexible transparent metal structures, if they are used as-is.

A method to overcome this is to engineer the silver nanowire surface to be flat but still maintain nanowire interconnectivity. If you utilize a known flat surface, then it is possible to mold a material to that surface, creating a very smooth interface. If you engineer that known surface's energy, then it is possible to peel the known flat
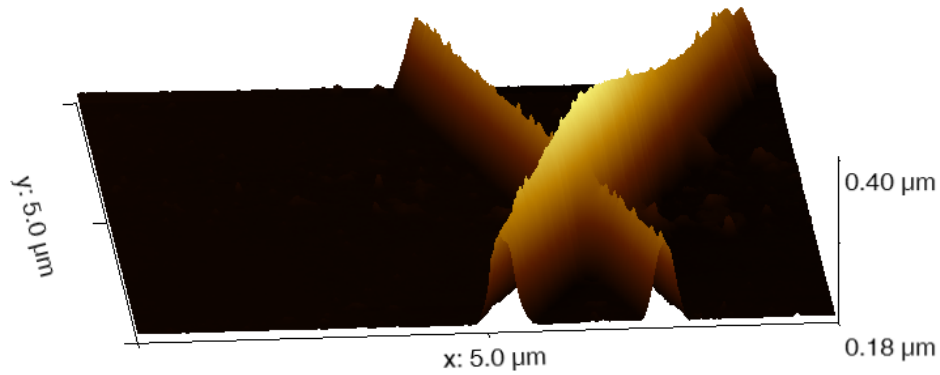
Figure 4-1: AFM images of two nanowires crossing. This shows how large of an aspect ratio this can be.

substrate and the material away from each other with ease. In this way, a new surface can be engineered with the properties of the old, thereby overcoming limitations of known deposition methods and traditional surface geometry.

Using the previous methods, nanowires meshes are inherently unable to fully conform to a surface as their properties are due to their networked nature. In order to take advantage of this approach for a transparent conductor, a composite must be fabricated, so that the wires can sit at the substrates surface and an infilling material can be molded to the surface. Once peeled, the new surface would have patches of nanowires as a conductive filler material and patches of a matrix material that smooths out the nanowire surface. If the peeled surface is smooth enough, this would allow for further processing of thin film materials. A schematic description of the process can be seen in Figure 4-2.
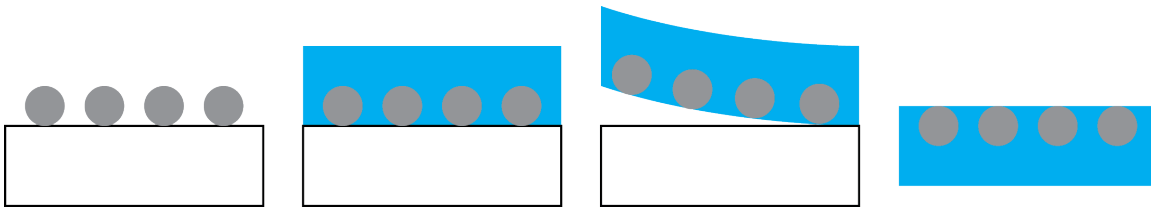
Figure 4-2: A simple description of the smoothing process. From left to right: Nanoparticles are deposited on a flat surface. A matrix materiel is infilled and encapsulates the particles. The encapsulation matrix material and the particles are peeled off the surface, thereby revealing a smooth surface. The nanoparticles sit on this smooth surface and are semi-exposed.

4.2 Initial Fabrication Process

Fabrication begins with the fluorosilane treatment of a borosilicate or a silicon wafer as described in the previous section. The substrate is washed with soap, in this case Micro90, and then sonicated in deionized water, acetone and then boiled in isopropanol. After removing from the isopropanol the sample are blown dry with nitrogen and stored faced down in dished fluoroware. After sample cleaning, a 15 mL, 5 mM solution of Trichloro(1H,1H,2H,2H-perfluorooctyl)silane in anhydrous ethanol was mixed in air. The Trichloro(1H,1H,2H,2H-perfluorooctyl)silane is stored in a glovebox and small amounts were removed when needed. The substrates were then oxygen plasma cleaned for 5 minutes. Upon completion, the substrates were placed face up in a petri dish, (glass or plastic) and then the silane solution poured over the sample. The petri dish was covered and the substrates were allowed to sit overnight.

The next day, the substrates were removed from the silane solution and rinsed with anhydrous alcohol, either ethanol or isopropanol. If the samples are not clear, or have white residue (an indication of precipitated silane), the samples are washed again with soap, DI, acetone and IPA. Finally, before usage, the substrates surface energy was checked with a goniometer. The contact angle was determined to be around 89° with DI water.

Silver nanowire ink preparation was as follows: Wires are initially synthesized as described in a previous section. After prices on silver nanowires dropped, additional experiments used purchased nanowires from Sigma Aldrich (product number 739448-

25mL and 808032-25mL) with an average length of 20-40uL and diameter 115nm. In 20mL vial, 12.5 mL of 0.2 mg/mL solution of silver nanowires in IPA was mixed, (roughly 12mL IPA : 0.5mL of stock solution). To break up clumps that form during dilution, the solution is sonicated for 10 seconds. Sonicating for over 10 seconds results in wire breaking. The solution should look wispy and silver in color. Depending on the nanowire manufacturer, it may also have a slight yellow appearance due to particle contamination or wire diameter (in the range of 70 nm, which would have a plasmonic resonance in green, therefore making the solution look orange/ yellow due to absorption and scattering). The solution is prepared right before spray coating to avoid wire settling, clumping and oxidation.

After surface treatment and cleaning and ink preparation, the substrates and taken to the spray coater and placed in the sample holder. The bed temperature is set to 85^oC and allowed to equilibrate for 30 minutes. The samples are covered loosely with aluminum foil to prevent dust setting and allow priming of the spray head. The ink is mounted in the vial holder and the spray head is primed using a 2-second purge. Once heating is done the foil is removed and the spray program is started. Once the program is done, the samples are rotated 180 degrees to maintain uniformity and the process is repeated. The samples are then removed from the bed. If more samples are needed, they are loaded into the sample holder and the process repeated. Patterning can be accomplished by using a static-adhered vinyl sticker or using an etched metal masked taped and pressed against the substrates surface.

Once spray coating of the wires is finished, the samples are loaded into the parylene chamber and the chamber is pumped down to 10^{-3} torr. The pyrolysis furnace is heated to 750^oC. The evaporation furnace is heated to 105 to 120^oC using the temperature to control a deposition rate of 3 Å per second. After around 1.6 μm is deposited, the evaporation furnace is tuned off and allowed to cool. During this time an additional 0.2 to 0.4 μm is deposited due to residual heating. After deposition has stopped, the evaporation genesis valve is closed and the pyrolysis furnace is allowed to cool. The chamber is vented, and the samples are removed from the front door, or transferred into high vacuum to be transferred into a high vacuum transfer system,
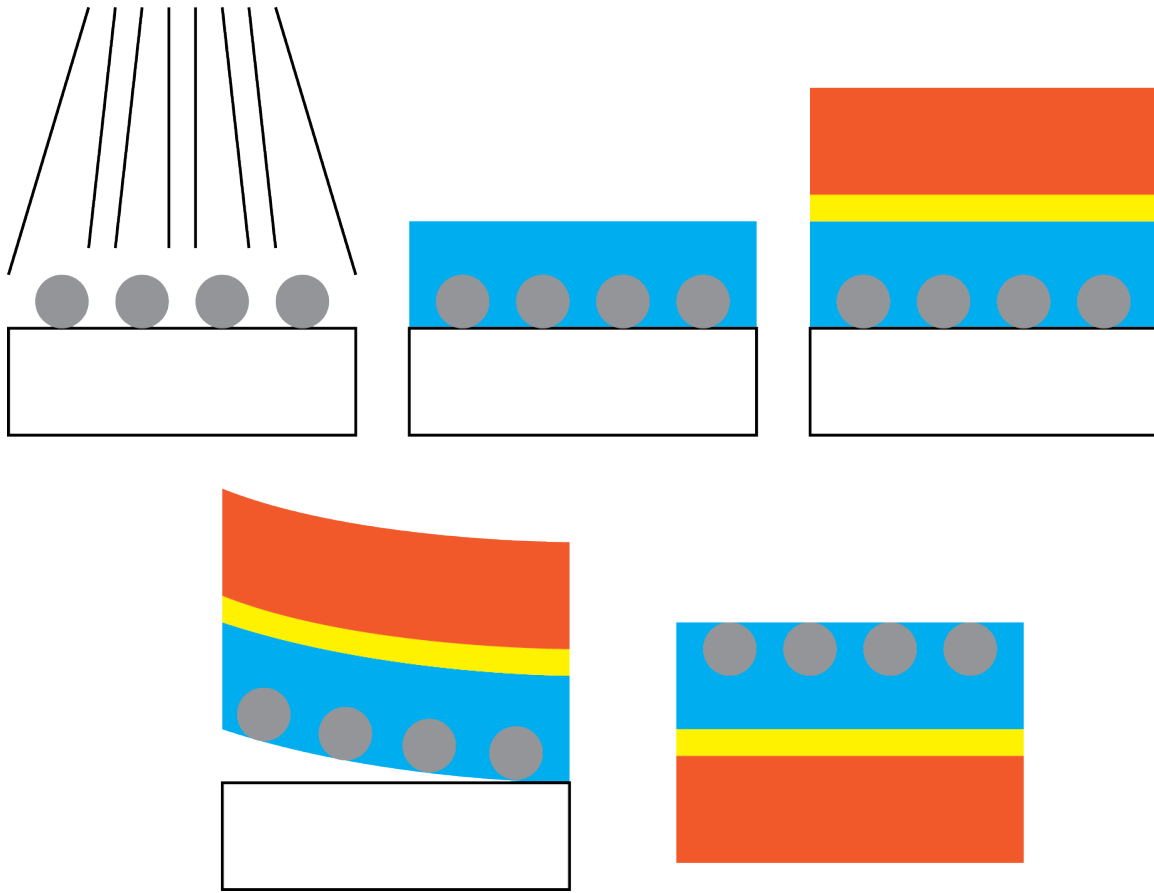
Figure 4-3: Initial fabrication process. From left to right: Nanowires are deposited on a flat surface via spray coating. Parylene is infilled and encapsulates the particles. The parylene is glued to PET using NO61 and the particles are peeled off the surface, thereby revealing a smooth surface. The nanowires sit on this smooth surface and are semi-exposed.

when can then be transferred into a glovebox. The entire process takes about 6 hours.

After parylene deposition, the samples are glued to 25 μm PET sheet using Norland 61 UV curing optical adhesive (NO61), and the nanowire-parylene-PET structure is peeled off of its fluorinated substrate. The sample is then trimmed to a one half inch size and either used as is, or glued to a piece of untreated glass for study on a more easily handled ridged substrate.

A pictorial description of the process can be seen in Figure 4-3.

4.3   Initial Results and Challenges With Uniformity

Initial AFM results using lab synthesized silver nanowires can be seen in Figure 4-4. Statistical quantities can be seen in Table 4.1. Initial SEM images can be seen in Figure 4-5. As shown, the technique allows for the creation of a smooth surface while allowing nanowires to protrude, allowing for contact to the conductive mesh.
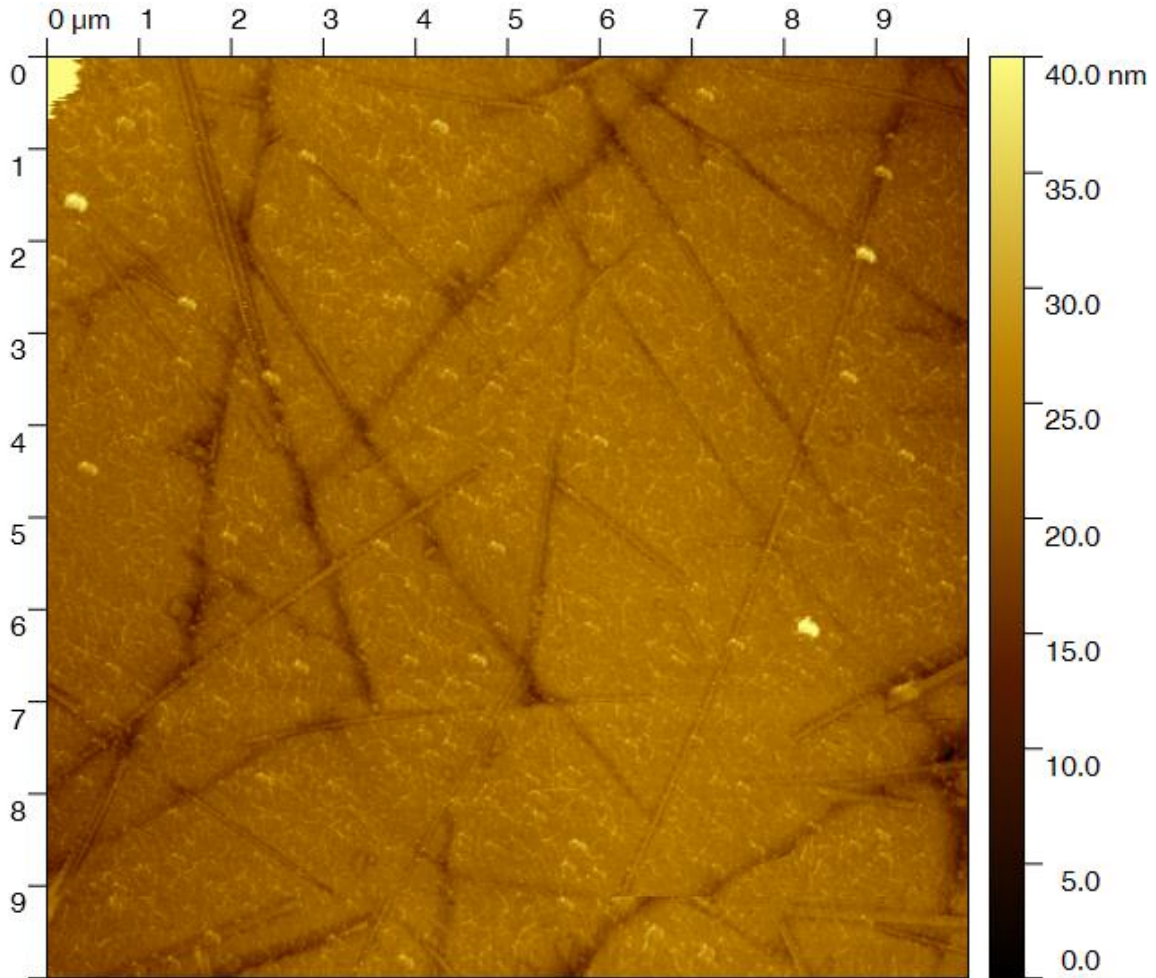
Figure 4-4: AFM image of the nanowire-parylene surface peeled from fluorinated glass. Nanowires were synthesized in-house. Statistical quantities are in 4.1
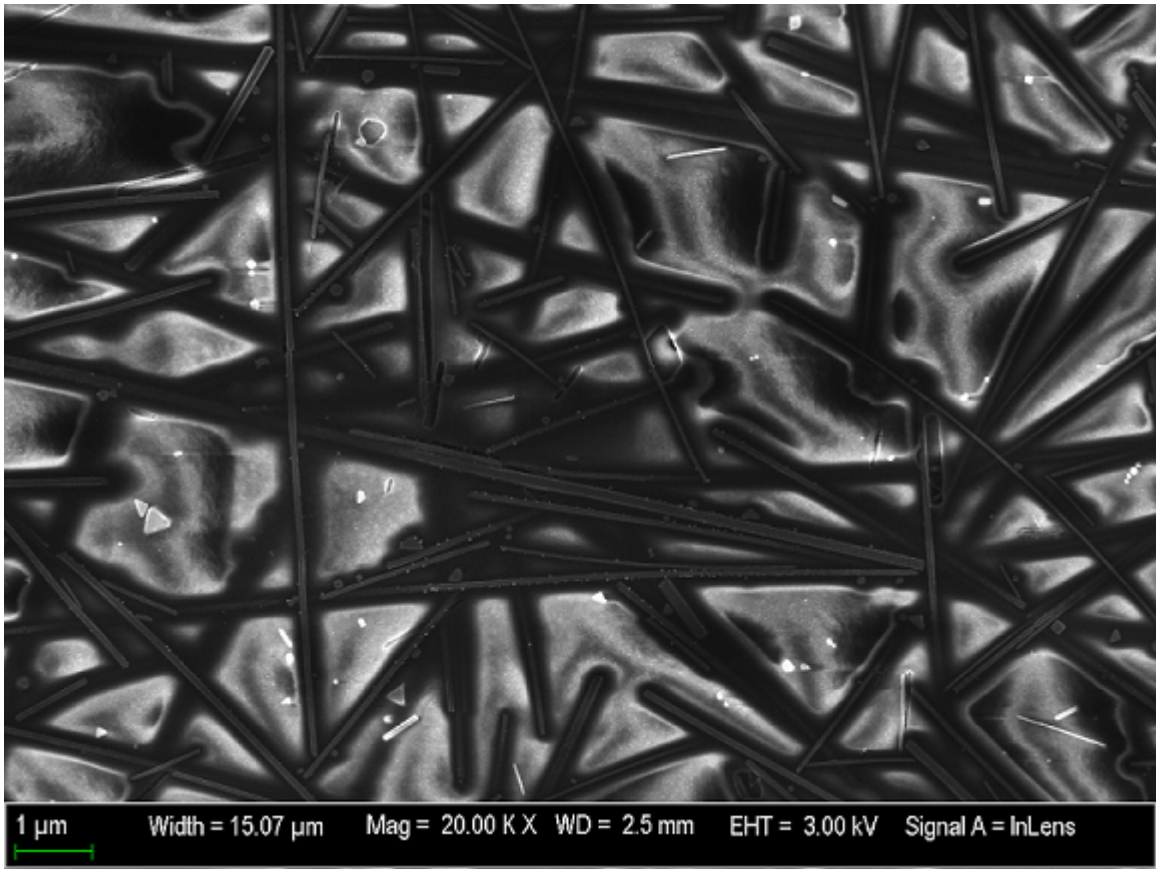
Figure 4-5: SEM image of the nanowire-parylene surface peeled from fluorinated glass. Nanowires were synthesized in-house.

Table 4.1: Statistical quantities for Figure 4-4

Quantity	Value
Minimum	0.00 nm
Maximum	133.40 nm
Average Value	21.92 nm
Median	22.10 nm
Ra (Sa)	3.30 nm
Rms (Sq)	3.30
Skew	9.63
Kurtosis	230.1
Projected Area	100.00 μm
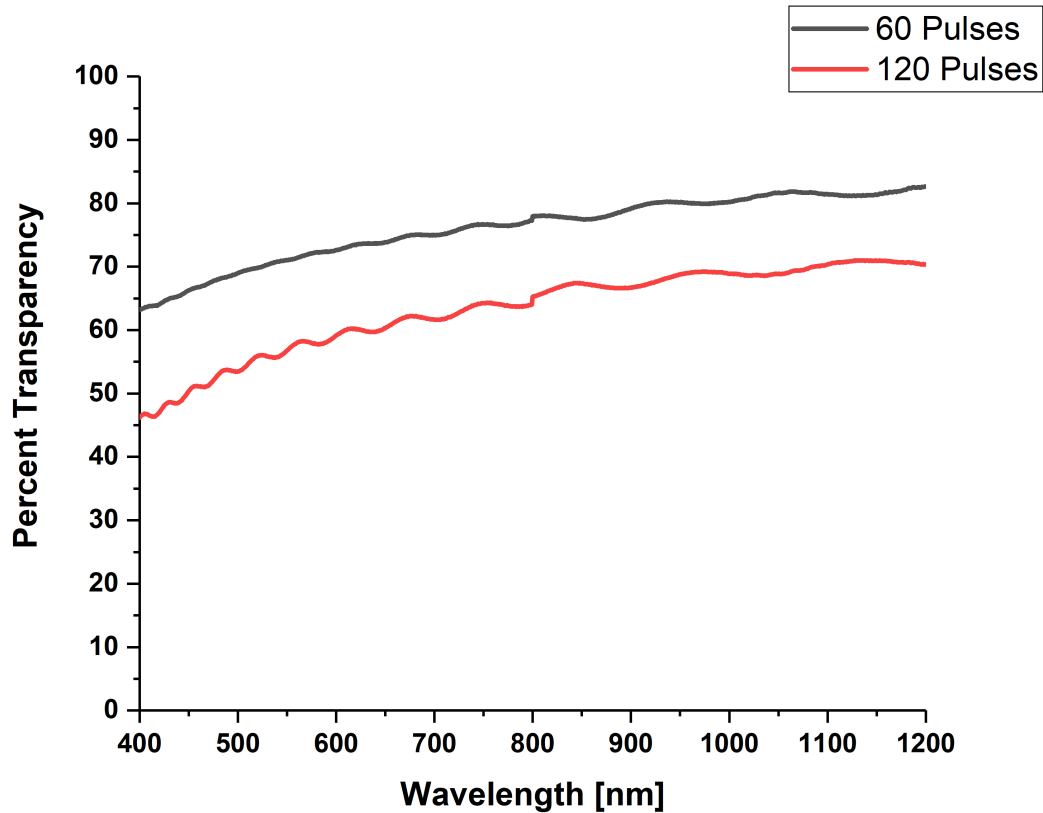
Figure 4-6: Transparency of silver nanowire-parylene composites with 60 and 120 pulses. Absorption is dominated by the nanowires. Nanowires were synthesized in-house and were at an as prepared concentration of about 0.15 mg/mL

In addition, since parylene is a transparent polymer over the entire visible spectrum, the composite still retains high transparency due to the low absolute absorption of the nanowire mesh network. Transparency over the visible spectrum and near IR can be seen in Figure 4-6.

However, conductivity in these films remained an issue. When measured with a standard 4-point probe, the measurements would either not make contact, show high sheet resistance $(1000\Omega/\square)$ or low sheet resistance $(20 - 100\Omega/\square)$. It would also depend on where the film was probed. Since the 4-point probe method is a small area measurement, it was theorized that there may be non-uniformity in the conductivity of the film due to the conformal nature of parylene. In this way, if wires are not directly touching, parylene may infill the network so much as to break long range
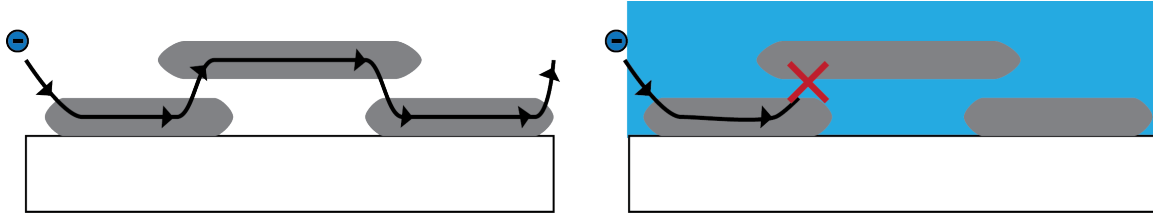
Figure 4-7: Proposed issues with conductivity after depositing parylene. Conduction is represented by the black line. Since not all nanowires are completely touching, conduction is possible before parylene infilling due to tunneling and not possible after.
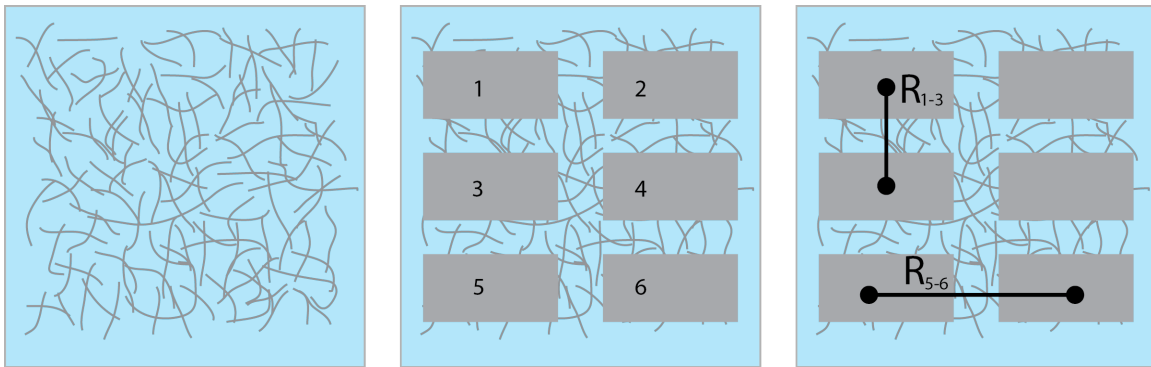
Figure 4-8: Simple measurement to determine uniformity on a one half inch square film. A nanowire-parylene film is prepared. Then six electrodes are evaporated along the full area. Resistance can then be measured between pads to get a sense of uniformity.

conduction. A description of this hypothesis can be seen in Figure 4-7. To confirm this theory, nanowire-parylene samples were fabricated and a 6 pad electrode mask was used to pattern 6 silver pads on the peeled surface. Resistivity measurements were then done between the pads to check the uniformity over the wire surface. A description of the measurement can be seen in Figure 4-8 and results can be seen in Table 4.2. As shown, conductivity is highly non-uniform over the peeled surface and there are even fully resistive gaps.

4.4 Wire Compression and Optimization

One solution to obtaining a more uniform film is to mechanically compress the wires so that all the wires are touching or the wires have a gap that do not get infilled

Table 4.2: Resistance values described in Figure 4-8 to understand film uniformity. Nanowires were purchased from Sigma and sprayed at 0.2mg/mL dilution. All measurements are in Ohms.

Sample Type	Position	Sample 1	Sample 2	Sample 3	Sample 4
40 Pulses	R_{1-2}	263.7	4.4	3.4	
	R_{3-4}	189.8	4.2	2.7	–
	R_{5-6}	–	4.5	3.4	–
	R_{1-3}	256.6	2.3	1.9	–
	R_{3-5}	314.1	–	1.8	–
	R_{2-4}	238.5	–	2.1	–
	R_{4-6}	841	–	2.3	–
30 Pulses	R_{1-2}	–	7.2	7.3	–
	R_{3-4}	–	9.0	5.3	–
	R_{5-6}	–	11.7	5.3	–
	R_{1-3}	–	3.9	5.3	–
	R_{3-5}	–	6.0	4.8	–
	R_{2-4}	–	3.1	3.4	–
	R_{4-6}	–	3.5	2.5	–
20 Pulses	R_{1-2}	144.4	117.1	121.3	–
	R_{3-4}	160.5	76.3	104.9	–
	R_{5-6}	1061	98.8	97.6	–
	R_{1-3}	–	88.0	53.0	–
	R_{3-5}	–	58.1	31.9	73.0
	R_{2-4}	100.5	90.4	228.5	1100
	R_{4-6}	200.1	155.8	198.9	177.3
10 Pulses	R_{1-2}	676	1163	303.8	966
	R_{3-4}	1902	–	230.3	267.4
	R_{5-6}	–	271.6	218.7	448.9
	R_{1-3}	–	124.6	–	455.4
	R_{3-5}	–	1267	113.9	235.5
	R_{2-4}	125.4	958	75.5	133.4
	R_{4-6}	–	1298	102.3	339.7
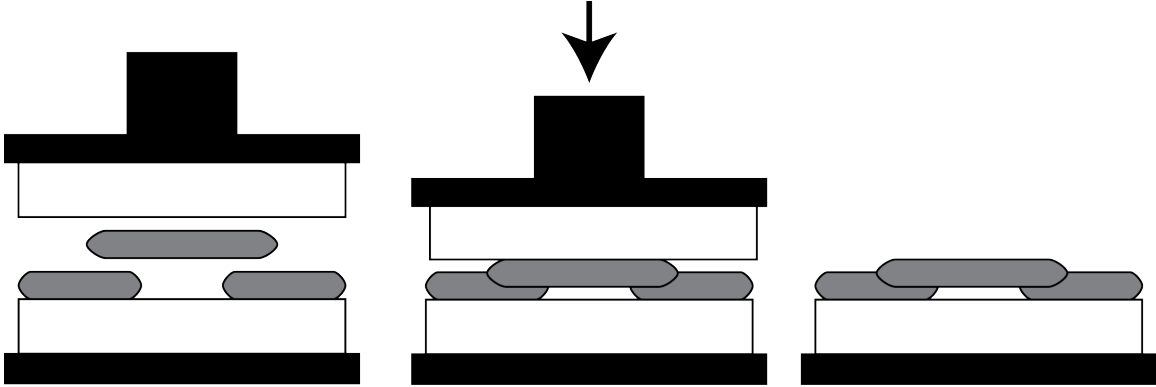
Figure 4-9: Description of the wire compression process. From left to right, wires samples are sandwiched with a second substrate and loaded into a press. Pressure forces the wires together, which when optimized leaves wires together after pressure and the second substrate is removed.

by parylene. Imprinting, and wire compression is a technique that has been used in literature to decrease nanowire sheet resistance [20] [40]. To test the effect of compression, samples were compressed or not compressed right after spray coating and before parylene deposition. Compression was done using a lab-built pneumatic press at around 40-60 psi on a half inch sample. Optimization was done on pressing time and pressing material to ensure that no damage was done to the nanowire and it was found that short periods of around 10s, at room temperature, with fluorosilane treated glass worked well to compress wires of smaller diameter. Heated pressing, at $85^{o}C$, with pressing times of 60 seconds using Kapton tape as the pressing material worked well for wires of thick diameter. A description of the process can be seen in Figure 4-9.

In addition, a larger area van-der-pawl technique was used to better determine large area uniformity. This was done by evaporating four contact pads at the corners of a $1cm^2$ area. A Keithley 2600 was then used as a current and source meter to measure conduction in the film. The technique is described in Figure 4-10. Equations 4.1, 4.2 and 4.3 can then be used to solve for sheet conductivity. If R_1 and R_2 are highly different from each other, it shows that there is a high amount of non-uniformity in the film, which may indicate other defects forming in the film. Sheet conductivity measurements vs nanowire density using this technique and the wire pressing method
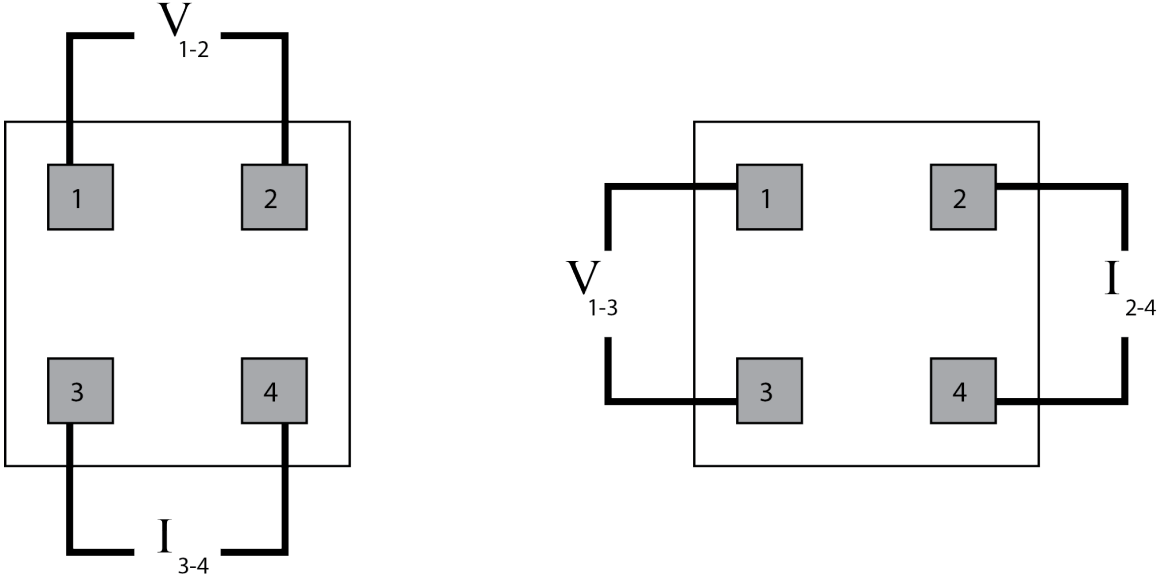
Figure 4-10: Description of the most basic form of the van-der-pawl sheet resistance measurement method. Current is applied along one set of electrodes and the voltage and measured along the other set, or vice versa

can be seen in Table 4.3. Non-conducting samples were because either the samples were glued upside down, by accidental destruction, or were not dense enough to measure (in the case of the 10 pulse samples).

$$R_1 = V_{1-2}/I_{3-4} \qquad (4.1)$$

$$R_2 = V_{1-3}/I_{2-4} \qquad (4.2)$$

$$e^{-\pi R_1/R_s} + e^{-\pi R_2/R_s} = 1 \qquad (4.3)$$

4.5   Final Fabrication Process

Fabrication begins with fluorosilane treatment as described in the previous section. In short: the substrates were allowed to sit in an anhydrous ethanol silane bath overnight to allow for silane self assembly. After treatment the samples were taken

Table 4.3: Van-der-pawl sheet resistance measurements on pressed and peeled nanowire samples

Density	Sample	$R_1[\Omega]$	$R_2[\Omega]$	$R_s[\Omega/\square]$
40 Pulses	1	–	–	–
	2	1.85	1.78	8.22
	3	1.77	1.52	7.44
	4	5.86	0.91	11.92
30 Pulses	1	1.53	2.10	8.15
	2	2.00	2.29	9.70
	3	1.42	1.32	6.21
	4	1.67	2.29	8.90
20 Pulses	1	3.81	2.87	15.03
	2	5.06	3.82	19.98
	3	–	–	–
	4	3.70	3.09	15.34
10 Pulses	1	43.43	29.25	162.63
	2	–	–	–
	3	185.2	4.38	210.71
	4	–	–	–

out and rinsed with ethanol. Additional post washing of the sample with soap and IPA was employed to help remove additional silane from the substrate surface if unreacted. After treatment and post washing the substrates were checked for proper surface treatment with a goniometer.

If proper surface treatment was achieved, the sample were coated with nanowires using a pulsed spray coating technique as described previously. In short: samples were loaded into the spray coater and allowed to heat to 85^oC. A dispersion of nanowires
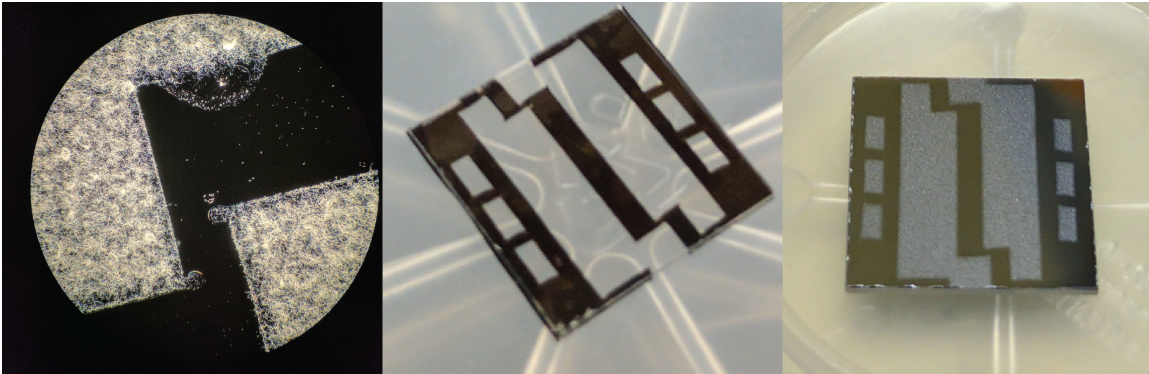
Figure 4-11: Patterning and edge sharpness via the vinyl sticker method

Table 4.4: Example machine parameters for a sample with wire density of 40 pulses. Samples were rotated 180° after finishing and the program was run again. In total, the program was run twice for a total of 40 pulses.

Head Number	Start Delay	On Time	Off Time	Pulses
1	0s	0.5s	5s	20

were then pulse sprayed onto the samples. Example machine parameters can be seen in Table 4.4. Patterning was done by either using statically adhered vinyl stickers (vinyl sheet cut in the shape of a mask) or with etched metal masks placed on the surface of the substrates. Dark field photos of the sharpness of the patterned edge can be seen in Figure 4-11 for the vinyl sticker method.

Nanowire coated samples were then taken over to a pneumatic press and compacted for 10 seconds at 60 PSI under a fluorinated piece of glass at room temperature. Compacted glass was then taken to the parylene chamber and 2um of parylene was deposited as described previously. After parylene deposition, the parylene was treated with a 1mM PVP solution in IPA and allowed to dry in air. The corners of the substrates were scribed with a razor blade, to disconnect the parylene film on the fluorinated surface from the edges of the substrate. After which, the parylene was adhered to 25μm PET film using Norland 61 as described previously and peeled. To prevent peeling defects, and keep constant peeling radius during peeling the samples were peeled using a 7-inch diameter jar. The peeled samples were either used as-is for study or adhered to glass using NO61 for further processing.

The complete fabrication process can be seen in Figure 4-12.

4.6   Results

Atomic force microscopy images of the final fabrication technique can be seen in Figure 4-13. A line scan over the a grouping of wires can be seen in Figure 4-14. As shown the surface has more wires at a similar transparency than the previous fabrication method, while keeping maintaining similar roughness. This is because the pressing method forces more wires to the substrates surface, meaning more of the
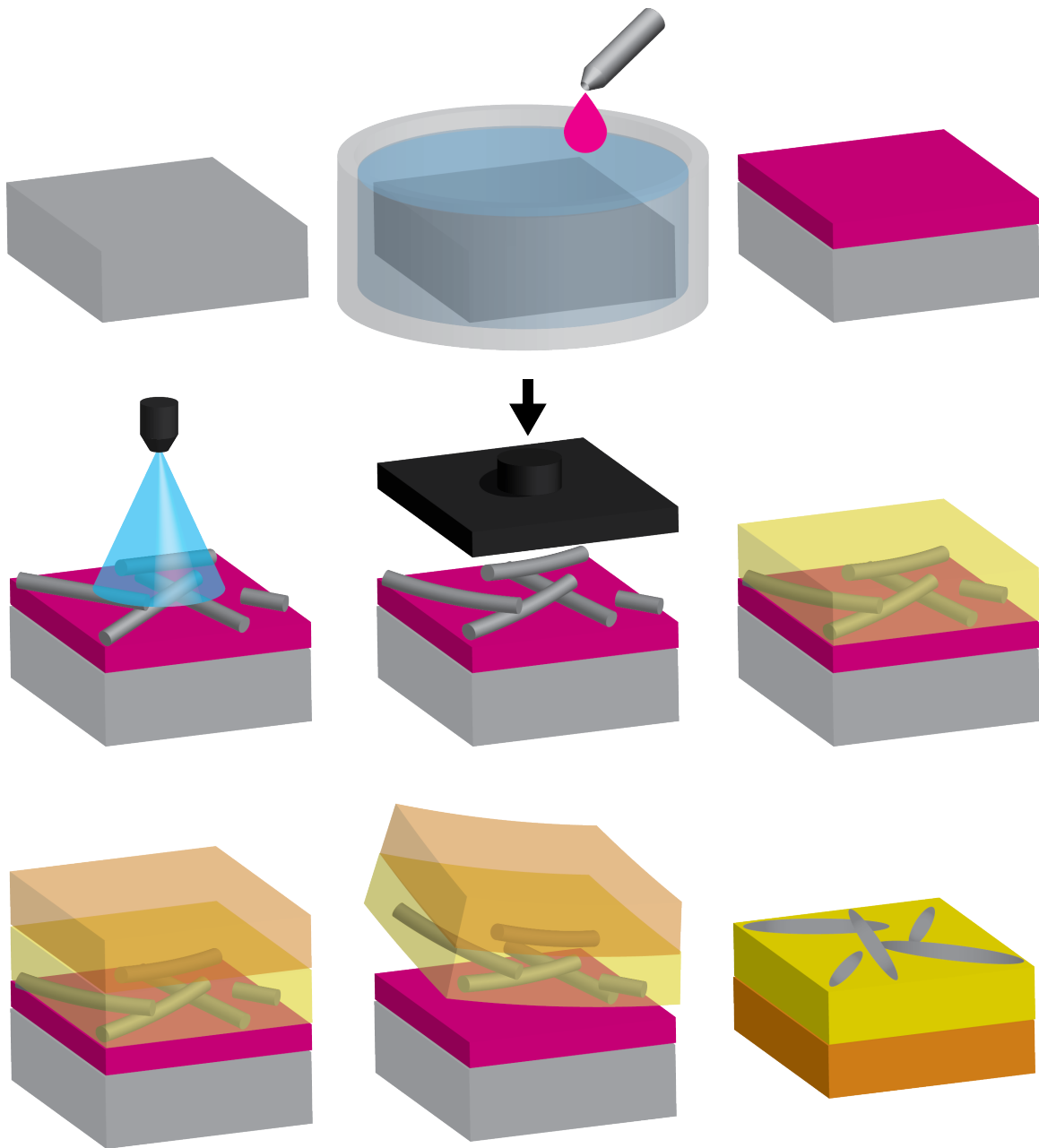
Figure 4-12: Fianl process for fabricating a smooth nanowire-parylene composite
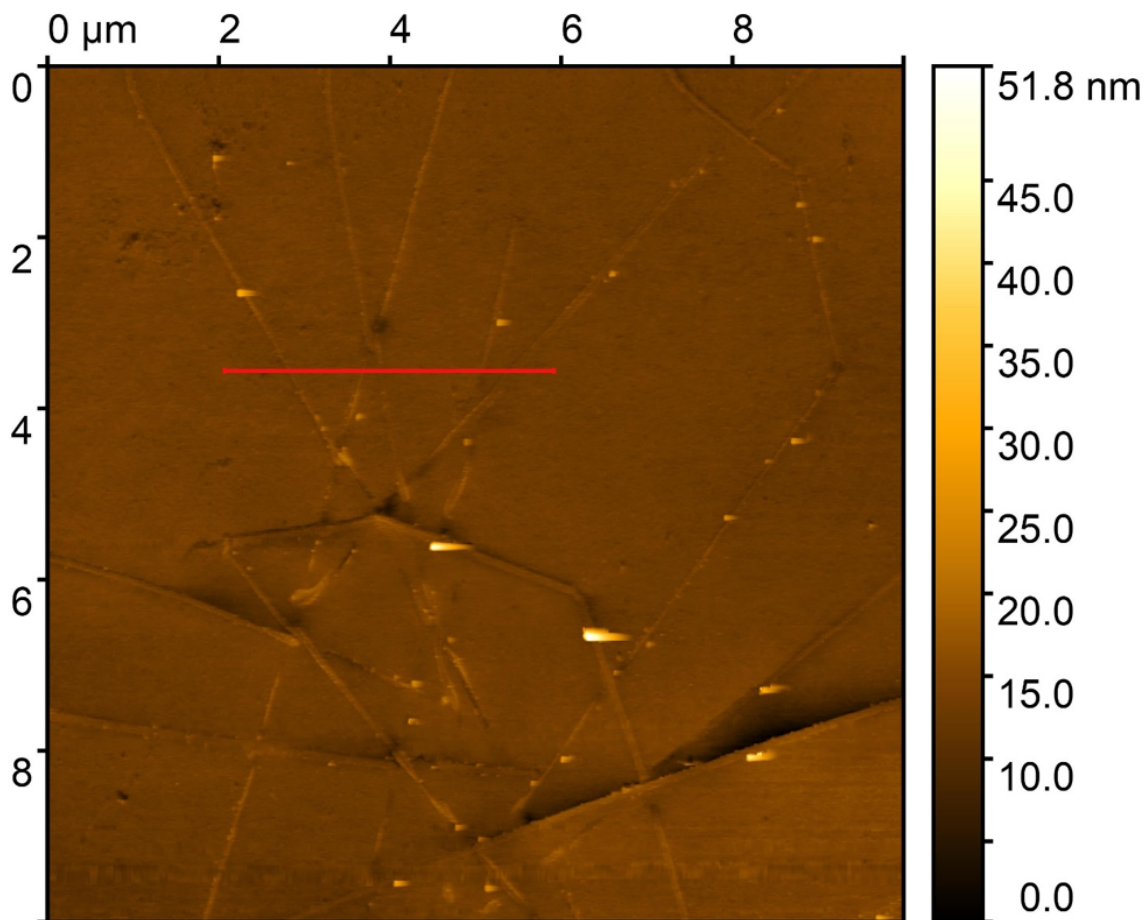
Figure 4-13: AFM image of the peeled nanowire-parylene surface. Surface roughness is 1.49 nm RMS. Wire density is 30 pulses. Red line scan is displayed in 4-14

wires are exposed after peeling. Statistics on this image can be seen in Table 4.5.

Transparency over the entire visible spectrum can be seen in Figure 4-15 for bare wires and Figure 4-16 for a fully completed composite stack mounted on glass. Bold lines are the averages of four samples and shaded regions are the deviation. Wire density was estimated from the size of the spray cone, roughly measured to be 4 cm in diameter, and the feed rate of the ink into the nozzle, which is roughly 1.1 mL per every 10 pulses. Therefore 0.015 mg/cm^2 equates to 10 pulses, 0.030 mg/cm^2 equates to 20, 0.045 mg/cm^2 equates to 30 and 0.060 mg/cm^2 equates to 40 pulses.

Transparency and sheet resistance trade-off can be seen in Figure 4-17. As shown, the nanowire-parylene composite is comparable to most traditional transparent electrodes like ITO and FTO, and has a maximum transparency to conductivity trade-off
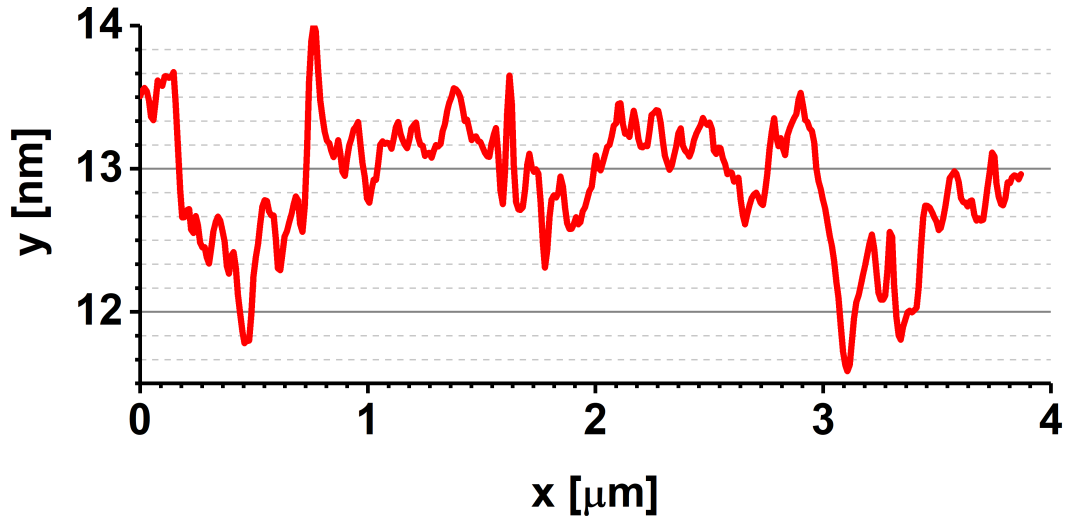
Figure 4-14: Line scan of the peeled nanowire-parylene surface marked in red in 4-13

Table 4.5: Statistical quantities for Figure 4-13

Quantity	Value
Minimum	0.00 nm
Maximum	51.80 nm
Average Value	12.90 nm
Median	12.89 nm
Ra (Sa)	0.85 nm
Rms (Sq)	1.49
Skew	3.66
Kurtosis	86.26
Projected Area	100.00 μm
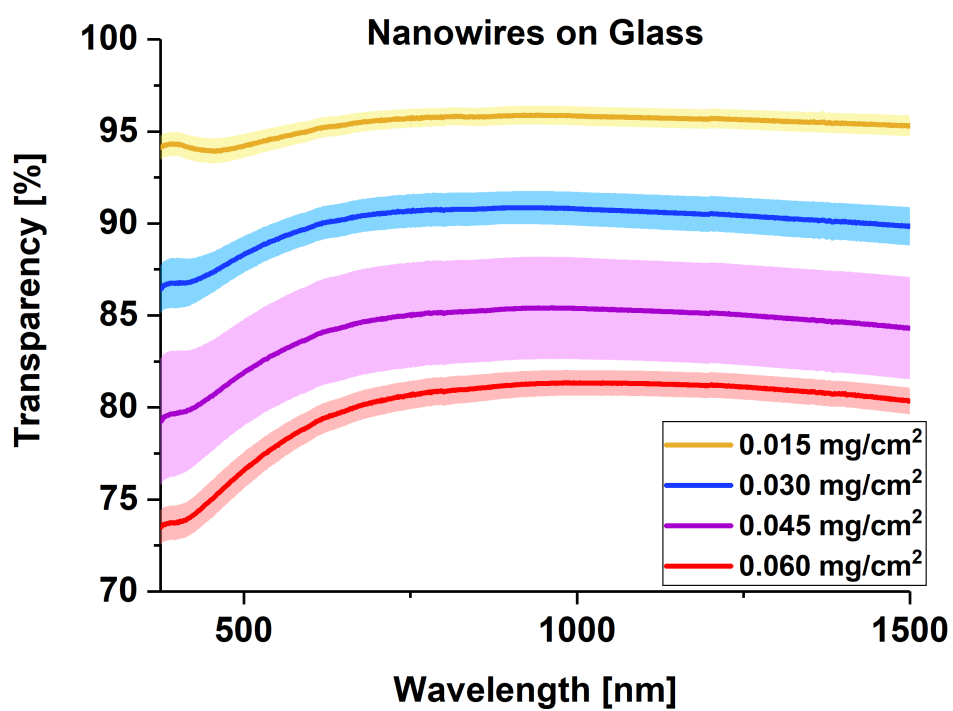
Figure 4-15: Transparency over the visible spectrum for bare nanowires at various densities.
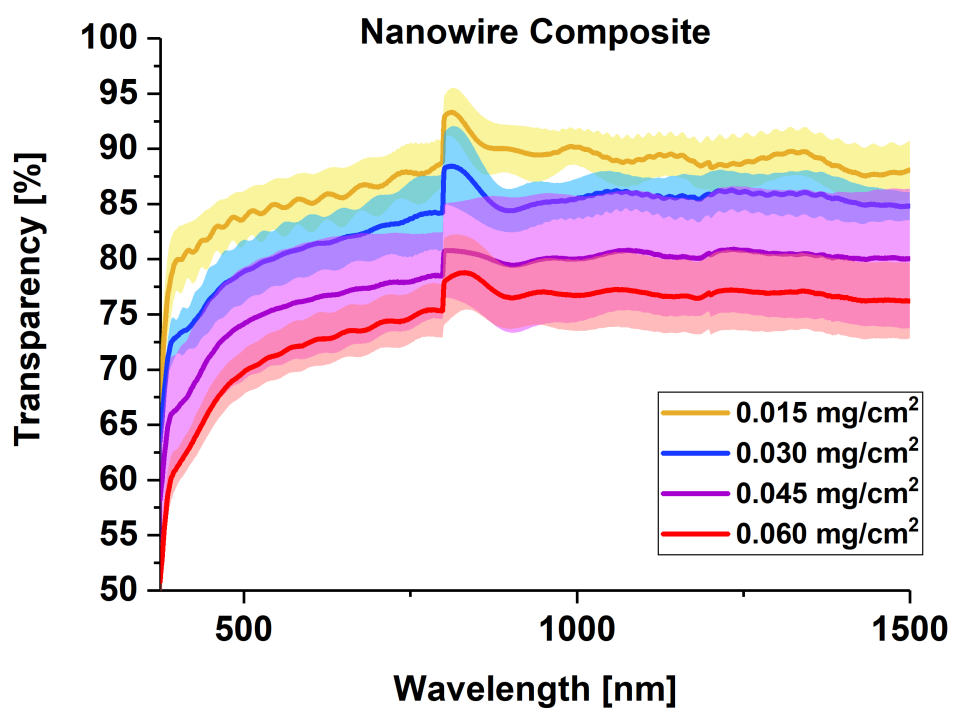
Figure 4-16: Transparency over the visible spectrum for nanowire-parylene composites mounted on glass at various nanowire densities.
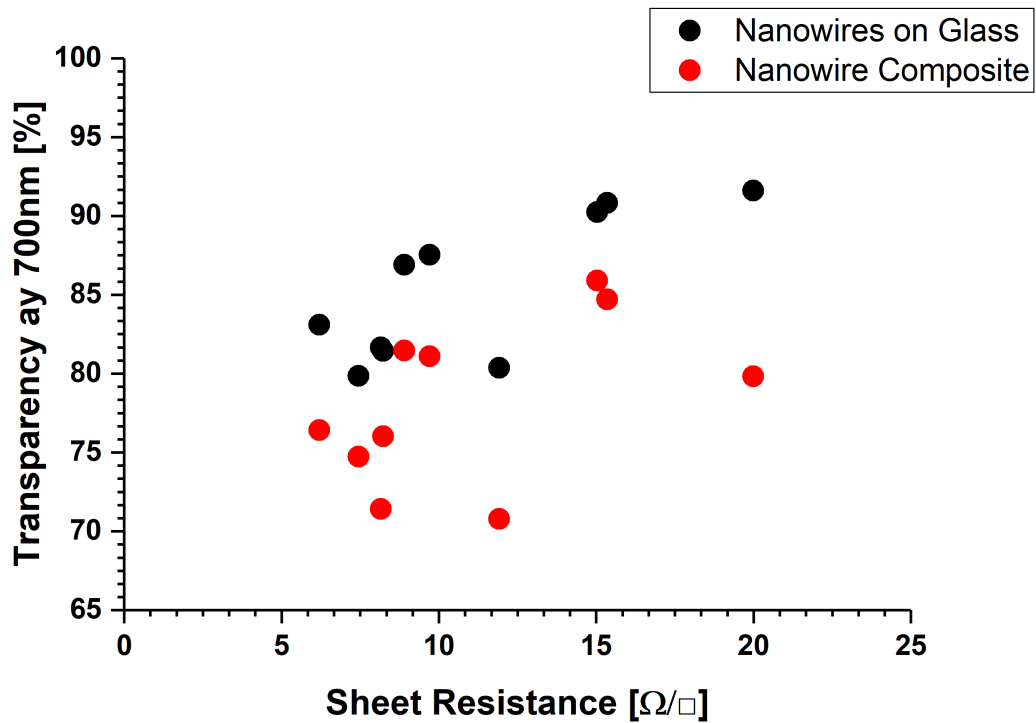
Figure 4-17: Transparency and conductivity trade-off of bare nanowires and the parylene-nanowire composite.

of about 85% transparent at 15 Ohm/sq.

Since parylene is also an electronic encapsulant, the stability of the nanowire matrix was determined by tracking the sheet resistance over the course of 4 weeks. Results can be seen in Figure 4-18. The wire composite is stable for over 500 hours to 95% of its original conductivity.
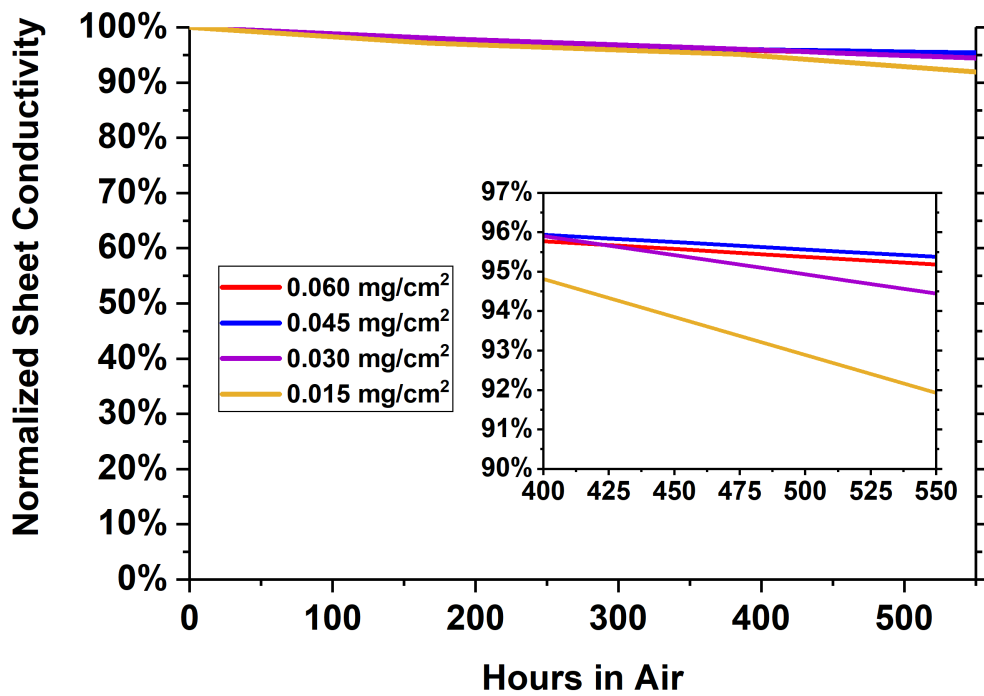
Figure 4-18: Stability of the nanowire-parylene composite measured via sheet conductivity over time.

Chapter 5

Concluding Remarks

The development of a smooth, conductive, flexible nanowire composite encompasses many facets of engineering: solution chemistry and rheology, thin film growth and most importantly surface engineering. This thesis has covered the potential of moving to flexible optoelectronic devices and the limitations imposed by brittle ceramic transparent conductors. It has covered the basics of solution thin film deposition and proposed a method for depositing colloidal nanoparticle dispersions in a scalable spray coating method. This spray coating method was developed into a working prototype with the help of CFD modeling and adequate control. Surface control and functionalization and its use in developing unique metal shapes like the metal nanowires, as well as creating fluorinated surfaces were explored both from a chemistry and experimental perspective. Lastly, all of these ideas were combined to create a nanowire-parylene composite that could be a suitable replacement for traditional transparent electrodes. It is smooth, transparent, conductive, atmospherically stable and flexible, making it a potential candidate for use in flexible optoelectronics. In addition, the techniques presented here are not limited to metal nanowire and parylene composites. These techniques could be applied additional systems in order to create smooth, planarized surfaces or uniform liquid processed thin films.

Figure 5-1: Image of a green OLED based on Alq3/NPD structure. Driving voltage was around 8V.

5.1 Future Studies

With every exploration and demonstration in engineering, it is important to discuss how the result can be improved or the technique be incorporated in new ways. Based on what is presented here in this thesis a few extensions will be discussed.

Devices

Initial usage of these films in optoelectronic devices show that it is possible to fabricate working devices using these nanowire films as a transparent electrode. A picture of an illuminated OLED device, based on an Alq3/NPD strucutre can be seen in Figure 5-1. A current voltage sweep of an organometallic perovskite solar cell can be seen in Figure 5-2 and a current voltage sweep of a Quantum Dot LED can be seen in Figure 5-3. As shown, all devices are working but lossy, mostly through series resistance. Therefore to completely demonstrate usage, understanding the electronic structuring and limitations of these films in working devices is imperative.
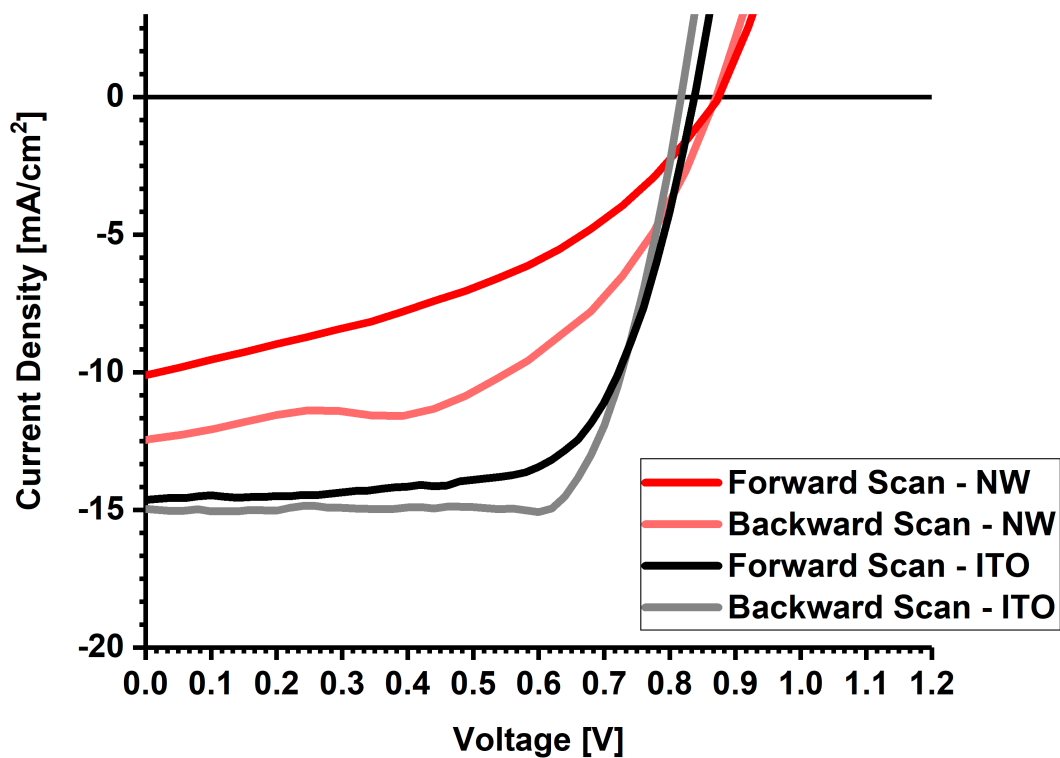
Figure 5-2: Current voltage sweep of a perovskite P-I-N device on nanowires.
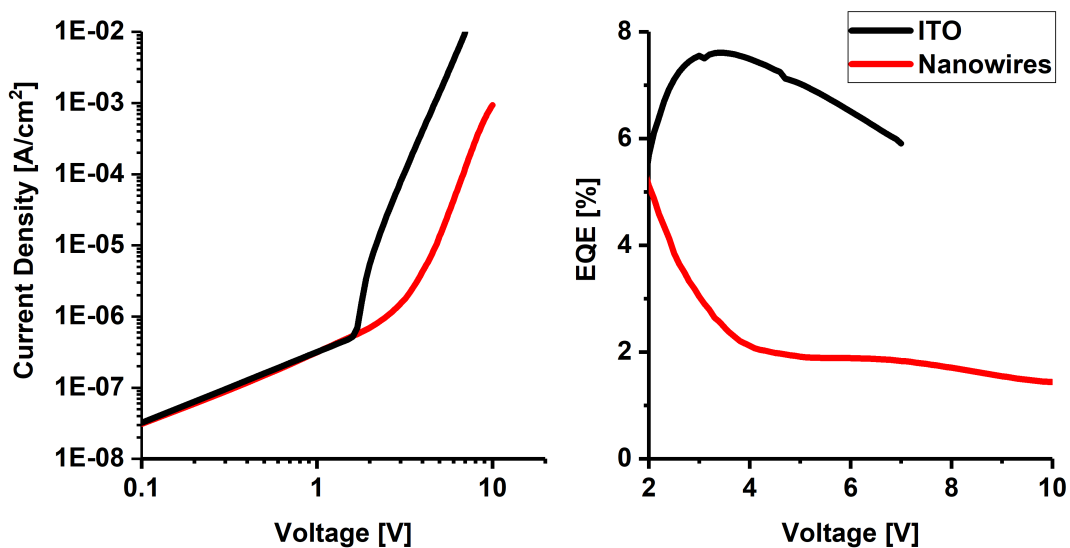
Figure 5-3: Current voltage sweep of a red quantum dot based LED on nanowires.

Additional Materials

Silver and parylene are good systems to demonstrate this manufacturing technique. However, they are not the only systems that can be used for a metal-mesh composite system. In recent years, development on the accuracy of metal mesh systems has continued. Metal wires are possible to synthesize cheaply in copper, nickel, and gold. Nickel is interesting due to being chemically stable as well as being cheap to produce. Therefore moving to a new wire system could have impacts on the ease of device development and yield something that is closer to becoming a true replacement.

Parylene, although useful for its encapsulating properties and uniformity could be replaced for a solution-processed alternative. This would make the entire manufacturing technique applicable for a roll-to-roll process and negate the need for transferring into vacuum.

Lastly, integrating electronic smoothing or injection layers like graphene or graphene flakes could increase environmental stability as well as chemical stability.

Plamonics

Tuning the metal ink to include plasmonic effects could be useful for single wavelength LEDs, lasers, as it has the potential to increase the out coupling from the semiconductor injection layers and active layers. This has the potential to increase eternal quantum efficiency (EQE) and therefore efficiency of the LED structure. The film could therefore serve two purposes, be a flexible transparent conductor but also improve efficiency. As this process creates a smooth surface, shorting would be a non-issue. A film of blue scattering plasmonic particles deposited by the pulsed spray coating technique can be seen in Figure 5-4.
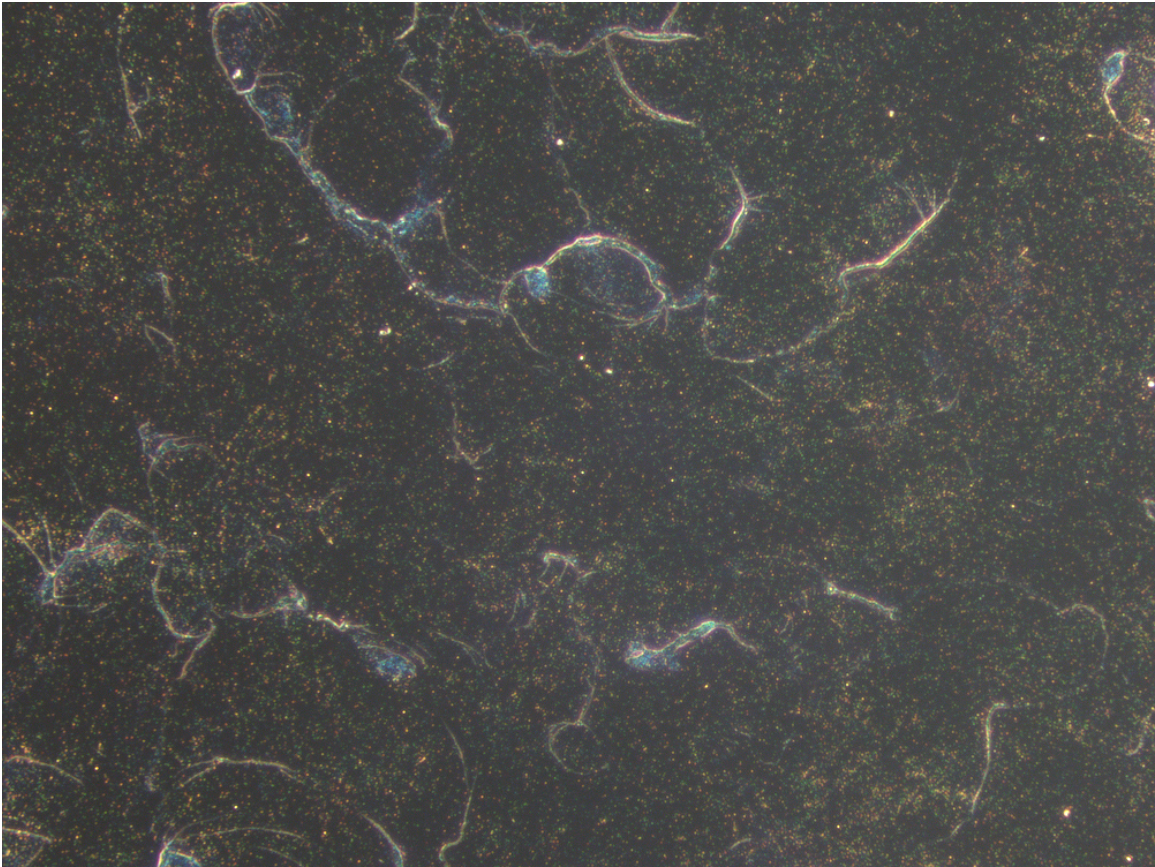
Figure 5-4: Dark field image of blue scattering plasmonic silver nanoparticles on glass, deposited by pulsed spray coating.

Appendix A

Python Code for Spray Coater

```
# -*- coding: utf-8 -*-
"""
Frontend for Spray Coater
version: 1
Last edited: 5/23/2016
Edited by: Richard Swartwout

"""
#import RPi.GPIO as GPIO
from tkinter import *
from tkinter import filedialog
from tkinter import scrolledtext
from time import sleep
'''
GPIO.setmode(GPIO.BOARD)
GPIO.setup(12,GPIO.OUT)
GPIO.setup(16,GPIO.OUT)
GPIO.setup(18,GPIO.OUT)
GPIO.setup(22,GPIO.OUT)
GPIO.setup(24,GPIO.OUT)
GPIO.setup(26,GPIO.OUT)
GPIO.setup(32,GPIO.OUT)
GPIO.setup(36,GPIO.OUT) #mixer 1
GPIO.setup(38,GPIO.OUT) #mixer 2
headpinout = [12, 16, 18, 22, 24, 26, 32]
'''
class main_window:
    def __init__(self,master):
        self.main = Frame(master, bg="")
        self.main.pack()
        self.openbutton=Button(self.main,text="OPEN", bg='yellow', width=20, command=self.opencode
            )
        self.openbutton.grid(row=1,column=0)
        self.savebutton=Button(self.main,text="SAVE", bg='orange', width=20,command=self.savecode)
        self.savebutton.grid(row=1,column=1)
        self.newbutton=Button(self.main,text="NEW", bg='pink', width=20, command=self.newcode)
        self.newbutton.grid(row=1,column=2)
        self.commandwindow=scrolledtext.ScrolledText(self.main,borderwidth=3)
        self.commandwindow.grid(row=0,column=0,columnspan=3)
        self.commandwindow.insert(END, "Head#;StartDelay;Cycles;TimeOn;TimeOff;\n")
```

```python
        self.textfeedback = scrolledtext.ScrolledText(self.main,borderwidth=3, bg='grey', fg='
            white',state=DISABLED)
        self.textfeedback.grid(row=0,column=3,columnspan=3)
        self.playbutton = Button(self.main, text="RUN", bg='green', width=40, command=self.runcode
            ) #runs the spray coater with a cetrain command
        self.playbutton.grid(row=1,column=3,columnspan=2)
        self.savelogbutton = Button(self.main,text="SAVE_LOG", bg='pink', width=20, command=self.
            savelog) #runs the spray coater stop command
        self.savelogbutton.grid(row = 1, column=5)

        self.purgebutton=Button(self.main,text="PURGE", bg='cyan', width=50, command=self.
            purgedialogcode)
        self.purgebutton.grid(row=2,column=0,columnspan=3)

        self.mixbutton=Button(self.main,text="MIX", bg='blue', width=50, command=self.
            mixdialogcode)
        self.mixbutton.grid(row=3,column=0,columnspan=3)

        self.quitbutton= Button(self.main,text="QUIT", bg='red', width=50, command=self.quitcode)
        self.quitbutton.grid(row=2,column=3,columnspan=3)


    def newcode(self):
        self.commandwindow.delete(1.0,END)
        self.commandwindow.insert(END, "Head#;StartDelay;Cycles;TimeOn;TimeOff;\n")
        self.textfeedback.config(state=NORMAL)
        self.textfeedback.delete(1.0,END)
        self.textfeedback.insert(END, "New_code_created\n")
        self.textfeedback.see(END)
        self.textfeedback.config(state=DISABLED)


    def opencode(self):
        file = filedialog.askopenfile(mode='r')
        self.commandwindow.delete(1.0,END)
        self.textfeedback.config(state=NORMAL)
        self.textfeedback.insert(END, "Spray_Code_Opened:_%s\n" %(file.name))
        self.textfeedback.see(END)
        self.textfeedback.config(state=DISABLED)
        self.commandwindow.insert(END, file.read())
        file.close()


    def savecode(self):
        file = filedialog.asksaveasfile(mode='w')
        file.write(self.commandwindow.get(1.0, END))
        self.textfeedback.config(state=NORMAL)
        self.textfeedback.insert(END, "Code_saved_to:_%s\n" %(file.name))
        self.textfeedback.see(END)
        self.textfeedback.config(state=DISABLED)
        file.close()


    def runcode(self):
        breakpoint = 0
        code = self.commandwindow.get(1.0, END)
        code = code.strip('_;\n')
        code = code.replace("_","")
        code = code.split('\n')
        for i in range(1,len(code)): #removes first line because reasons
            code[i] = code[i].strip('_;')
            code[i] = code[i].replace("_","")
            code[i] = code[i].split(';')
            #print(code)
            if len(code[i]) != 5:
```

```python
                    self.textfeedback.config(state=NORMAL)
                    self.textfeedback.insert(END, "Not_the_right_amount_of_inputs_on_line_%i\n" %(i))
                    self.textfeedback.see(END)
                    self.textfeedback.config(state=DISABLED)
                    breakpoint = 1
                    break
            for n in range(0,len(code[i])):
                try:
                    float(code[i][n])
                except ValueError:
                    self.textfeedback.config(state=NORMAL)
                    self.textfeedback.insert(END, "Problem_with_input_on_line_%i_value_%i\n" %(i
                        +1,n+1))
                    self.textfeedback.see(END)
                    self.textfeedback.config(state=DISABLED)
                    breakpoint =1
                    break
                code[i][n] = float(code[i][n])
        if breakpoint == 0:
            for line in code[1:len(code)]: #actually run the program
                self.textfeedback.config(state=NORMAL)
                self.textfeedback.insert(END, "Running_Spray_Head_%i_\n_Delaying_for_%f_seconds_\n
                    _Running_%i_cycles_of_%f_seconds_ON_and_%f_seconds_OFF\n" %(int(line[0]),line
                    [1],int(line[2]),line[3],line[4]))
                self.textfeedback.see(END)
                self.textfeedback.config(state=DISABLED)
                root.update_idletasks()
                sleep(line[1])
                for cycle in range(0,int(line[2])):
                    self.textfeedback.config(state=NORMAL)
                    self.textfeedback.insert(END, "_Cycle_%i....._" %(cycle))
                    self.textfeedback.see(END)
                    self.textfeedback.config(state=DISABLED)
                    root.update_idletasks()
                    #RPI code goes here
                    #GPIO.output(headpinout[int(line[0])-1],True)
                    sleep(line[3])
                    #RPI code goes here
                    #GPIO.output(headpinout[int(line[0])-1],False)
                    sleep(line[4])
                    self.textfeedback.config(state=NORMAL)
                    self.textfeedback.insert(END, "Done\n")
                    self.textfeedback.see(END)
                    self.textfeedback.config(state=DISABLED)
                    root.update_idletasks()
        #GPIO.cleanup()


def savelog(self):
    file = filedialog.asksaveasfile(mode='w')
    self.textfeedback.config(state=NORMAL)
    file.write(self.textfeedback.get(1.0, END))
    self.textfeedback.insert(END, "Log_saved_to:_%s\n" %(file.name))
    self.textfeedback.see(END)
    self.textfeedback.config(state=DISABLED)
    file.close()


def purgedialogcode(self):
    self.purgedialog=Toplevel()
    self.purgedialog.title("PURGE")

    self.headvar = StringVar(self.purgedialog)
```

```python
        self.headvar.set('Head_1')
        self.headlist = OptionMenu(self.purgedialog, self.headvar, 'Head_1','Head_2','Head_3','
            Head_4','Head_5','Head_6','Head_7')
        self.headlist.grid(row=0,column=0,padx=5)

        self.secondbox = Entry(self.purgedialog) #, height=0,width=5)
        self.secondbox.insert(END,'3.00')
        self.secondbox.grid(row=0,column=1)

        self.secondlabel = Label(self.purgedialog, text='SECONDS')
        self.secondlabel.grid(row=0,column=2)

        self.purge = Button(self.purgedialog, text='Purge', bg ='cyan', command=self.purgecode)
        self.purge.grid(row=0, column=3,padx=5)

        self.purgequit = Button(self.purgedialog, text = 'QUIT', bg ='red', command=self.
            purgedialog.destroy)
        self.purgequit.grid(row=0,column=4,padx=5)

    def mixdialogcode(self):
        self.mixdialog=Toplevel()
        self.mixdialog.title("MIX")

        self.mixonevar = IntVar()
        self.mixtwovar = IntVar()

        self.mixone = Checkbutton(self.mixdialog,text="Mix_1", variable=self.mixonevar)
        self.mixone.grid(row=0,column=0,padx=5)

        self.mixtwo = Checkbutton(self.mixdialog,text="Mix_2", variable=self.mixtwovar)
        self.mixtwo.grid(row=0,column=1,padx=5)

        self.mix = Button(self.mixdialog, text='Mix', bg ='cyan', command=self.mixcode)
        self.mix.grid(row=0, column=2,padx=5)

        self.mixquit = Button(self.mixdialog, text = 'QUIT', bg ='red', command=self.mixdialog.
            destroy)
        self.mixquit.grid(row=0,column=3,padx=5)

    def purgecode(self):
        purgehead = self.headvar.get()
        purgesecond = self.secondbox.get()
        purgesecond = float(purgesecond.strip('_'))
        purgehead = int(purgehead.strip('Head_'))

        self.textfeedback.config(state=NORMAL)
        self.textfeedback.insert(END, "_Purging_Head_%i_for_%.2f_Seconds\n" %(purgehead,
            purgesecond))
        self.textfeedback.see(END)
        self.textfeedback.config(state=DISABLED)
        root.update_idletasks()

        #RPI code goes here
        #GPIO.output(headpinout[int(purgehead-1],True)
        sleep(purgesecond)
        #RPI code goes here
        #GPIO.output(headpinout[int(purgehead-1],False)
        sleep(1)

    def mixcode(self):
        mixheadone = self.mixonevar.get()
```

```python
            mixheadtwo = self.mixtwovar.get()

            if mixheadone == 1:
                #GPIO.output(36,True)
                self.textfeedback.config(state=NORMAL)
                self.textfeedback.insert(END, "Turning on mixer 1\n")
                self.textfeedback.see(END)
                self.textfeedback.config(state=DISABLED)
                root.update_idletasks()
            else:
                #GPIO.output(36,False)
                self.textfeedback.config(state=NORMAL)
                self.textfeedback.insert(END, "Turning off mixer 1\n")
                self.textfeedback.see(END)
                self.textfeedback.config(state=DISABLED)
                root.update_idletasks()

            if mixheadtwo == 1:
                #GPIO.output(38,True)
                self.textfeedback.config(state=NORMAL)
                self.textfeedback.insert(END, "Turning on mixer 2\n")
                self.textfeedback.see(END)
                self.textfeedback.config(state=DISABLED)
                root.update_idletasks()
            else:
                #GPIO.output(38,False)
                self.textfeedback.config(state=NORMAL)
                self.textfeedback.insert(END, "Turning off mixer 2\n")
                self.textfeedback.see(END)
                self.textfeedback.config(state=DISABLED)
                root.update_idletasks()

    def quitcode(self):
        #GPIO.cleanup()
        root.destroy()

root = Tk()
main = main_window(root)
root.mainloop()
```

Bibliography

[1] Yumi Ahn, Donghwa Lee, Youngjun Jeong, Hyungjin Lee, and Youngu Lee. Flexible metal nanowire-parylene C transparent electrodes for next generation optoelectronic devices. *Journal of Materials Chemistry C*, 5(9):2425–2431, 2017.

[2] Khalid Alzoubi, Mohammad M. Hamasha, Susan Lu, and Bahgat Sammakia. Bending Fatigue Study of Sputtered ITO on Flexible Substrate. *Journal of Display Technology*, 7(11):593–600, nov 2011.

[3] Barry Arkles. *Hydrophobicity, Hydrophilicity and Silane Surface Modification*, volume 1. 2015.

[4] M. A. Baldo, D. F. O'Brien, Y. You, A. Shoustikov, S. Sibley, M. E. Thompson, and S. R. Forrest. Highly efficient phosphorescent emission from organic electroluminescent devices. *Nature*, 395(6698):151–154, sep 1998.

[5] K K Caswell, C M Bender, and C J Murphy. Seedless, surfactantless wet chemical synthesis of silver nanowires. *Nano Letters*, 3(5):667–669, 2003.

[6] Nathan L. Chang, Anita Wing Yi Ho-Baillie, Doojin Vak, Mei Gao, Martin A. Green, and Renate J. Egan. Manufacturing cost and market potential analysis of demonstrated roll-to-roll perovskite photovoltaic cell processes. *Solar Energy Materials and Solar Cells*, 174:314–324, 2018.

[7] Moon Kee Choi, Jiwoong Yang, Kwanghun Kang, Dong Chan Kim, Changsoon Choi, Chaneui Park, Seok Joo Kim, Sue In Chae, Tae-Ho Kim, Ji Hoon Kim, Taeghwan Hyeon, and Dae-Hyeong Kim. Wearable red-green-blue quantum dot light-emitting diode array using high-resolution intaglio transfer printing. *Nature Communications*, 6(1):7149, dec 2015.

[8] Seth Coe, Wing Keung Woo, Moungi Bawendi, and Vladimir Bulović. Electroluminescence from single monolayers of nanocrystals in molecular organic devices. *Nature*, 420(6917):800–803, 2002.

[9] Sukanta De, Thomas M. Higgins, Philip E. Lyons, Evelyn M. Doherty, Peter N. Nirmalraj, Werner J. Blau, John J. Boland, and Jonathan N. Coleman. Silver Nanowire Networks as Flexible, Transparent, Conducting Films: Extremely High DC to Optical Conductivity Ratios. *ACS Nano*, 3(7):1767–1774, jul 2009.

[10] R.D. Deegan, O. Bakajin, T.F. Dupont, G. Huber, S.R. Nagel, and T.A. Witten. Capillary flow as the causes of ring stains from dried liquid drops. *Nature, London*, 389:827–829, 1997.

[11] Bing Deng, Po-Chun Hsu, Guanchu Chen, B. N. Chandrashekar, Lei Liao, Zhawulie Ayitimuda, Jinxiong Wu, Yunfan Guo, Li Lin, Yu Zhou, Mahaya Aisijiang, Qin Xie, Yi Cui, Zhongfan Liu, and Hailin Peng. Roll-to-Roll Encapsulation of Metal Nanowires between Graphene and Plastic Substrate for High-Performance Flexible Transparent Electrodes. *Nano Letters*, 15(6):4206–4213, jun 2015.

[12] Klaus Ellmer. Past achievements and future challenges in the development of optically transparent electrodes. *Nature Photonics*, 6(12):809–817, dec 2012.

[13] Christopher J.M. Emmott, Antonio Urbina, and Jenny Nelson. Environmental and economic assessment of ITO-free electrodes for organic solar cells. *Solar Energy Materials and Solar Cells*, 97:14–21, feb 2012.

[14] J. B. Fortin and T. M. Lu. A model for the chemical vapor deposition of poly(para-xylylene) (parylene) thin films. *Chemistry of Materials*, 14(5):1945–1949, 2002.

[15] Yulia Galagan, Jan Eric J.m. Rubingh, Ronn Andriessen, Chia Chen Fan, Paul W.m. Blom, Sjoerd C. Veenstra, and Jan M. Kroon. ITO-free flexible organic solar cells with printed current collecting grids. *Solar Energy Materials and Solar Cells*, 95(5):1339–1343, 2011.

[16] Erik C. Garnett, Wenshan Cai, Judy J. Cha, Fakhruddin Mahmood, Stephen T. Connor, M. Greyson Christoforo, Yi Cui, Michael D. McGehee, and Mark L. Brongersma. Self-limited plasmonic welding of silver nanowire junctions. *Nature Materials*, 11(3):241–249, mar 2012.

[17] Roy G. Gordon. Criteria for Choosing Transparent Conductors. *MRS Bulletin*, 25(08):52–57, aug 2000.

[18] William F. Gorham. A New, General Synthetic Method for the Preparation of Linear Poly-p-xylylenes. *Journal of Polymer Science Part A-1: Polymer Chemistry*, 4(12):3027–3039, 1966.

[19] Huizhang Guo, Na Lin, Yuanzhi Chen, Zhenwei Wang, Qingshui Xie, Tongchang Zheng, Na Gao, Shuping Li, Junyong Kang, Duanjun Cai, and Dong-Liang Peng. Copper nanowires as fully transparent conductive electrodes. *Scientific reports*, 3:2323, 2013.

[20] Liangbing Hu, Han Sun Kim, Jung-Yong Lee, Peter Peumans, and Yi Cui. Scalable Coating and Properties of Transparent, Flexible, Silver Nanowire Electrodes. *ACS Nano*, 4(5):2955–2963, may 2010.

[21] Joel Jean, Annie Wang, and Vladimir Bulović. In situ vapor-deposited parylene substrates for ultra-thin, lightweight organic solar cells. *Organic Electronics*, 31:120–126, apr 2016.

[22] S.K.M Jönsson, J Birgerson, X Crispin, G Greczynski, W Osikowicz, A.W Denier van der Gon, W.R Salaneck, and M Fahlman. The effects of solvents on the morphology and sheet resistance in poly(3,4-ethylenedioxythiophene)-polystyrenesulfonic acid (PEDOT-PSS) films. *Synthetic Metals*, 139(1):1–10, aug 2003.

[23] R.L. Kaas and J.L. Kardos. The Interacion of Alkoxy Silane Coupling Agents with Silica Surfaces. *Polymer Engineering Science*, 11:11, 1971.

[24] Martin Kaltenbrunner, Getachew Adam, Eric Daniel Głowacki, Michael Drack, Reinhard Schwödiauer, Lucia Leonat, Dogukan Hazar Apaydin, Heiko Groiss, Markus Clark Scharber, Matthew Schuette White, Niyazi Serdar Sariciftci, and Siegfried Bauer. Flexible high power-per-weight perovskite solar cells with chromium oxide-metal contacts for improved stability in air. *Nature Materials*, 14(10):1032–1039, oct 2015.

[25] Martin Kaltenbrunner, Matthew S. White, Eric D. Głowacki, Tsuyoshi Sekitani, Takao Someya, Niyazi Serdar Sariciftci, and Siegfried Bauer. Ultrathin and lightweight organic solar cells with high flexibility. *Nature Communications*, 3(1):770, jan 2012.

[26] Juho Kim, Jeongwoo Hwang, Kwangsun Song, Namyun Kim, Jae Cheol Shin, and Jongho Lee. Ultra-thin flexible GaAs photovoltaics in vertical forms printed on metal surfaces without interlayer adhesives. *Applied Physics Letters*, 108(25):253101, jun 2016.

[27] Yong Hyun Kim, Christoph Sachse, Michael L. Machala, Christian May, Lars Müller-Meskamp, and Karl Leo. Highly Conductive PEDOT:PSS Electrode with Optimized Solvent and Thermal Post-Treatment for ITO-Free Organic Solar Cells. *Advanced Functional Materials*, 21(6):1076–1081, mar 2011.

[28] Kylee Korte. Rapid Synthesis of Silver Nanowires. *National Nanotechnology Infrastructure Network*, pages 28–29, 2007.

[29] Peter Kovacik, Gabriella del Hierro, William Livernois, and Karen K. Gleason. Scale-up of oCVD: large-area conductive polymer thin films for next-generation electronics. *Materials Horizons*, 2(2):221–227, 2015.

[30] Daniel Langley, Gaël Giusti, Céline Mayousse, Caroline Celle, Daniel Bellet, and Jean-Pierre Simonato. Flexible transparent conductive materials based on silver nanowire networks: a review. *Nanotechnology*, 24(45):452001, nov 2013.

[31] Daniel Langley, Gaël Giusti, Céline Mayousse, Caroline Celle, Daniel Bellet, and Jean-Pierre Simonato. Flexible transparent conductive materials based on silver nanowire networks: a review. *Nanotechnology*, 24(45):452001, nov 2013.

[32] J. D. Le Grange, J.L. Markham, and C. R. Kurkjian. Effects of Surface Hydration. *Langmuir*, (9):1749–1753, 1993.

[33] Jung-Yong Lee, Stephen T. Connor, Yi Cui, and Peter Peumans. Solution-Processed Metal Nanowire Mesh Transparent Electrodes. *Nano Letters*, 8(2):689–692, feb 2008.

[34] Mainak Majumder, Clint S. Rendall, J. Alexander Eukel, James Y.L. Wang, Natnael Behabtu, Cary L. Pint, Tzu Yu Liu, Alvin W. Orbaek, Francesca Mirri, Jaewook Nam, Andrew R. Barron, Robert H. Hauge, Howard K. Schmidt, and Matteo Pasquali. Overcoming the "coffee-stain" effect by compositional marangoni-flow-assisted drop-drying. *Journal of Physical Chemistry B*, 116(22):6536–6542, 2012.

[35] Yong-Jin Noh, Seok-Soon Kim, Tae-Wook Kim, and Seok-In Na. Cost-effective ITO-free organic solar cells with silver nanowire-PEDOT:PSS composite electrodes via a one-step spray deposition method. *Solar Energy Materials and Solar Cells*, 120:226–230, jan 2014.

[36] Y. Park, V. Choong, Y. Gao, B. R. Hsieh, and C. W. Tang. Work function of indium tin oxide transparent conductor measured by photoelectron spectroscopy. *Applied Physics Letters*, 68(19):2699–2701, may 1996.

[37] Kaustubha Parkhi. Global Markets, Technologies and Applications for Flexible Displays. *BBC Research*, page 165, 2017.

[38] A. E. Rakhshani, Y. Makdisi, and H. A. Ramazaniyan. Electronic and optical properties of fluorine-doped tin oxide films. *Journal of Applied Physics*, 83(2):1049–1057, jan 1998.

[39] Erin M. Sanehira, Ashley R. Marshall, Jeffrey A. Christians, Steven P. Harvey, Peter N. Ciesielski, Lance M. Wheeler, Philip Schulz, Lih Y. Lin, Matthew C. Beard, and Joseph M. Luther. Enhanced mobility CsPbI 3 quantum dot arrays for record-efficiency, high-voltage photovoltaic cells. *Science Advances*, 3(10):eaao4204, oct 2017.

[40] William J. Scheideler, Jaewon Jang, Muhammed Ahosan Ul Karim, Rungrot Kitsomboonloha, Andre Zeumault, and Vivek Subramanian. Gravure-Printed Sol-Gels on Flexible Glass: A Scalable Route to Additively Patterned Transparent Conductors. *ACS Applied Materials and Interfaces*, 7(23):12679–12687, 2015.

[41] William J. Scheideler, Jeremy Smith, Igal Deckman, Seungjun Chung, Ana Claudia Arias, and Vivek Subramanian. A robust, gravure-printed, silver nanowire/metal oxide hybrid electrode for high-throughput patterned transparent conductors. *Journal of Materials Chemistry C*, 4(15):3248–3255, 2016.

[42] R Schlaf, H Murata, and Z.H Kafafi. Work function measurements on indium tin oxide films. *Journal of Electron Spectroscopy and Related Phenomena*, 120(1-3):149–154, oct 2001.

[43] W. A. Sirignano and Chris F. Edwards. *Fluid Dynamics and Transport of Droplets and Sprays*, volume 122. 2000.

[44] Zhaoning Song, Chad L. McElvany, Adam B. Phillips, Ilke Celik, Patrick W. Krantz, Suneth C. Watthage, Geethika K. Liyanage, Defne Apul, and Michael J. Heben. A technoeconomic analysis of perovskite solar module manufacturing with low-cost materials and techniques. *Energy & Environmental Science*, 10(6):1297–1305, 2017.

[45] Joshua A. Spechler, Tae-Wook Koh, Jake T. Herb, Barry P. Rand, and Craig B. Arnold. A Transparent, Smooth, Thermally Robust, Conductive Polyimide for Flexible Electronics. *Advanced Functional Materials*, 25(48):7428–7434, dec 2015.

[46] W Steckelmacher. Introduction to surface and thin film processes. *Vacuum*, 62(4):387–388, 2001.

[47] Kuan Sun, Shupeng Zhang, Pengcheng Li, Yijie Xia, Xiang Zhang, Donghe Du, Furkan Halis Isikgor, and Jianyong Ouyang. Review on application of PEDOTs and PEDOT:PSS in energy conversion and storage devices. *Journal of Materials Science: Materials in Electronics*, 26(7):4438–4462, jul 2015.

[48] Zhi-Kuang Tan, Reza Saberi Moghaddam, May Ling Lai, Pablo Docampo, Ruben Higler, Felix Deschler, Michael Price, Aditya Sadhanala, Luis M. Pazos, Dan Credgington, Fabian Hanusch, Thomas Bein, Henry J. Snaith, and Richard H. Friend. Bright light-emitting diodes based on organometal halide perovskite. *Nature Nanotechnology*, 9(9):687–692, sep 2014.

[49] W. Tang and D.C. Cameron. Aluminum-doped zinc oxide transparent conductors deposited by the sol-gel process. *Thin Solid Films*, 238(1):83–87, jan 1994.

[50] Arthur A. Tracton. *Coatings Technology Fundamentals,Testing, And Processing Techniques*. 2007.

[51] Xuan Wang, Linjie Zhi, and Klaus Müllen. Transparent, Conductive Graphene Electrodes for Dye-Sensitized Solar Cells. *Nano Letters*, 8(1):323–327, jan 2008.

[52] Jonathan K. Wassei and Richard B. Kaner. Graphene, a promising transparent conductor. *Materials Today*, 13(3):52–59, mar 2010.

[53] Junbo Wu, Héctor A. Becerril, Zhenan Bao, Zunfeng Liu, Yongsheng Chen, and Peter Peumans. Organic solar cells with solution-processed graphene transparent electrodes. *Applied Physics Letters*, 92(26):263302, jun 2008.

[54] Younan Xia, Yujie Xiong, Byungkwon Lim, and Sara E. Skrabalak. Shape-Controlled Synthesis of Metal Nanocrystals : Simple. *Angewandte Chemie International Edition*, 48(1):60–103, 2009.

[55] Woon Seok Yang, Byung-Wook Park, Eui Hyuk Jung, Nam Joong Jeon, Young Chan Kim, Dong Uk Lee, Seong Sik Shin, Jangwon Seo, Eun Kyu Kim, Jun Hong Noh, and Sang Il Seok. Iodide management in formamidinium-lead-halide-based perovskite layers for efficient solar cells. *Science*, 356(6345):1376–1379, jun 2017.

[56] Zhiqiang Yang, Haijun Qian, Hongyu Chen, and Jeffrey N. Anker. One-pot hydrothermal synthesis of silver nanowires via citrate reduction. *Journal of Colloid and Interface Science*, 352(2):285–291, 2010.

[57] Xiao-Yan Zeng, Qi-Kai Zhang, Rong-Min Yu, and Can-Zhong Lu. A New Transparent Conductor: Silver Nanowire Film Buried at the Surface of a Transparent Polymer. *Advanced Materials*, 22(40):4484–4488, oct 2010.

[58] Jingbo Zhao, Yunke Li, Guofang Yang, Kui Jiang, Haoran Lin, Harald Ade, Wei Ma, and He Yan. Efficient organic solar cells processed from hydrocarbon solvents. *Nature Energy*, 1(2), 2016.